

# NAVAL POSTGRADUATE SCHOOL

## Monterey, California



# THESIS

DEFINITION STUDY AND MODEL FOR  
A TETHERED SOUNDING ROCKET

by

Yoon, Sang Il

December 1988

Thesis Adviser:

Richard C. Olsen

Approved for public release: distribution is unlimited



REPORT DOCUMENTATION PAGE

1a. REPORT SECURITY CLASSIFICATION <b>Unclassified</b>		1b. RESTRICTIVE MARKINGS	
2a. SECURITY CLASSIFICATION AUTHORITY		3. DISTRIBUTION/AVAILABILITY OF REPORT Approved for public release; distribution is unlimited	
2b. DECLASSIFICATION/DOWNGRADING SCHEDULE			
4. PERFORMING ORGANIZATION REPORT NUMBER(S)		5. MONITORING ORGANIZATION REPORT NUMBER(S)	
6a. NAME OF PERFORMING ORGANIZATION Naval Postgraduate School	6b. OFFICE SYMBOL (If applicable) 61	7a. NAME OF MONITORING ORGANIZATION Naval Postgraduate School	
6c. ADDRESS (City, State, and ZIP Code) Monterey, California 93943-5000		7b. ADDRESS (City, State, and ZIP Code) Monterey, California 93943-5000	
8a. NAME OF FUNDING / SPONSORING ORGANIZATION	8b. OFFICE SYMBOL (If applicable)	9. PROCUREMENT INSTRUMENT IDENTIFICATION NUMBER	
8c. ADDRESS (City, State, and ZIP Code)		10. SOURCE OF FUNDING NUMBERS	
		PROGRAM ELEMENT NO.	PROJECT NO.
		TASK NO.	WORK UNIT ACCESSION NO.
11. TITLE (Include Security Classification) Definition Study and Model for a Tethered Sounding Rocket			
12. PERSONAL AUTHOR(S)			
13a. TYPE OF REPORT Master's Thesis	13b. TIME COVERED FROM _____ TO _____	14. DATE OF REPORT (Year, Month, Day) 1988 December	15. PAGE COUNT 109
16. SUPPLEMENTARY NOTATION The views expressed in this thesis are those of the author and do not reflect the official policy or position of the Department of Defense or the U. S. Government			
17. COSATI CODES		18. SUBJECT TERMS (Continue on reverse if necessary and identify by block number)	
FIELD	GROUP	Tether deployment system, Plasma contactor Hollow Cathode, Flight program, Model of system electrodynamic behavior study	
19. ABSTRACT (Continue on reverse if necessary and identify by block number)			
<p>The HOCAT experiment is a sounding rocket payload to measure the coupling of large currents (up to 1 A) from a satellite into the ambient plasma, and the return path through the plasma. The devices to be used to establish electrical contact with the plasma are hollow cathode plasma sources, using Xenon propellant. Two satellite sections will be connected by a 100-m cable, which can be used to bias the two satellites with respect to each other. The current through the connecting cable will be monitored, along with the particle fluxes to the satellites. A fiber-optic technique will be used to measure the return current flowing through the ambient plasma. Electric fields, densities, and plasma waves will be monitored with floating probes. We intend to launch this payload from Wallops Flight Facility two years after funding begins.</p>			
20. DISTRIBUTION/AVAILABILITY OF ABSTRACT <input checked="" type="checkbox"/> UNCLASSIFIED/UNLIMITED <input type="checkbox"/> SAME AS RPT. <input type="checkbox"/> DTIC USERS		21. ABSTRACT SECURITY CLASSIFICATION Unclassified	
22a. NAME OF RESPONSIBLE INDIVIDUAL Professor Richard Christopher Olsen		22b. TELEPHONE (Include Area Code) (408) 646 - 2019	22c. OFFICE SYMBOL 61 Os

Approved for public release; distribution is unlimited.

Definition Study and Model for a Tethered  
Sounding Rocket

by

Yoon, Sang Il  
Major, Republic of Korea Army  
B.S., Republic of Korea Military Academy, 1979

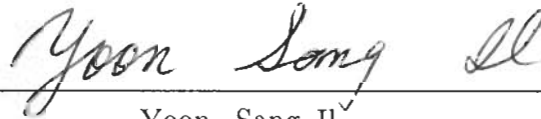
Submitted in partial fulfillment of the  
requirements for the degree of

MASTER OF SCIENCE IN PHYSICS

from the

NAVAL POSTGRADUATE SCHOOL  
December 1988

Author:



Yoon, Sang Il

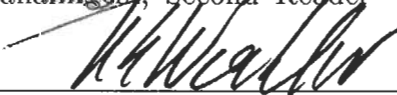
Approved by:




Richard C. Olsen, Thesis Advisor



S. Gnanalingam, Second Reader



Karlheinz E. Woehler, Chairman,  
Department of Physics



Gordon E. Schacher,  
Dean of Science and Engineering

## ABSTRACT

The HOCAT experiment is a sounding rocket payload to measure the coupling of large currents (up to 1 A) from a satellite into the ambient plasma, and the return path through the plasma. The devices to be used to establish electrical contact with the plasma are hollow cathode plasma sources, using Xenon propellant. Two satellite sections will be connected by a 100 m cable, which can be used to bias the two satellites with respect to each other. The current through the connecting cable will be monitored, along with the particle fluxes to the satellites. A fiber-optic technique will be used to measure the return current flowing through the ambient plasma. Electric fields, densities, and plasma waves will be monitored with floating probes. We intend to launch this payload from Wallops Flight Facility two years after funding begins.

## TABLE OF CONTENTS

I.	INTRODUCTION	1
	A. A HISTORY OF TETHER CONCEPTS	1
	B. ELECTRODYNAMIC TETHERS	6
	1. Basic Concept	6
	2. Electrodynamic Tether Applications	7
	3. Tether Experiments	8
	a. Tethered Satellite System-1 Experiment	8
	b. US-JAPAN Charge Rocket Experiment	10
	c. MAIMIK Rocket Experiment	11
	C. PLASMA CONTACTORS	13
	1. Basic Concept (Requirements and Future Mission)	13
	2. Plasma Contactor Flight History	15
	a. Balloons	15
	b. Electron Gun	17
	c. Neutral Gas Releases	18
	d. Ion Beams	20
	e. Ion Engine	21
	f. Hollow Cathodes	29
	D. PROPOSED EXPERIMENT	30
II.	TETHER DEPLOYMENT	31
	A. BASIC DYNAMICS	31

B.	HOCAT DEPLOYMENT OBJECTIVES.....	32
1.	US-JAPAN Joint Experiment Deployment System.....	34
2.	MAIMIK Rocket Experiment Deployment System.....	38
3.	CANADIAN OEDIPUS Experiment Deployment System.....	39
4.	Tethered Satellite System-1 Deployment System.....	42
III.	PLASMA CONTACTOR HOLLOW CATHODES.....	43
A.	LABORATORY STUDIES.....	43
B.	THEORETICAL STUDIES.....	50
C.	FLIGHT EXPERIMENT DATA.....	52
IV.	EXPERIMENTAL FLIGHT PROGRAM.....	54
A.	ENVIRONMENT.....	54
B.	LAUNCH VEHICLE.....	60
C.	DEPLOYMENT SYSTEM.....	62
D.	FLIGHT SCENARIO.....	63
E.	PAYLOAD.....	63
1.	Hollow Cathode.....	64
2.	Experiment Control and PCM Encoder.....	65
3.	Electric Field Instruments.....	66
4.	Thermal Plasma Analyzer (Ions and Electrons).....	67
5.	Direct Current Measurements (Current Loop).....	71
6.	TV Camera.....	73
7.	Magnetometer.....	74
V.	MODEL OF SYSTEM ELECTRODYNAMIC BEHAVIOR.....	75
A.	PROBE THEORY.....	75

B. MODIFICATIONS DUE TO PLASMA CONTACTOR.....	86
1. Electron Emission.....	86
2. Election Collection.....	87
C. SUMMARY.....	89
VI. CONCLUSIONS AND RECOMMENDATIONS.....	90
LIST OF REFERENCES.....	92
INITIAL DISTRIBUTION LIST.....	97

## LIST OF FIGURES

Fig. 1.1	Gemini–Titan Space Vehicle Configuration·····	2
Fig. 1.2	Agena Target Vehicle Configuration·····	3
Fig. 1.3	Gemini Spacecraft·····	3
Fig. 1.4	Tethered Spacecraft/Target Vehicle·····	3
Fig. 1.5	Effect of Damping on the Oscillation of Tethered System··	4
Fig. 1.6	Effect of Relative Velocity on Motion of Gravity–Grad····	5
Fig. 1.7	Electrodynamic Tether System·····	7
Fig. 1.8	TSS–1 Satellite System·····	9
Fig. 1.9	Payload Configuration of fourth TPE Experiment·····	11
Fig. 1.10	Individual Liquid Metal Ion Emitter·····	14
Fig. 1.11	Collector Screen in the Deployed Configuration·····	16
Fig. 1.12	Configuration of ATS–5 Ion Thruster·····	22
Fig. 1.13	Configuration of ATS–6 Ion Engine·····	23
Fig. 1.14	Spacecraft Plasma Current Diagram of SERT–II·····	26
Fig. 1.15	Distribution of Emission Currents·····	27
Fig. 1.16	Excess Neutralizer Emission·····	28
Fig. 2.1	Dumbbell Tether Model·····	31
Fig. 2.2	Hollow Cathode Configuration·····	33
Fig. 2.3	Plot of Tether Wire Extension Velocity vs Time·····	36
Fig. 2.4	Plot of Tether Separation Distance vs Time·····	37
Fig. 2.5	Deployment Velocity of fourth US–JAPAN Experiment·····	38
Fig. 2.6	Plot of Separation Velocity vs Time·····	40
Fig. 2.7	Plot of Separation Distance vs Time·····	41

Fig. 2.8	TSS-1 Reel and Boom Mechanism.....	42
Fig. 3.1	Perturbing Effect of Vacuum Tank Wall.....	45
Fig. 3.2	Contactor Anode-to Ambient Plasma Potential Difference vs Electron Emission Current.....	46
Fig. 3.3	Plasma Potential Contour around Hollow Cathode.....	47
Fig. 3.4	Hollow Cathode Ignited mode Configuration.....	48
Fig. 3.5	Current to Contactor vs Bias Voltages.....	49
Fig. 3.6	Bias-to-Plasma Potential Difference.....	49
Fig. 3.7	Current vs Contactor Potential.....	50
Fig. 3.8	2-Dimensional Cut.....	52
Fig. 4.1	Ionospheric Electron Density (daytime).....	56
Fig. 4.2	Ionospheric Electron Density (nighttime).....	56
Fig. 4.3	SPEAR-1 Neutral Pressure Data.....	57
Fig. 4.4	Electron Temperature and Thermal Velocity.....	58
Fig. 4.5	Ion Temperature, Mass and Thermal Velocity.....	58
Fig. 4.6	Debye Length.....	59
Fig. 4.7	Electron Collision Frequency and Mean Free Path.....	59
Fig. 4.8	NASA Sounding Rocket Performance.....	60
Fig. 4.9	HOCAT Black Brant X Payload.....	61
Fig. 4.10	Hollow Cathode Design.....	64
Fig. 4.11	Dimensions of Hollow Cathode.....	64
Fig. 4.12	UAH Fast Event System.....	66
Fig. 4.13	Electric Field and Density Data.....	68
Fig. 4.14	Electrostatic Analyzer.....	69
Fig. 4.15	ESA Included Mass Resolution.....	69

Fig. 4.16	ATS-6 ESA.....	70
Fig. 4.17	Spectrometer Results from SPEAR-1.....	72
Fig. 4.18	Principle of the Current Loop Measurement.....	73
Fig. 5.1	Plot of Electron Current Density vs Positive Potential.....	77
Fig. 5.2	Plot of Ion Current Density vs Negative Potential.....	79
Fig. 5.3	Plot of Bias Potential vs Current Density.....	80
Fig. 5.4	Schematic Diagram of System.....	81
Fig. 5.5	Sphere Current Data from SPEAR-1.....	83
Fig. 5.6	Plot of $\frac{I}{I_0}$ vs Positive Potential.....	84
Fig. 5.7	Plot of Radius vs Bias Potential.....	85
Fig. 5.8	Plasma Cloud Expansion Model.....	88

## ACKNOWLEDGEMENTS

I wish to express my gratitude and appreciation to thesis advisor, Professor Richard Christopher Olsen and my second reader, Professor S. Gnanalingam for the instruction, guidance and friendly advices throughout this study.

I wish to thank the numerous scientists who contributed Figures and data for this work, particularly, Dr. Ira Katz, S-Cubed; Dr. Paul Wilbur and Mr. John Williams, Colorado State University; Dr. Roy Torbert, University of Alabama in Huntsville; Mr. John Patterson, NASA/LeRC; and Dr. John Raitt, Utah State University.

Finally, many thanks to my wife, Hye-Soog and my daughter, Ye-Ji, for their love and being healthy and patient for two and half years in Monterey, California.

## I. INTRODUCTION

### A. A HISTORY OF TETHER CONCEPTS

The concept of using a long thin structure in space was first documented by Tsiolkovsky in 1895 in the form of a tower reaching from the Earth's equator to beyond geostationary altitudes. This grandiose idea has received further attention in the modern space era for the purpose of lifting payloads into space, and concepts have been developed under the titles "space elevator", and "orbital tower", with some scaled down but still ambitious variations proposed in the 60's and 70's. [Ref. 1]

The Smithsonian Astrophysical Observatory (SAO) proposed and initiated the rigorous investigation of the feasibility of tether systems. For example, a Shuttle-borne radio physics facility that included a 20–100 km long, vertical, thin-wire antenna was proposed by Mario D. Grossi in 1972. In 1974, G. Colombo, recognizing the potential of more general uses of the shuttle-borne tether, provided with a rigorous analysis the proof of dynamic feasibility. He identified several additional applications, including a scheme for the measurement of gravity gradients at orbital heights. Since 1974, a series of investigations has made it possible to explore several critical aspects of feasibility in such areas as tether dynamics, tether electrostatics, tethered constellations, tether-induced dynamic noise in the subsatellite, etc.[Ref. 2]

The "Space elevator" capable of crawling in a controlled manner along a deployed tether appears to have a number of potential Space Station applications. These include a variable microgravity laboratory, transportation unit between two

tethered bodies, system center-of-gravity management, tether inspection and repair device, and carrier for re-entry probe.

The first actual demonstration of a thin tether connecting two vehicles in space occurred in the Gemini program in 1966. The Gemini program was undertaken for the purpose of space-flight capabilities during the period between Mercury and Apollo. Two modes of tethered space vehicle operations were explored during the Gemini program. One mode was rotating tethered vehicles. The other mode studied gravity gradient effects. Two separate missions conducted experiments requiring tethered attachment of the manned Gemini spacecraft to a spent Atlas-Agena D booster stage.

The Gemini XI flight was launched on September 12, 1966. The launch configuration of the Gemini-Titan Space vehicle and Spacecraft is shown in Figure 1.1. Figure 1.2 shows the Agena target vehicle configurations. Figure 1.3 shows the Gemini spacecraft configuration which is composed of adapter and re-entry module.[Ref. 3]

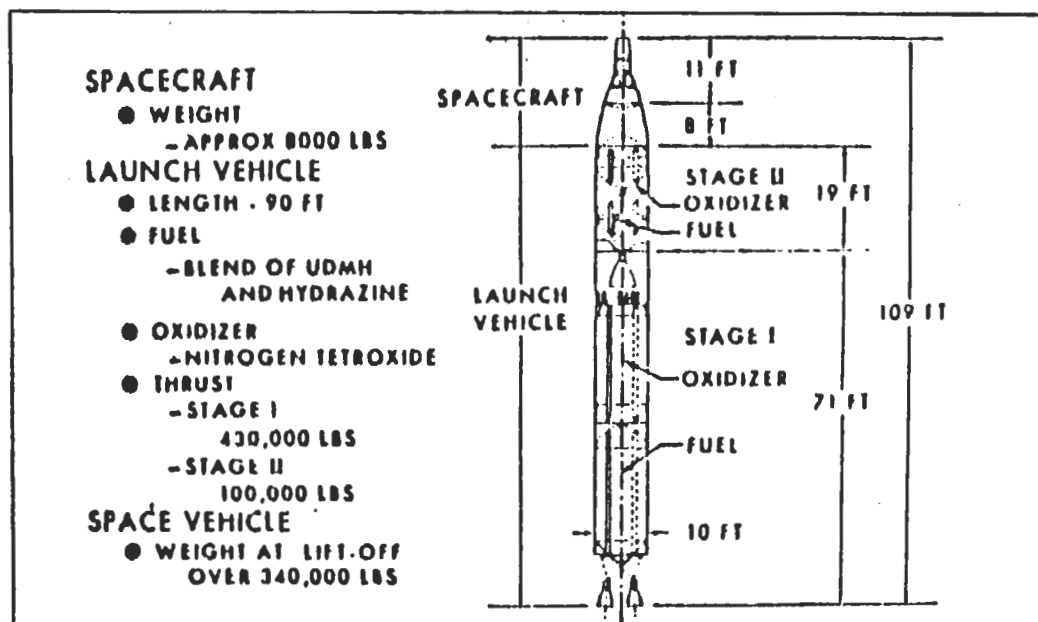


Fig. 1.1 Gemini-Titan Space Vehicle Configuration[Ref. 3]

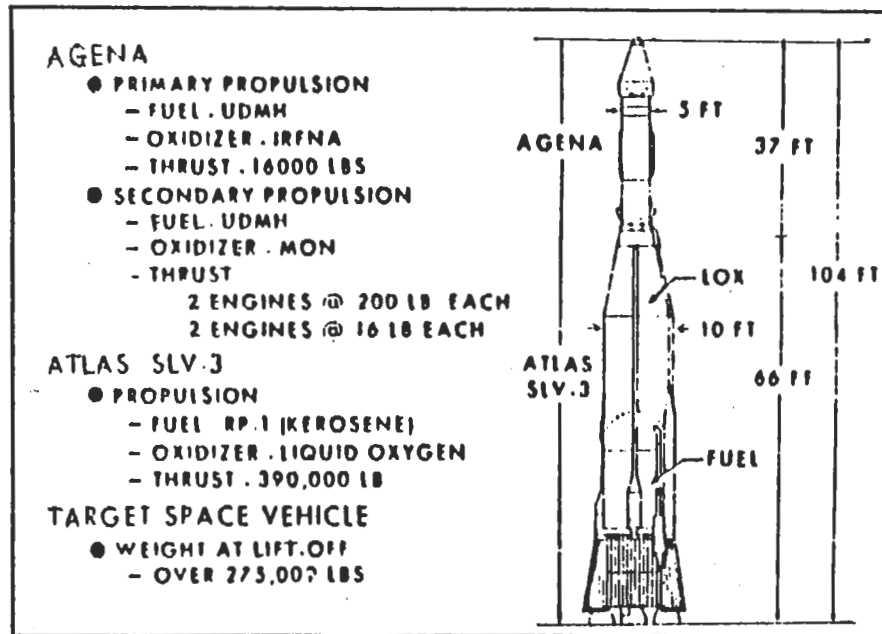


Fig. 1.2 Agena Target Vehicle Configuration [Ref. 3]

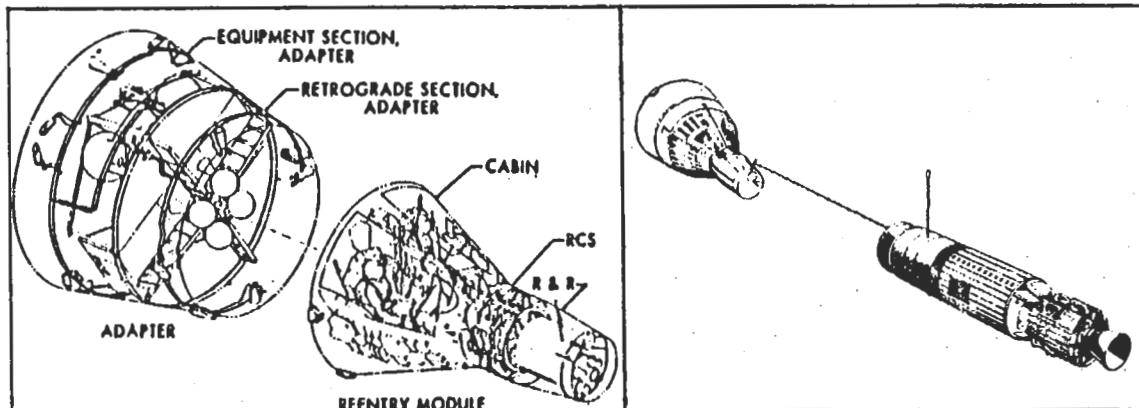


Fig. 1.3 Gemini Spacecraft

Fig. 1.4 Tethered Spacecraft/Target Vehicle

Figure 1.4 shows the tethered configuration of Gemini spacecraft/target vehicle. The unstretched tether length was 100 ft. The tether was constructed from Dacron webbing with a breaking strength of 800 pounds. The total lateral thrusting of 13 seconds gave rise to a final spin rate of 0.9 deg/sec. The maximum diameter of both vehicles was 10 ft. [Ref. 4]

On Gemini XI, a spin-up maneuver was successfully conducted with no evidence of significant cable-dynamics effects. This confirmed that cable dynamics were not critical in the rotational behavior (i.e. a spin-stabilized configuration was shown to be feasible). The procedure for spinning up the tethered spacecraft/target vehicle system consisted of backing the spacecraft away from the target vehicle until the tether was almost taut, then firing the translational thrusters to provide thrust on the spacecraft normal to the line between the vehicles. The spin-up moment on the system was supplied entirely by the spacecraft translation-control system.

Figure 1.5 illustrates the spin-up behavior with and without damping. The damping is quite effective in eliminating a slack/taut tether oscillation. The bottom half of Figure 1.5 presents a time history of tension in the tether, and the yaw angle of the spacecraft relative the target vehicle. It can be seen that the tether tension was strongly affected by damping.

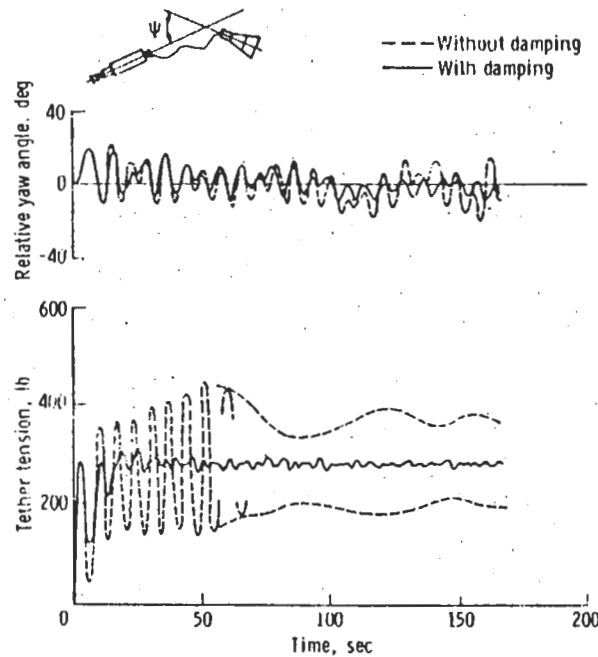


Fig. 1.5 Effect of Damping on the Oscillation of Tethered System[Ref. 3]

The Gemini XII flight experiment was launched on 11 november, 1966. Gemini XII studied the feasibility of gravity gradient stabilization. The system was initialized by various translational and attitude thruster maneuvers by the spacecraft. This was followed by an active stabilization of the target vehicle using the target-vehicle attitude control system. The proper starting conditions consisted of a slightly taut tether, initial alignment along a local vertical, approximately circular orbit, and a relative velocity of 0.138 ft/s for a 100 ft tethered spacecraft/vehicle combination. Figure 1.6 illustrates typical result obtained from the point mass analysis on the sensitivity of the system motion to initial relative velocity between the point masses. The main requirement was that the initial orientation be vertical. The result of this experiment for gravity gradient stabilization were that with a properly functioning control system operated by the crew, the initial conditions necessary for the tethered system could be accomplished with relative ease. The gravity-gradient stabilization orientation was successfully demonstrated in Gemini XII.

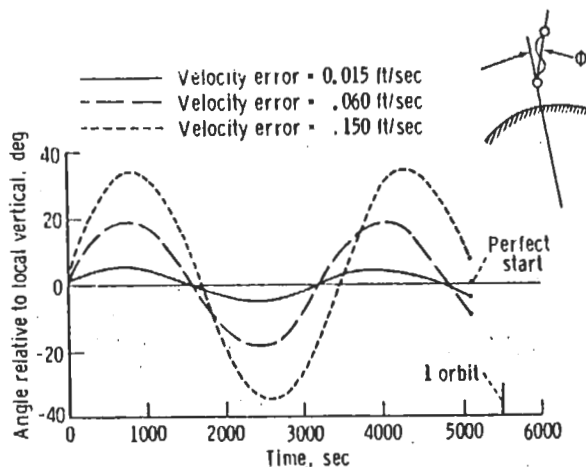


Fig. 1.6 Effect of Relative Velocity on Motion of Gravity-Grad[Ref. 3]

This concept has evolved into the set of Tethered Satellite System experiments. Electrodynamic applications will be tested with the upward-deployed

TSS-1 experiment for the first shuttle borne tether experiment. The general areas of current interest include scientific experimentation, transportation applications, tethered platforms, and propellant storage and transfer. Tether shows particular promise for resolving the problem of de-orbiting in wasting mass from the space station—a task shuttle will not be able to meet. Many of these areas are now receiving serious attention, and the concepts are progressing from the initial idea generation stage to the detailed analysis and proof-of-concept testing stage.

There is a gravity gradient for a vertically aligned tether system. The lower satellite experiences a greater gravitational force than the higher one, which causes tension on the tether. In an experimental or operational system, the tethered vehicles require proper starting conditions so that subsequent motions will be limited in amplitude. In particular, it is desirable that oscillations of the system about local vertical be limited in amplitude. Once the system is properly established, a number of electrodynamic applications are possible.

## B. ELECTRODYNAMIC TETHERS

### 1. Basic Concept

A tethered payload system in which two separate payloads in space are connected with an insulated conductive wire forms an electrodynamic tether. Electrodynamic tethers make use of interactions between a moving conductor (the tether wire), the earth's magnetic field, and the ambient plasma for propulsion and braking, power generation, science and communications.

A  $(\mathbf{v} \times \mathbf{B}) \cdot \mathbf{L}$  potential difference develops across the tether due to its motion through the geomagnetic field. In order to generate electrical power or thrust electrical contact must be made with the ambient plasma at each tether end to close the circuit to the environment. The tether circuit is made complete by conduction of electrons along B-field lines in the environment.[Ref. 5]

Figure 1.7 shows the electrodynamic tether system with electrodynamic drag. Typical ionospheric values, for an orbiting system, result in induced voltage of several kilovolts for a 5–10 km system.

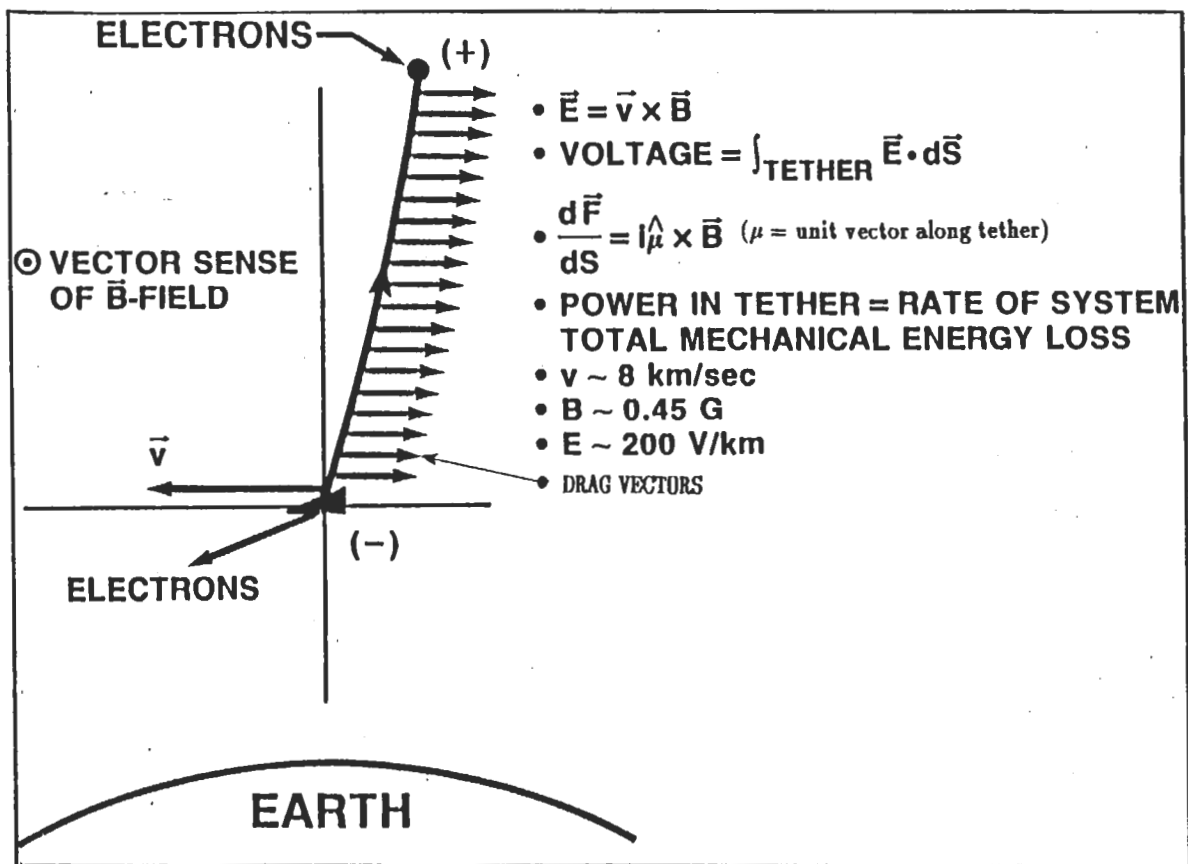


Fig. 1.7 Electrodynamic Tether System [Ref. 5]

Typical ionospheric densities of  $10^4$ – $10^6$  electrons/cm<sup>3</sup>, and collecting areas of a few square meters, suggest that currents of a few amperes can be collected, to give a net power of kilowatts. Of course, this requires that electrons be emitted at the same current level at the opposite end of the tether.

## 2. Electrodynamic Tether Applications

A number of possible applications exist. By applying a voltage between two payloads connected with a conductive wire, the response of ionospheric plasma

to potential differences between collector and plasma can be studied. By regulating the current collected (emitted) at the ends, the tether current can be controlled. By modulating the tether current, low frequency radio waves with long wave length such as Whistler and Alfvén modes, can be excited.

An electrodynamic tether system can be used for electrodynamic propulsion and braking by using the interaction force between the tether electrical current and the ambient magnetic field. In principle it can be applied as an electrical power generator up to MW level. In this (braking) mode, the kinetic energy lost by the orbiting system is converted to electrical energy. For ionospheric science, an electrodynamic tether system can be used to induce controlled, large-scale perturbations which can be tracked and measured.

### 3. Tether Experiments

Besides the early Gemini experiments, relatively few experiments have been conducted. The major planned experiment is TSS-1 which is described next.

#### a. **Tethered Satellite System-1 Experiment**

Space shuttle engineering tests of the space tether concept are planned for the early 1990s using the tether satellite system which is being developed jointly by Italy and the US. The TSS goal is to test the feasibility of deploying, controlling and retrieving a tethered satellite from space shuttle, as well as to demonstrate the system's usefulness for scientific research. The TSS will provide a unique, reusable facility for conducting research based from the Space Shuttle and for conducting proof-of-concept demonstrations of tethered satellite systems in space.

TSS-1 mission, planned now for late 1992, will be an engineering verification flight. It will also perform limited electrodynamic science. Figure 1.8 shows the configuration of TSS-1 satellite system in space. A 20 km-long

electrically conductive tether will be deployed above the shuttle (spaceward) to study the electrodynamic properties of the ionosphere as well as conduct plasma physics experiments.

This mission will test the feasibility of generating electricity with the insulated conductive tether. This process could be an important source of power for future spacecraft and space station. As the shuttle moves in earth orbit, the tether will cut through the planet's magnetic field and interact with the ionospheric plasma.

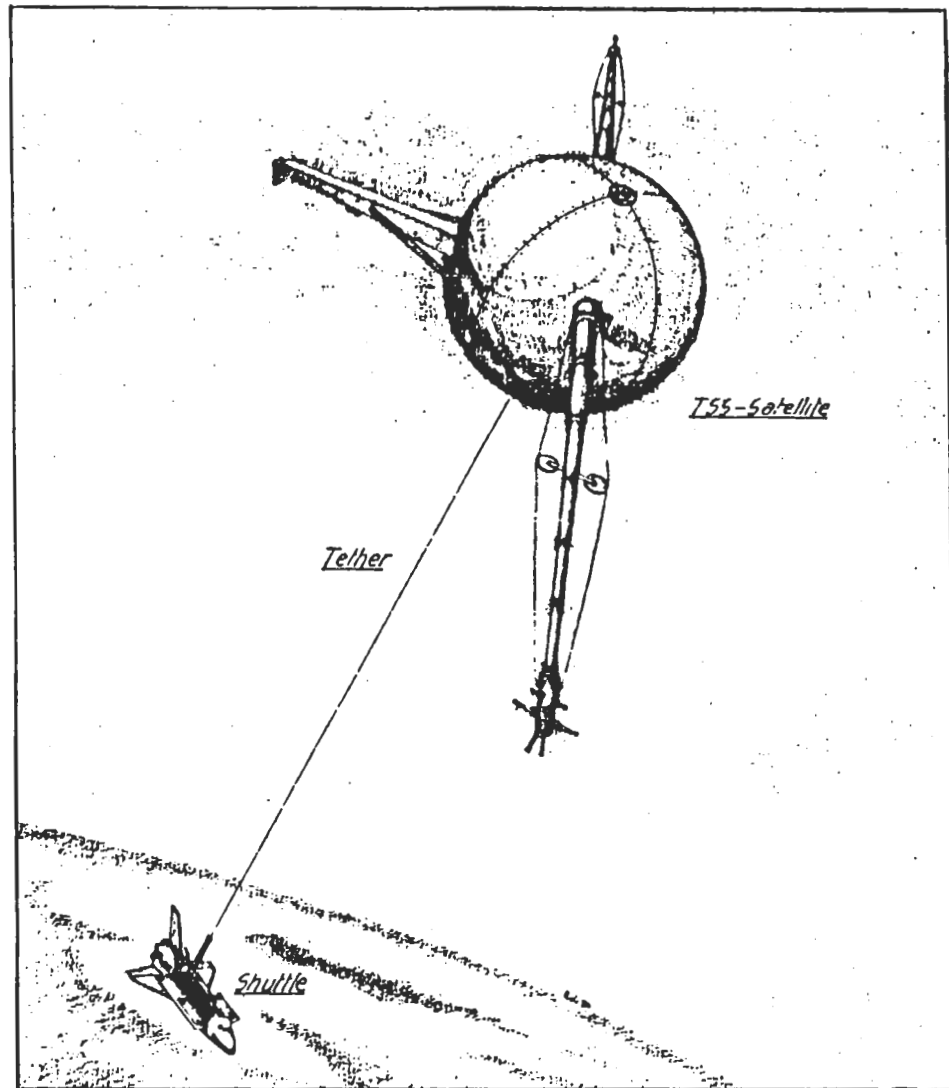


Fig. 1.8 TSS-1 Satellite System [Ref. 6]

The electrically positive deployed satellite will collect electrons from the ionosphere. These will be emitted back into space by an electron gun or plasma source on the shuttle orbiter. This causes a net current to flow upward through the conductive tether. The intended current is 0.75 A, voltage of up to 3 kV, for a power of a few kW. The tether resistance is about 0.2  $\Omega$ /m which will limit the conducted current in the 20 km cable to the above values.[Ref. 6]

**b. US–JAPAN Charge Rocket Experiment**

Tethered sounding rocket experiments have been underway since 1980 as part of a joint US–JAPAN program (Tethered Payload Experiment; TPE). Its objective is to obtain technical and scientific data in support of the space shuttle electrodynamic tethered subsatellite experiments on the space shuttle Tethered Satellite System–1 mission. The goal of the rocket program has been to perform active plasma experiments, by ejecting an electron beam from the tethered mother–daughter payload system. In the third and fourth rocket flights, the conductive tether wire was successfully deployed more than 400 m. Figure 1.9 shows the payload configuration of the fourth Tethered Payload Experiment. These latter payloads have been dubbed charge 1 and charge 2.

The electron gun generated a narrow electron beam of 1 kV, 80 mA in DC and multi–pulse modes. The floating/Langmuir probe array consisted of 4 cylindrical probes installed on a rod every 25 cm. Two 35 mm cameras with high sensitivity color film were installed. One was operated synchronized with the beam firings to observe the beam trajectory. Another was synchronized with flashing of a strobe light to illuminate the reflective tape attached to the daughter rocket.

Two photometers filtered at 3914  $\text{\AA}$  were used to detect the light emission from the interaction of the electron beam with the atmosphere and the charge sheath around the rocket surface. The charge probe was installed to apply a

high voltage up to 500 V between the two payloads. The deployment system was installed on the daughter payload with deployment monitoring system of 0.1 m resolution.

It was found that the tether wire acted as an antenna. Current in the tether wire apparently resulted in the generation of waves in the MHz frequency range. Vehicle charging due to beam emission up to 80 mA was repeatedly measured in the series of the experiments. Beam energies up to 500 eV were used. The 80 mA emission experiments displayed clear evidence for the ignition of a beam plasma discharge, as measured by photometers and wave receivers.[Ref. 7]

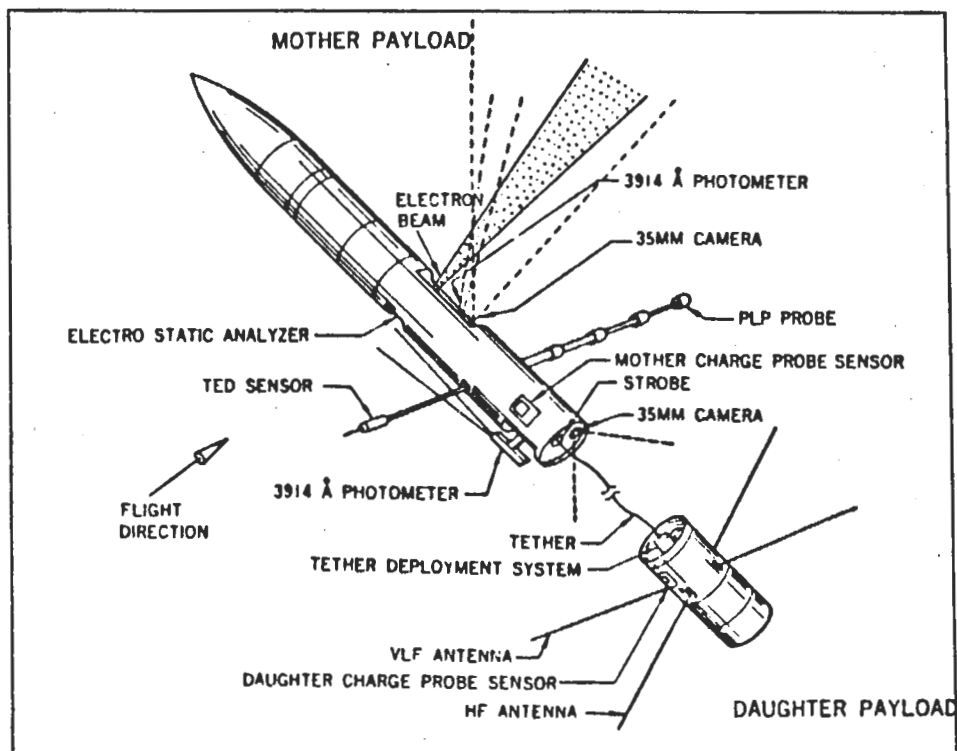


Fig. 1.9 Payload Configuration of fourth TPE Experiment[Ref. 7]

### c. MAIMIK Rocket Experiment

The "mother-daughter" payload Maimik was launched out of Andoya Rocket Range November 10 1985 on Terrier/Black Brant VC rocket motor.

The two payloads were connected by a tether, and the "daughter" payload carried an accelerator which emitted pulse of electrons at energies of approximately 8 keV. The main aims of this program were to study the interactions between the electron beam and the environment for various boundary conditions, to conduct studies of various physical processes have been conducted, including plasma modifications, wave generation, and optical excitation studies, and to study the physical processes associated with the neutralization of electrically charged vehicles in an ionospheric plasma. It was launched when the geomagnetic conditions were exceptionally quiet which eliminated the need to disentangle artificial from natural processes and during the period with very low background plasma density.

In this experiment, the tether wire was to be cut on the mother and daughter payload independently. Apparently, the tether was cut on the daughter 112.6 sec after launch at an altitude of 192 km. The wire was cut in conjunction with the injection of an 800 mA electron pulse, and the daughter may have charged to a very high potential due to this pulse. The early squib firing may have been due to arcing on the daughter.[Ref. 8]

The daughter payload was charged to several kilovolts every time the beam current was equal to or higher than 80 mA. This result apparently differs from previous sounding rocket experiments, such as the ECHO series. This suggest that electron collection at altitudes near (or above) 200 km, is not as effective as previous experience suggested. This may indicate improper analysis of the results of earlier experiments, and probably indicates the need for improved plasma contactors.

## C. PLASMA CONTACTORS

### 1. Basic Concept (Requirements and Future Mission)

The ongoing need to establish electrical contact between satellites and the ambient plasma environment has resulted in studies of devices generically termed "PLASMA CONTACTORS" which enable low impedance electrical contact with the ionosphere. This type of device is needed for bidirectional electric current operation of an electrodynamic tether and stable spacecraft electric reference potentials.

A plasma contactor might be a large conducting surface, such as an aluminized mylar balloon. Charged particle emitters such as electron and ion guns are traditionally thought of in this context. Neutral gas releases can produce enhanced levels of conductivity. The most effective techniques typically utilize neutral plasma emission.

Plasma contactor performance can be characterized by plotting the contactor current versus the contactor potential measured relative to the local space plasma. Ideal performance is approached if the effective collecting area (for the appropriate species) is equal to or greater than the associated tether current divided by the ambient space current density ( $N_e \sqrt{KT/m}$ ). The collecting area can be physical, or simply the enhanced plume area of a plasma source or neutral gas cloud.

Plasma sources have been extensively studied for the purpose of active charge control. The need for charge control technology has been apparent since the early 1970's, when it was recognized that satellite charging at geosynchronous orbit reached kilovolt levels, and that such charging might be related to satellite failures. In this regime, current levels of microamps are typically found.[Ref. 9]

The European Space Agency CLUSTER spacecraft scheduled to be launched in the mid-1990's will have conducting surfaces so that the behavior of

their potential should be similar to that of the GEOS and ISEE spacecraft. The GEOS and ISEE experience has been that the potential is determined by the balance between photoelectron emission and ambient electron collection as long as the spacecraft is outside the plasmasphere and in sunlight. In order to reduce expected positive potentials of 5–10 V to near zero, a liquid–metal ion gun is included part of the payload. Currents of 10–20  $\mu\text{A}$  will be emitted at 7 kV. Indium ions are emitted from needle shaped sources in this design as shown in Figure 1.10.[Ref. 10] The Liquid Metal Ion Source (LMIS) is suited for formation of microfocused ion beams and has wide application in microelectronic technology. This method has advantages of low power consumption, high mass efficiency, compactness and low mass. Unfortunately, it is unipolar, that is, it only emits positive charge.

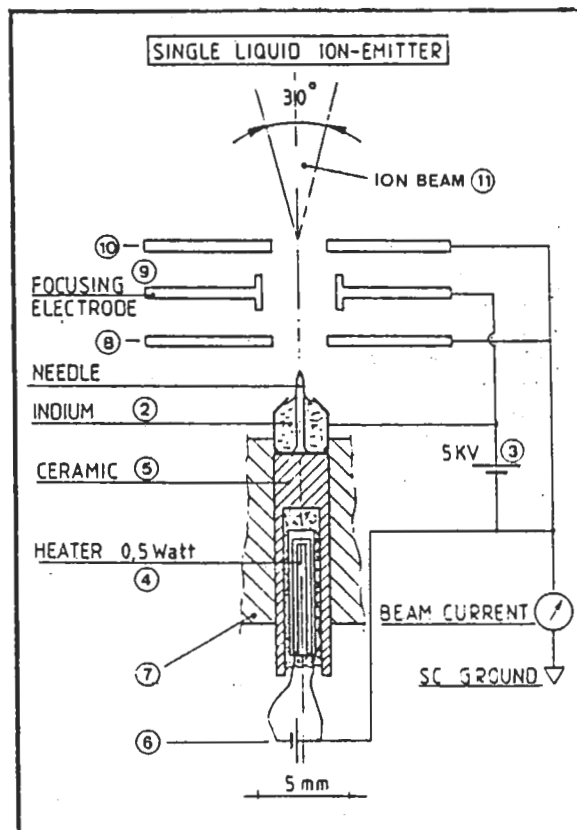


Fig. 1.10 Individual Liquid Metal Ion Emitter [Ref. 10]

The scientific objectives of many sounding rocket active experiments have been to study the propagation of plasma beams through the ionospheric plasma in the presence of the earth's magnetic field. Recent interest has been stimulated by active experiments on the space shuttle orbiter, such as the former SPACELAB payload, SEPAC, a large electron gun experiment(1A, 10 kV), which will be reflown as part of the ATLAS payload.

The 1983 SEPAC experiments included large positive potentials on the shuttle orbiter. To prevent such charging, net positive (e.g. ion) currents of ampere or more are desired. This would allow the fundamental mission objective of transmitting an electron beam through the ionosphere to the top of the atmosphere to be achieved. The joint Italian–American Tethered Satellite System (TSS–1) is scheduled for a late 1992 flight on the shuttle orbiter. In the case of TSS–1, plasma sources are needed to collect and emit the estimated 1 A current which will flow along the tether wire to the orbiter.

It is anticipated that charge control technology will be needed for the space station, particularly if active plasma experiments are to be conducted from that platform. Orbital systems which emit large fluxes of charged particles presently being considered for defense purposes will also require this technology.

## 2. Plasma Contactor Flight History

### a. **Balloons**

The free space capacitance of a typical rocket payload is so small that ejection of even a 1 mA beam will charge the vehicle to more than 10 kV in less than 1 msec. Consequently, if the electron beam current is not neutralized by ejection of an equal positive ion current, sustained ejection of electrons will require the collection of an electron return current through the ionosphere plasma.

The assurance of an adequate collection of return current can be addressed by deploying a large collecting surface. For this purpose, a large inflation-deployed electron collection screen was developed and fabricated for the first US rocket-borne electron accelerator experiment. The experiment carried electron guns capable of up to 490 mA at 9.5 keV. This artificial aurora experiment was launched on an Aerobee 350 from Wallops Island in January, 1969. The rocket payload included an aluminized mylar disk, 26 m in diameter, with an inflatable hub and rim and four inflatable spokes. The collector is illustrated in Figure 1.11. The deployment was apparently incomplete, due to a malfunction in a pressure regulator. Nevertheless, the technique was at least partially successful.[Ref. 11]

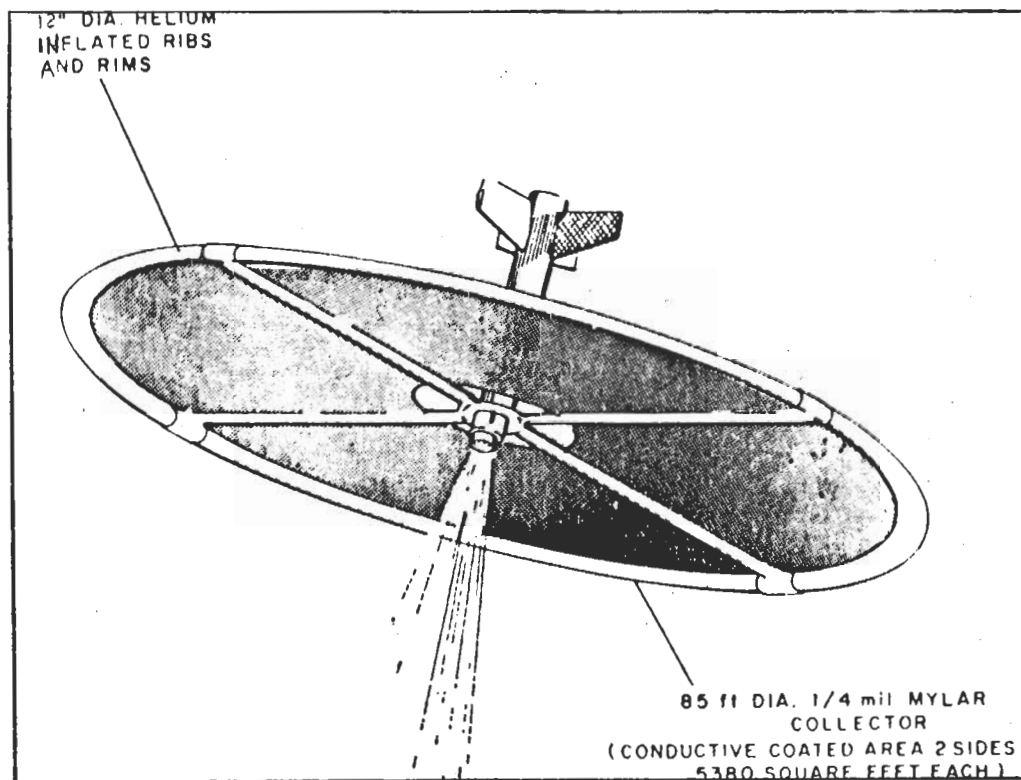


Fig. 1.11 Collector Screen in the Deployed Configuration[Ref. 11]

ECHO 1 was launched on 13 August, 1970. This experiment apparently showed that the conducting rocket body could collect a sufficient return current for beam neutralization without a special collector disc or other devices.[Ref. 12]

## b. Electron Gun

Electron guns are a primary form of a plasma contactor. Electron guns have been used in space at current levels from microamperes to amperes. Examples of flight experiments are as follows:

The first was the above mentioned Artificial aurora experiment. This experiment was a first feasibility test in the development of a system for the study of magnetospheric field configurations through the controlled injection of monoenergetic electron beams on to magnetic-field lines. Energies up to 9.5 keV and beam currents up to 490 mA were used. In this experiment, the vehicle neutralization was accomplished by collecting an ionospheric current using aluminized mylar foil deployed perpendicular to the magnetic field.[Ref. 11]

In the ECHO series of sounding rocket experiments, electron guns with energies of 40 kV and current levels of 100 mA and above have been used to study magnetospheric plasma phenomena. Beginning with ECHO I, it was found that sufficient beam electrons escaped to the top of the atmosphere to generate an artificial aurora. In this sense, the 'contactor' was adequate to couple 10's–100's mA to the environment.[Ref. 13]

Space Experiments with Particle Accelerator (SEPAC) was designed to perform an active experiment in space by ejecting a high power electron beam up to 5 kV, 300 mA (e.g. kilowatt power) from shuttle orbit. It apparently failed in this function, due to shuttle charging, and the occurrence of a beam plasma discharge, which disrupted the beam.[Ref. 14]

A second (French) payload carried on the same spacelab mission was dubbed PICPAB. This lower power electron gun (10 mA, 8 kV) was designed to study wave generation. Diagnostics were inconclusive, but appear to indicate the beam resulted in low potentials, and hence the beam escaped.[Ref. 15]

A series of the US/JAPAN tethered rocket experiments used electron guns of 1 kV, 80 mA in DC and multi-pulse modes as described previously. The CHARGE rockets have been at least partially successful in propagating beams away from the vehicles.

The MAIMIK experiment used an electron gun with 1–3.2 kV and 20–800 mA. The MAIMIK experiments, were also successful. These experiments resulted in some observations indicating that the vehicle charged to near or above beam energy, however, limiting the emitted current. In fact, it appears that a virtual cathode formed, and only 1–10 % of the beam escaped. The escaping electrons were accelerated to 110–120 % of the beam energy.

The ATS–5 filament neutralizer was used as an electron emitter at microampere current levels at geosynchronous orbit. ATS–5 electron emitting operations succeeded in reducing the magnitude of the negative eclipse charging potentials on the satellite, However, the spacecraft was rarely discharged completely. This was the result of differential charging on the satellite surface limiting the emitted current.

This means that on high altitude satellites with substantial portions of the satellite covered with insulators, electron emitters are generally ineffective as plasma contactors. SCATHA experiments used an electron gun at levels ranging from 1  $\mu$ A to 13 mA, and from 50 V to 3 kV. SCATHA experiments showed that even with high energy beams differential charging prevented beam emission.[Ref. 16]

### c. Neutral Gas Releases

The injection of a plasma or a neutral gas is one way to neutralize the spacecraft. The mechanisms which are important are those which result in substantial ionization of the neutral gas cloud. This may be due to the beam itself,

the return (collected) electron flux, or perhaps even secondary electron emission from the vehicle surface. Under some conditions, it is believed that as the ionization process proceeds, electrostatic waves are set up, which increase the ionization rate, instigating a Beam–Plasma Discharge (BPD).[Ref. 17]

Neutral gas releases were used on ECHO I. No direct evidence of effective vehicle neutralization was obtained. Indeed, the ECHO I results have been traditionally interpreted with the thought that the rocket body provided adequate return current collection. ECHO IV experiment considered again the effect of a neutral gas release. The 40 kV, 80 mA beam was fired through an N<sub>2</sub> plume which had densities were obtained by means of a photometer calibrated at 3914 Å. The return current was enhanced by the neutral N<sub>2</sub>. [Ref. 18]

Possible occurrences of BPD during sounding rocket experiments are described by J. R. Winckler. The BPD conditions are that:

$$I_c = C \frac{V^{1.5}}{B^{0.7}PL} \quad (1)$$

where V is the accelerating voltage, B the magnetic field, P the pressure and L the scale length of the experiment. Since beam perveance is generally of the form  $I \propto V^{1.5}$ , it is clear that beam perveance determines the occurrence. Winckler concludes that BPD has been observed.[Ref. 19]

This technique was also used in the SEPAC experiments with beam energy of 2.9 keV and current of 200 mA. The neutral gas plume (NGP) emitted 10<sup>23</sup> molecules of nitrogen (N<sub>2</sub>) in a 100 ms pulse. The gas release resulted in a neutral gas pressure increase in the shuttle bay, from 10<sup>-6</sup> Torr to 2 – 3×10<sup>-6</sup> Torr. This technique was apparently successful, but appears to have involved substantial interactions with the ambient neutrals and plasma. One curious aspect

of these experiments was that the 8 keV, 10 mA PICPAB beam did not result in substantial ionization of the emitted neutrals. This may be related to the relatively low shuttle potentials induced by PICPAB ( $\sim +10$ ).[Ref. 20] There is substantial disagreement in the literature over occurrence of BPD in the SEPAC experiments.[Ref. 21]

#### d. Ion Beams

A non-neutral ion beam is a form of plasma contactor. The ARCS series experiments used Argon ion beams to study the electrodynamics in the ionosphere. A 100 mA, 25 eV Ar<sup>+</sup> ion beam was used on experiments beginning with a sounding rocket ARCS-1, launched on 27 January, 1980. Electrons were observed to be accelerated toward the beam emitting payload during ion beam operations. This effect was ascribed to the creation of an electric field parallel to the geomagnetic field. There also appear to have been substantial electron heating, apparently due to wave turbulence associated with beam operations.[Ref. 22]

ARCS-3 was launched on 10 February, 1985. This experiment showed that the injection of particles parallel or perpendicular to the geomagnetic field consistently resulted in the appearance of a population of ions at low energy ( $\sim 15$  eV) and at 90° pitch angle. These ions apparently are scattered out of the beam. These experiments indicate that the sounding rockets are able to draw neutralizing currents to the beam and rocket via complex processes which accelerate and thermalize the ambient plasma. It appears that the beams do escape.[Ref. 23]

Another form of ion beam is ACED (Accelerator with Closed Electron Drift). ACED was initiated in the United States but appears to have been abandoned in the mid-60's. Subsequently, it was taken up in the USSR. An ACED thruster was used to adjust the near synchronous orbit of one of the "Meteor" satellites. The ACED ion beam source delivered 4 A of Xenon ions at 200 eV.[Ref. 24]

It was supplied by the Soviet participants for the West–German "Porcupine" program of rocket experiments in the auroral ionosphere. Porcupine rockets F3 and F4 were launched in March, 1979 from the European Space Research Range. The Xenon ion beam was injected perpendicular to the ambient magnetic field into the collisionless ionospheric plasma at altitudes ranging from 190 to 450 km. These experiments showed that the beam propagated nearly undistorted across the plasma. The beam was not current neutralized.[Ref. 25]

**e. Ion Engine**

An ion engine is a device which combines an ion beam with a charge and current balancing electron source. There is generally little net current. The first major ion engine flight experiment was ATS–4 launched on August 10, 1968. ATS–4 was intended to be a geosynchronous satellite but the booster failed to achieve a second burn. ATS–4 remained attached to its Centaur Stage booster, and remained in a low parking orbit. In spite of this failure, a number of successful ion engine tests were run. Two ion thruster systems were on board, and a spacecraft potential monitor that employed one of the gravity gradient booms as a Langmuir probe.[Ref. 26]

The boom was deployed prior to the last of five ion engine test periods. The large ram ion currents available from the relatively dense ambient plasma (altitude 218 to 760 km, density  $10^{10}/\text{m}^3$ , ambient pressure  $10^{-9}$ – $10^{-6}$  Torr, current  $330 \mu\text{A}$ , spacecraft potential  $-132 \text{ V}$ ) precluded the achievement of appreciable neutralizer emission current except for a few brief periods. With the exception of the emission limited behavior of the neutralizer during test 5, both ion engines performed normally in all respects. Particularly gratifying were the complete absence of detectable electromagnetic interference, and the lack of arcing.

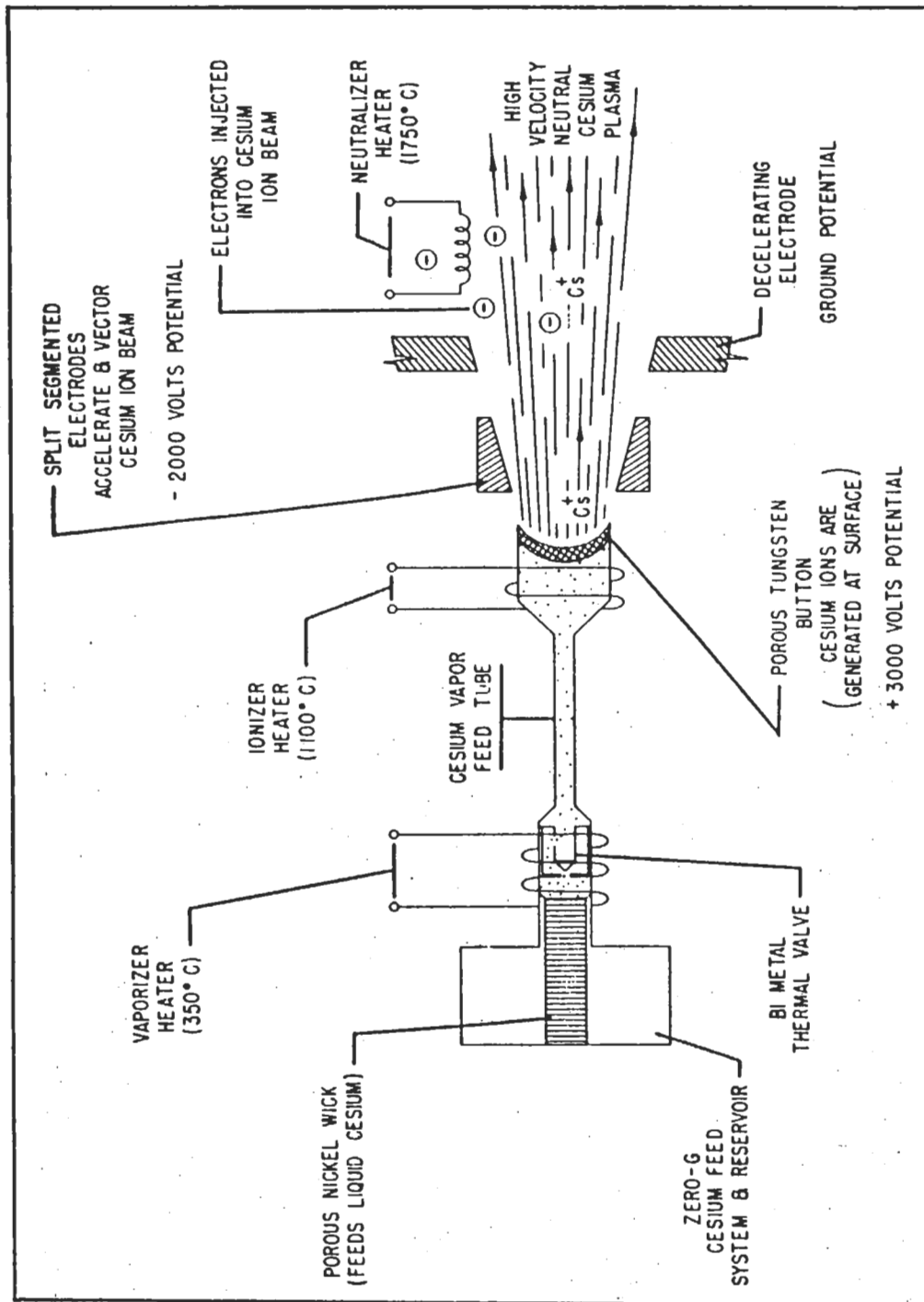


Fig. 1.12 Configuration of ATS-5 Ion Thruster[Ref. 16]

ATS-5 carried a cesium contact ion engine and filament neutralizer. ATS-5 was launched into synchronous orbit on August 12, 1969 and stationed at 105 ° W longitude. Again, there was a launch failure. ATS-5 was to be gravity gradient stabilized, but ended up spinning at 100 rpm. The ATS-5 ion engine is shown in Figure 1.12. The ion engine worked well in spite of the spin problem. Coupling potentials of less than 50 V resulted from engine operation. Induced charging experiments (no neutralization) with the ion beam in sunlight resulted in induced charging to near the beam energy. These experiments indicate the effectiveness of neutral beam emission.[Ref. 16]

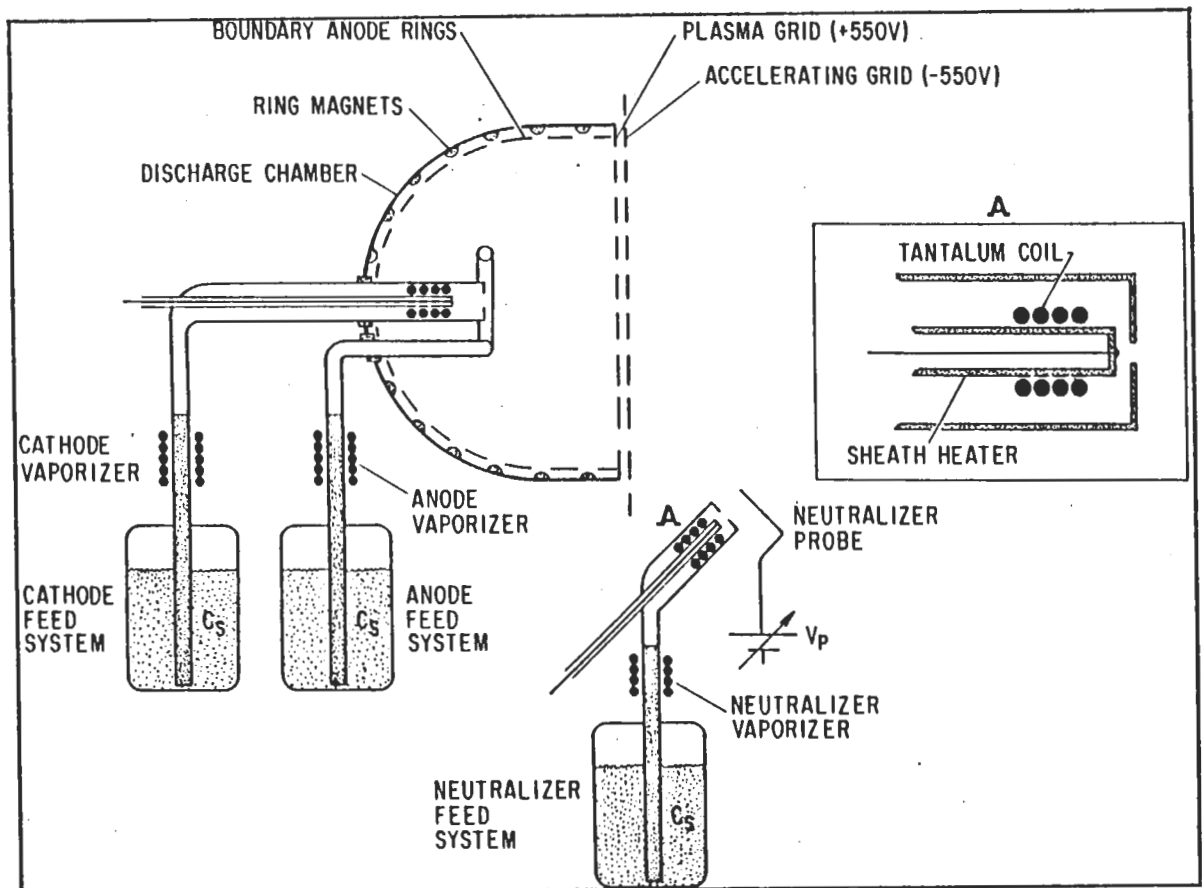


Fig. 1.13 Configuration of ATS-6 Ion Engine[Ref. 16]

ATS-6 carried twin cesium thrusters designed to test ion engine technology and their usefulness for stationkeeping on the three-axis-stabilized

satellite, It was launched in 1974. Figure 1.13 shows the ATS-6 ion engine schematic with neutralizer. ATS-6 engine operations were successful, and had the beneficial side effects of discharging the mainframe and all differentially charged surfaces. The plasma bridge neutralizer alone could also discharge large negative potentials in sunlight or eclipse. A 92 hour operation of the ion engine at 160 mA, 3 kV was successfully conducted.

A geophysical rocket was used to launch an automatic ionosphere space-flight laboratory (SFL). Experiments with this rocket were conducted by the USSR in November, 1969 and August, 1970. These experiments made use of an ion engine using surface ionization of cesium on tungsten to study the operation of the various systems of this engine. The maximum value of the ion beam current was 100 mA (240 sec) and the effective accelerating voltage was about 2400 V. The magnitude of the potential was about -1700 V and the thickness of the space charge layer surrounding the SFL was about 7 m.[Ref. 27]

SERT-II (Space Electric Rocket Test II), carrying dual 15 cm diameter mercury electron bombardment ion thrusters, was launched on February 3, 1970 into a polar, sun-synchronous orbit at 1000 km altitude. The primary purpose of SERT-II was a long duration (6-month) test of a mercury ion thruster. A secondary objective was investigation of the interaction between the ion thruster, the spacecraft, and the ambient space environment.[Ref 28]

Emissive probes flown on the SERT-II spacecraft in conjunction with the prime ion thruster experiment allowed an investigation of the interaction between the spacecraft, the ion thruster, and the ambient space plasma. One thruster operated for 5-months and the other operated for 3-months. Both thrusters failed due to sudden shorts between the high voltage grids. It was determined that the cause was sputtering of grid surfaces. The specific impulse was

about 4200 sec, and thrust was a 28 mN for a thruster input power of 850 W. The main objectives were largely reached. The engines were operated at 253 mA, 3 kV for 600 hours. They demonstrated thrust, and an absence of harmful interactions with the vehicle.[Ref. 29]

The mean SERT-II spacecraft equilibrium potential with the engine off was  $-6$  to  $-8$  V. This relatively high negative potential was due to the presence of exposed solar array interconnections at high positive potentials (36 Volts). The space probe measurements indicated that photoemission had no detectable effect on spacecraft potentials. It was possible to control the potential difference between the spacecraft and the space plasma, using the neutralizer bias. This effect could be used to minimize electrostatic influence on the space plasma of an ion thruster bearing spacecraft. The ion beam neutralizer potential difference was constant for all neutralizer biases (with respect to the spacecraft ground) with a constant neutralizer emission current.[Ref. 30]

In 1973, new goals were added for the still functional SERT-II spacecraft which included, i) demonstration of thruster restability after long space storage, ii) study of factors limiting thruster restarting, iii) demonstration of the space lifetime of thruster system components, such as propellant feed systems, closed loop control systems, insulator shields, and power processor units, iv) measurement of main solar array degradation after years of space exposure, and , v) verification of the compatibility of the spacecraft system with sustained thruster efflux. Minor components of the spacecraft had failed, but this did have not interfere with the functional status of the spacecraft. The short between the engine grids removed itself, apparently due to mechanical stress.[Ref. 31]

In 1974, the spacecraft was placed into a spin-stabilized mode in order to be ready for the next period of complete solar-array illumination. In 1979,

additional goals were added : 1) demonstration of steady state operation of an ion thruster system 9 years after launch, 2) measurement and comparison the performance of this aged thruster with that of a new thruster, and 3) long term operation of the ion thruster system to determine its life limiting factor. Again, the engines worked well after 9 years in orbit. During the first quarter of 1979, thruster 2 was operated for nearly 600 hours at 85 mA beam current. The performance of the thruster was found to be unchanged in the 9 years. The spacecraft remained functional and had only experienced minor failures of a battery in the telemetry system and the loss one of one tape recorder.[Ref. 32]

Of particular interest are the plasma contactor aspects of the SERT-II experiments, particularly the beam neutralization. The SERT-II neutralizers were hollow cathode, plasma bridge neutralizers. Figure 1.14 shows a

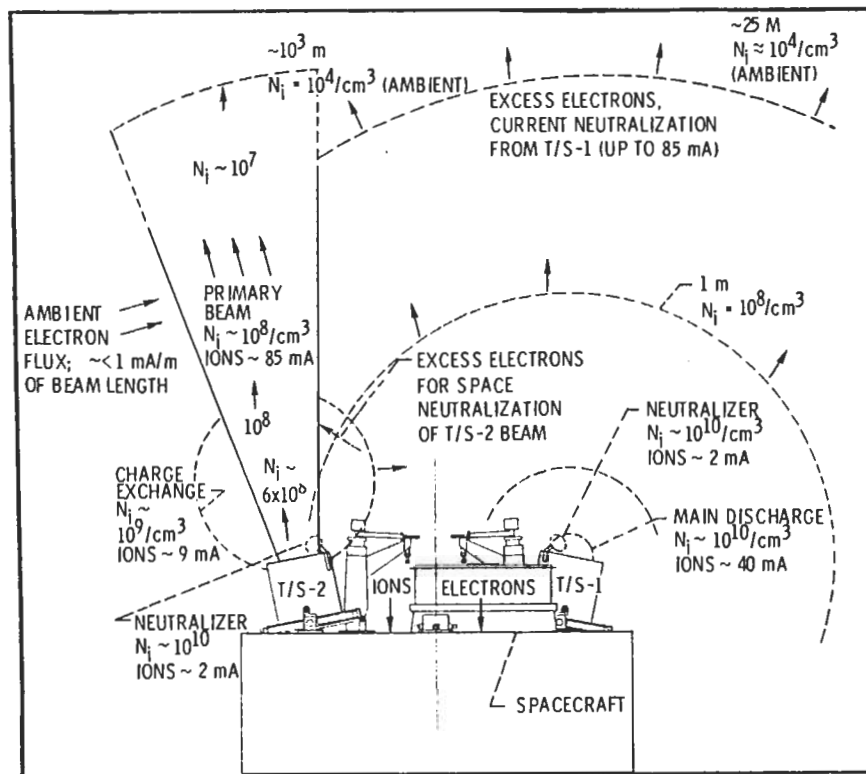


Fig. 1.14 Spacecraft Plasma Current Diagram of SERT-II[Ref. 33]

spacecraft plasma current diagram of SERT-II experiment. Operation of the two SERT-II thrusters with one grounded and the other biased positive permits a comparison of flight data with theoretical coupling characteristics. Experiments in beam neutralization were conducted. A plume penetration model was developed which showed qualitative agreement with flight data. The average of the total neutralizer emission of SERT-II data was 72 mA. The SERT-II neutralizer currents with negative neutralizer biases were up to about twice the theoretical predictions for electron collection by the ground screen.[Ref. 33]

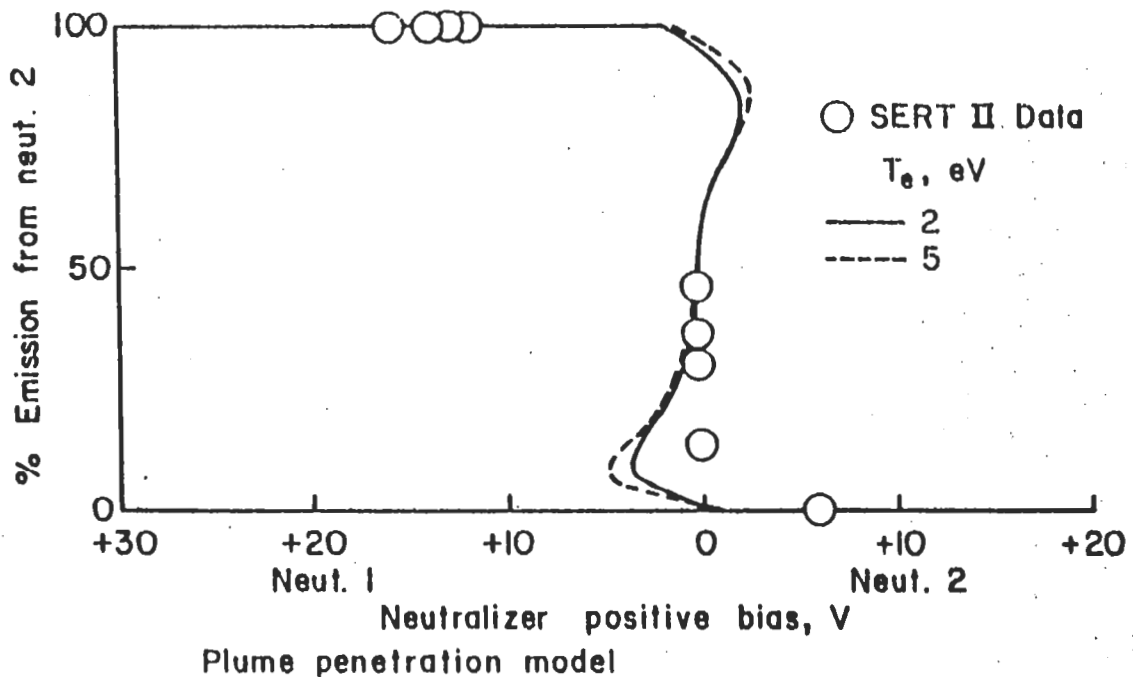


Fig. 1.15 Distribution of Emission Currents[Ref. 34]

Figure 1.15 shows the shift in neutralization current between the two neutralizers for various positive biases for plume penetration model. One thruster (No. 1) was in discharge only mode and the other was in normal operating mode (HV on). The discharge only thruster emitted sufficient discharge-chamber electrons to neutralize the associated ion beam. The experimental data show a shift

from neutralizer 2 emission at a neutralizer 1 bias of 12–16 V to all neutralizer 1 emission at a neutralizer 2 positive bias of 6 V.[Ref. 34]

The data from SERT–II experiment indicate that a hollow cathode provides large electron emission capability and it only takes a few volts to extract currents of 0.1 A. The data also indicate that an ion beam in space need not be neutralized by a physically close electron source. Electrons may be emitted 1 meter away between the electron source and the ion beam. The neutralizers of the SERT–II thrusters were operated negative of the spacecraft showing large excess neutralizer currents. Figure 1.16 show excess neutralizer emission as a function of negative neutralizer bias for normal operation. It indicates that a significant electron current to the ground screen may exist in the absence of a negative neutralizer bias (5 eV).

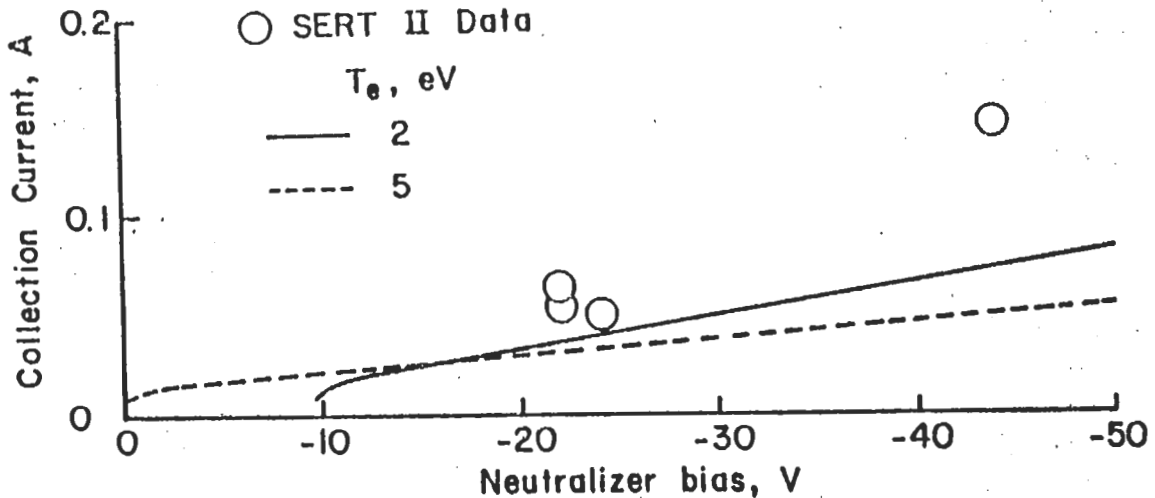


Fig. 1.16 Excess Neutralizer Emission[Ref. 34]

A modified form of an ion engine is the MPD arcjet. Essentially an magnetoplasmadynamic arcjet is a hollow–cathode discharge source, in which an arc is struck between a cylindrical rod anode on the axis, and a hollow cylindrical cathode forming the outer wall of the device. A strong azimuthal magnetic field

created by current flowing along anode yields the propulsive force along the axis which is proportional to the square of the current. Thus an MPD arcjet works best at high current because it expels much neutral gas along with the jet of plasma. A MPD arcjet was used to neutralize the SEPAC electron beam Spacelab-1. It differs from the designs flown on the SERT and ATS series in that it does not produce a continuous current. The SEPAC arcjet generated  $10^{19}$  argon ion-electron pairs, during a 1 ms pulse. The neutralization effect persisted for tens of milliseconds. The main features of this neutralization have been explained by existence of a cold secondary plasma near the orbiter. The cold secondary plasma was produced by charge exchange processes between the released neutral gas atoms and injected high speed plasma ions. This result suggested that the production of plasma that will remain near a vehicle will effectively neutralize the charged spacecraft. This limits the usefulness of this design as a plasma contactor.[Ref. 35]

#### f. Hollow Cathodes

One successful form of a plasma contactor is the hollow cathode. Hollow cathodes are effective sources of dense, low energy (1 eV) plasma. They are particularly effective as low impedance electron sources. The original satellite use for hollow cathode technology was in association with ion engines. In this application, hollow cathodes are utilized as electron sources inside ion engine discharge chambers, and as electron emitters to balance the charge and current contained in the emitted ion beam. They have worked well in this regard on the SERT-II and ATS-6 missions.

Hollow cathode technology has been extensively considered for the purpose of charge (potential) control on satellites. Hollow cathodes operating at low current levels (microamperes) were effective in controlling satellite charging at high altitudes (geosynchronous orbit).[Ref. 36]

Hollow cathodes have been operated as high current sources (100 mA) in association with the SERT-II ion engine experiments as described in the previous section.

#### **D. PROPOSED EXPERIMENT**

We propose to test hollow cathode technology for application as plasma contactors, using a tethered system, deployed from a sounding rocket.

In this study, deployment systems of different tethered rocket experiments will be investigated in order to choose a proper deployment system for the hollow cathode rocket experiment. Modeling of tethered deployment system will be studied using the numerical integration method. This modeling work will be compared with our experimental configurations.

## II. TETHER DEPLOYMENT

### A. BASIC DYNAMICS

The dominant tether dynamic behavior, when tip masses are present, is the rigid-body in-plane libration. If we assume that the tether is massless, then the system behaves as a dumbbell subject to only trajectory dynamic effects. The geometry is shown in Figure 2.1. The tether length  $l$ , is allowed to vary as a controlled function of time, since the deploying rate will be used as a control input for precise positioning of the tether tip.

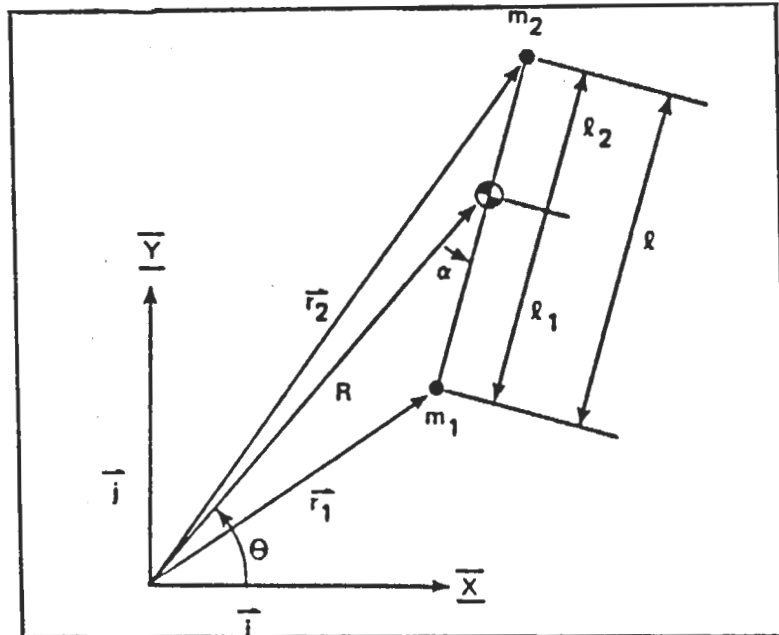


Fig. 2.1 Dumbbell Tether Model

The nature of the tether dynamics suggests two different control inputs. The first is tether reeling acceleration. This can be used to achieve the desired tether length and reeling rate. The second technique is to use small thrusters on the tether tip vehicle. These can be cycled on or off to control the tether pitch angle and

pitching rate. Only one dimensional separation dynamics of the tether are considered here, thus allowing reeling motions along the tether length.

## B. HOCAT DEPLOYMENT OBJECTIVES

The configuration we are proposing for HOCAT is illustrated in Figure 2.2. The subsatellite would be deployed gradually to a maximum extent of about 100 meters. This separation distance has been selected for practicality (e.g. a reasonable distance in the available time), and as a logical step up from the 1–10 m vacuum chambers currently in use for testing hollow cathodes.

The intention for HOCAT is to utilize the same tether used previously on the ISEE–1 satellite. This material consists of a Kevlar strand with 8 inner conductors, shielded with a conducting outer sheath. It has a tensile strength of about 600 Newton. Several other versions of higher strength are available with only a small weight penalty. The conductors have a resistance of about one ohm per meter so that we would power the sub–payload with separate, local batteries.

The tether link can be used to carry commands to the daughter payload, and return command verification and instrument parameters to the main payload, where the telemetry systems would reside. The tether will provide us the capability to electrically isolate, connect or drive the potential of the sub–satellite and the tether independently, in order to study the operational characteristics of an electrodynamic tether, particularly the plasma contactor aspects.

Two main options were initially considered. These were a spinning, or bolo configuration versus an inertial system. In order to be capable of measuring the conductor's effects at a variety of aspect angles to the magnetic field, the entire configuration should be rotating about a common center of mass. The tensile strength largely determines the spin rate of the satellite system.

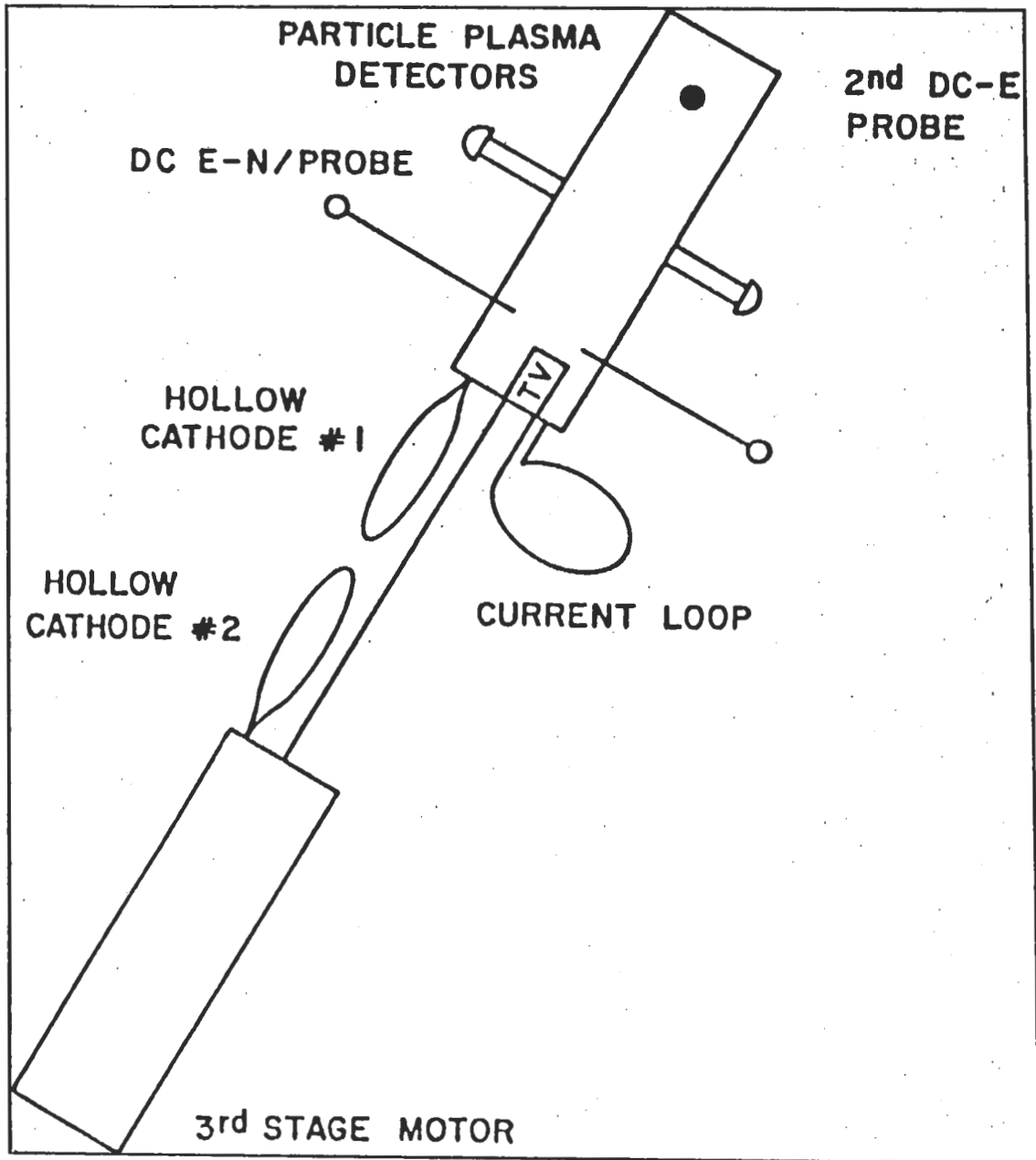


Fig. 2.2 Hollow Cathode Configuration

An initial spin rate of 30 rpm, will result in a final spin of near zero at maximum deployment (For an initial separation of 1 meter, and end masses of 100 kg, a centripetal force of about 500 Newton results, and hence a reasonable tension). This configuration does put a substantial strain on the deployer, however, and complicates that design. For simplicity, therefore, an inertial system is focused on in the remaining work.

In order to minimize mechanical design costs, we wish to make use of experience obtained by other experiments. The major previous experiments, are the Japanese CHARGE, and Norwegian MAIMIK experiments. Two future experiments are Canadian OEDIPUS and TSS-1

#### 1. US-JAPAN Joint Experiment Deployment System

The tether wire was deployed at mother-daughter separation by a multiple spring system. Separation speed was set at 0.5, 1.0, 1.5 and 1.05 m/s in the first, second, third and fourth experiment respectively. In the first two experiments, the deployment speed gradually decreased with time, and finally stopped abruptly at 38 m and 65 m respectively, due to a frictional force in the tether deployment system. However, in the last two experiments, an improved deployment system, called a Reaction Control System (RCS) was used on the daughter rocket. The RCS operated with gas jets every 40 sec to compensate for the friction.

This system is characterized by a non-constant deployment speed. Mechanically, the deployer design is similar to a spinning reel (e.g. a fishing reel). McCoy has adopted a similar strategy for his Plasma Motor Generator test. To model the deployment system, without a RCS, from the above data, the equation of motion for the separation of the tethered payload system can be solved by expanding the separation distance in a Taylor series where the separation distance is expressed as a function  $F(t)$ :

$$F(t+\Delta t) = F(t) + F'(x)\Delta t + F''(t) \frac{\Delta t^2}{2!} + \dots + F^n(t) \frac{\Delta t^n}{n!} \quad (2)$$

The first neglected term provides an estimate of the local discretization error. The equation of motion of the separating system can also be expressed:

$$\ddot{x} + \frac{c}{m} \dot{x} = 0 \quad (3)$$

where  $x$  is the separation distance,  $m$  is mass of the daughter payload, and  $c$  is a combination of the different frictional constants.

Equation (3) was first solved analytically to obtain the constant  $c/m$ , by using the known values of the initial velocity, and time from the first two experiments (e.g.  $\frac{V_f - V_i}{\Delta t} = \frac{c}{m}$ ). In anticipation of less linear systems, numerical integration was used to model the separation. The coefficient  $c/m$  was determined to be 0.0002, which gives a separation distance of 35.4 m and 71 m for initial separation velocities 0.5 m/s, and 1 m/s respectively. In the second experiment, the maximum separation was 65 m, which indicates that the acceleration is not linear with velocity. To model this nonlinearity in the drag, a quadratic or cubic term was included, making the differential equation;

$$\ddot{x} = c_1 \dot{x} + c_2 \dot{x}^3 \quad (5)$$

Trial and error solutions yielded  $c_1$  0.0001817 and  $c_2$  0.0000599 for the quadratic equation, giving rise to 34.7 m and 65.4 m for 0.5 m/s, and 1 m/s. For the cubic equation, the analytical values of  $c_1$  and  $c_2$  are 0.000196, 0.0000499 giving the separation distances of 34.93 m and 65.1 m for 0.5 m/s and 1 m/s respectively. This agree very well with the practical data of US–JAPAN experiment

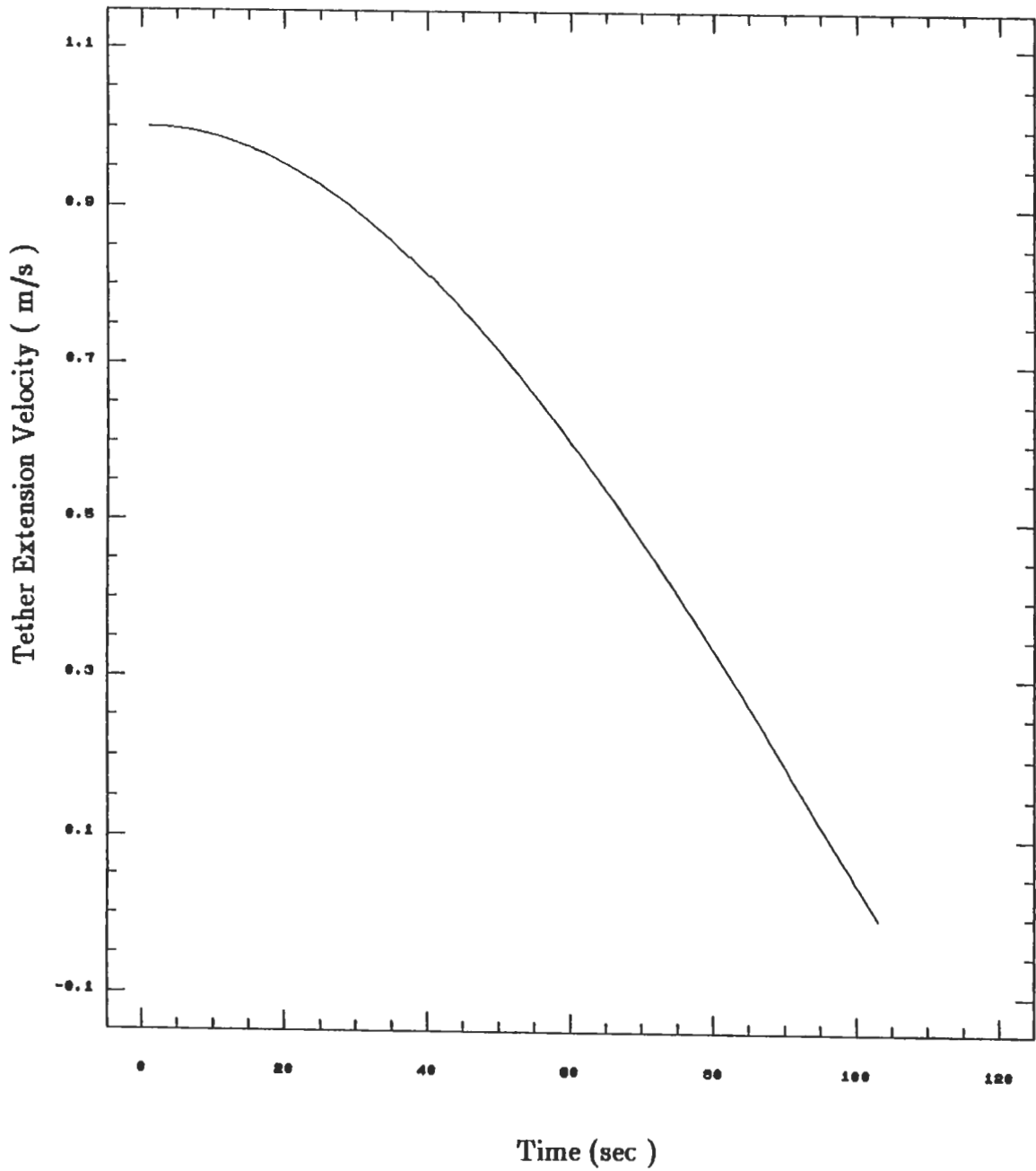


Fig. 2.3 Plot of Tether Wire Extension Velocity vs Time

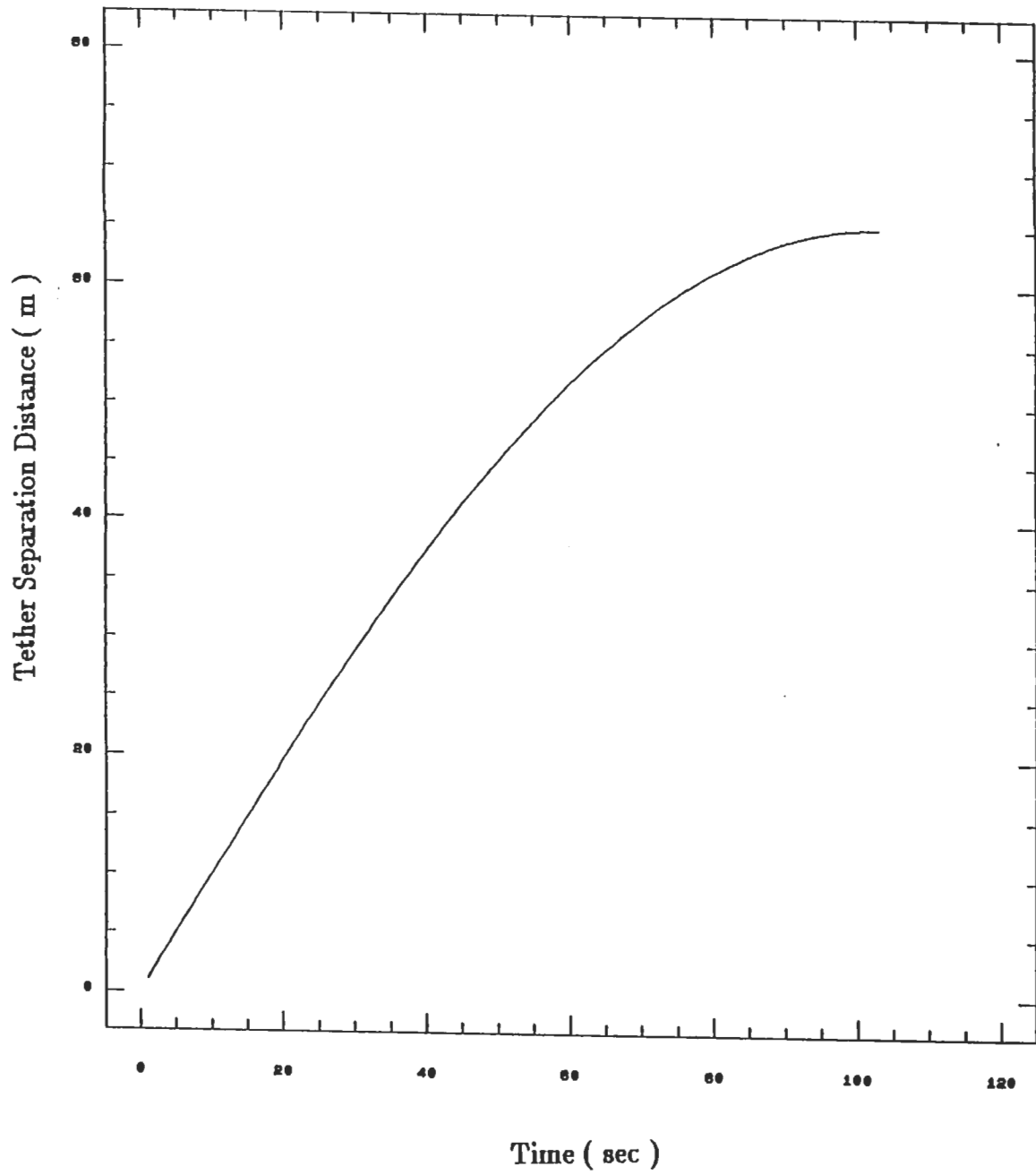


Fig. 2.4 Plot of Tether Separation Distance vs Time

without RCS. Figures 2.3 and 2.4 show how the velocity and separation distance change with respect to time for a system with initial velocity 1 m/s, and drag similar to the US–JAPAN experiment. In the third and fourth experiment, the tether deployed to a length of 418 m during 283 second and 426 m during 290 second respectively. Figure 2.5 shows the wire deployment for the velocity of fourth experiment with the Reaction Control System on board.

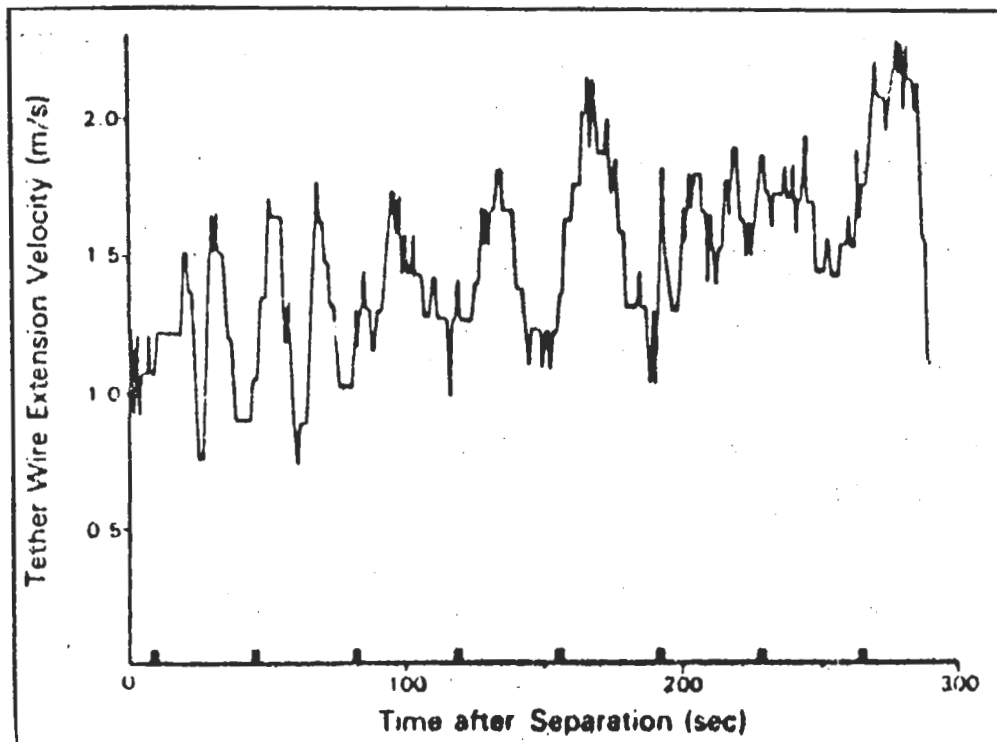


Fig. 2.5 Deployment Velocity of fourth US–JAPAN Experiment[ref. 7]

## 2. MAIMIK Rocket Experiment Deployment System

The MAIMIK rocket payloads were separated at an altitude of 86.5 km some 62 second after launch with relative speed of 0.8 m/s. During the separation, the payloads axes were tilted at an angle of  $23 \pm 2$  degrees relative to the local geomagnetic field vector. Hence, the relative cross-field daughter velocity was 0.3 m/s.

### 3. CANADIAN OEDIPUS Experiment Deployment System

A Canadian experiment team has developed a deployment system which appears optimal for HOCAT. By contrast to the Japanese approach, this is a "trolling" reel. The daughter payload is accelerated in the first 10 sec with attitude control jets. The velocity is increased up to 20 ft/s. It then decelerates until the velocity drops to zero. This takes 328 sec with a constant deceleration rate of 0.0819 m/s<sup>2</sup>. The satellites maximum separation distance of 1 km. We can apply this approach to our system, where the initial acceleration would be the same as Canadian's of 0.6096 m/s<sup>2</sup>. A deceleration rate of 0.005 m/s<sup>2</sup> would give a maximum separation distance of 100 m at apogee for the chosen conditions. If there is negligible friction, which means constant acceleration and deceleration, the acceleration and deceleration can be easily calculated using;

$$x = \frac{1}{2} \ddot{x} t^2 \quad (6)$$

and

$$\dot{x} = \ddot{x} t \quad (7)$$

For the OEDIPUS deployment system, the initial acceleration was 0.6096 m/s<sup>2</sup> which gives rise the separation distance of 0.8 m at the maximum velocity 1 m/s, and is valid for our system. The deceleration should be different, because of the differences in maximum separation distances and initial separation velocities. It takes just 1.64 sec to reach the required velocity of 1 m/sec, and takes 200 sec for the velocity to drop to zero. This gives a total time of 201.64 sec from separation to apogee. We know that the acceleration is linear with velocity which is different from US-JAPAN experiment. This deployer model meet our experimental

requirements. Figure 2.6 and 2.7 show that the velocity and separation distance with respect time.

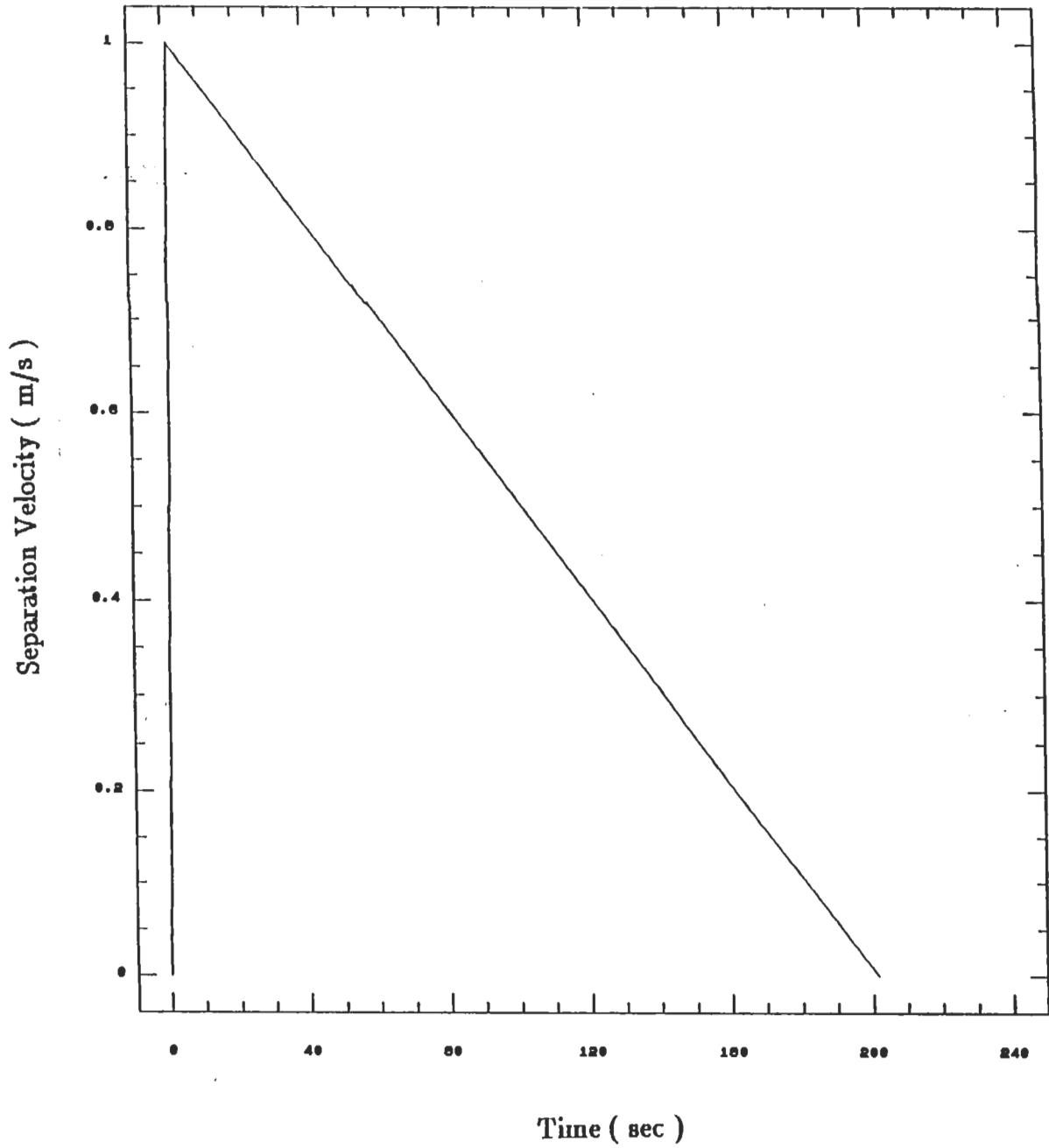


Fig. 2.6 Plot of Separation Velocity vs Time

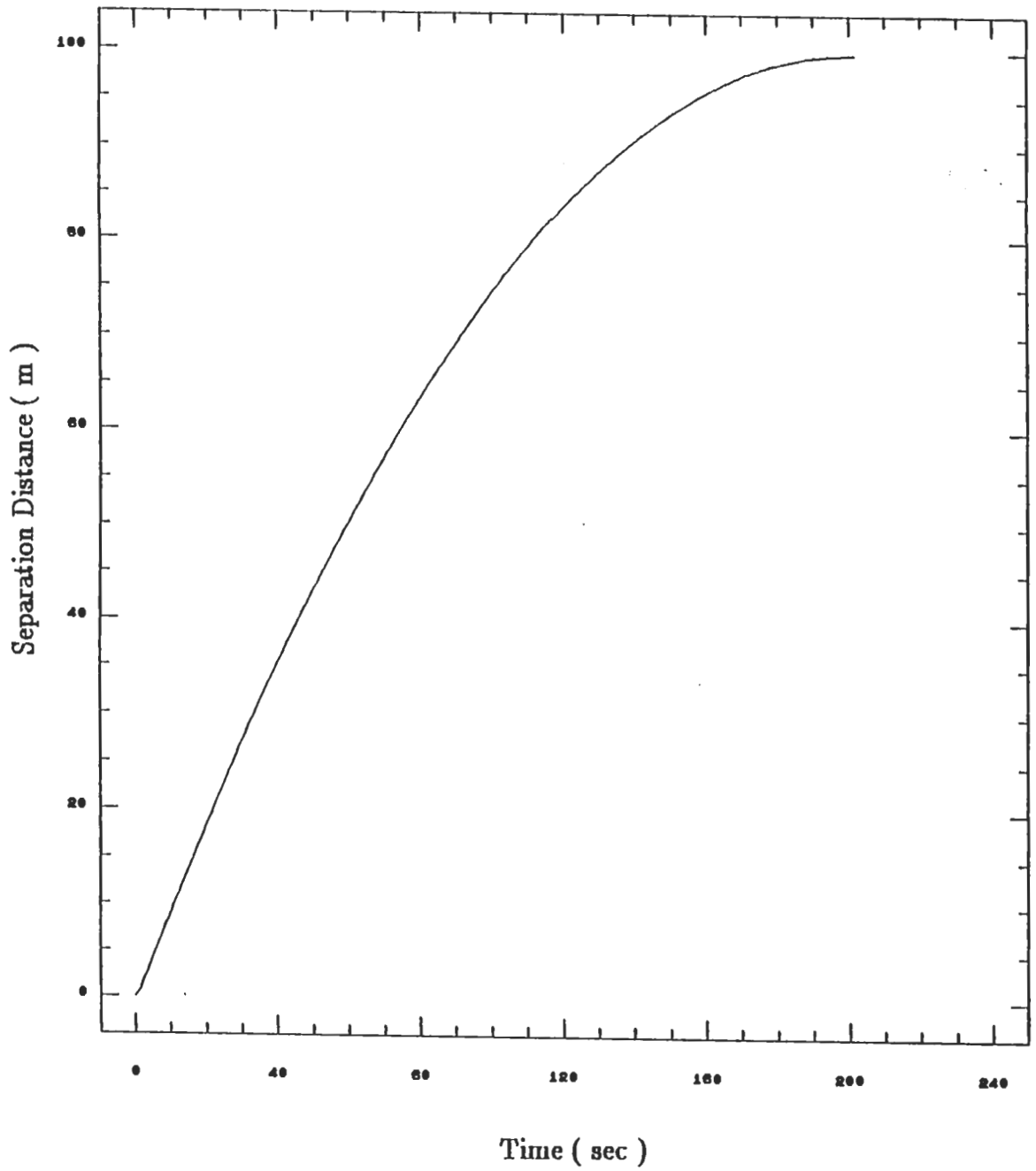


Fig. 2.7 Plot of Separation Distance vs Time

#### 4. Tethered Satellite System-1 Deployment System

To complete the consideration of past and future tether systems, the TSS-1 system is illustrated. Deployment of the tether and TSS-1 satellite is a stable maneuver, requiring 5-8 hours in the case of a 20 - 100 km tether to reach the desired altitude region upward direction from the orbiter. Stabilization of the satellite at the desired deployment position is accomplished by introducing damping through the tether tension. Swing motions of the tether can be converted to stretching motions, which are damped by the reel control mechanism. During the course of the experiment, it should be possible to change the length of the tether to permit observations at various altitudes. The system should have a capability for controlling dynamic trajectories of the satellite in the 1-10 km zone surrounding the orbiter. Figure 2.8 shows the tethered satellite system reel and boom mechanism for TSS-1 mission.

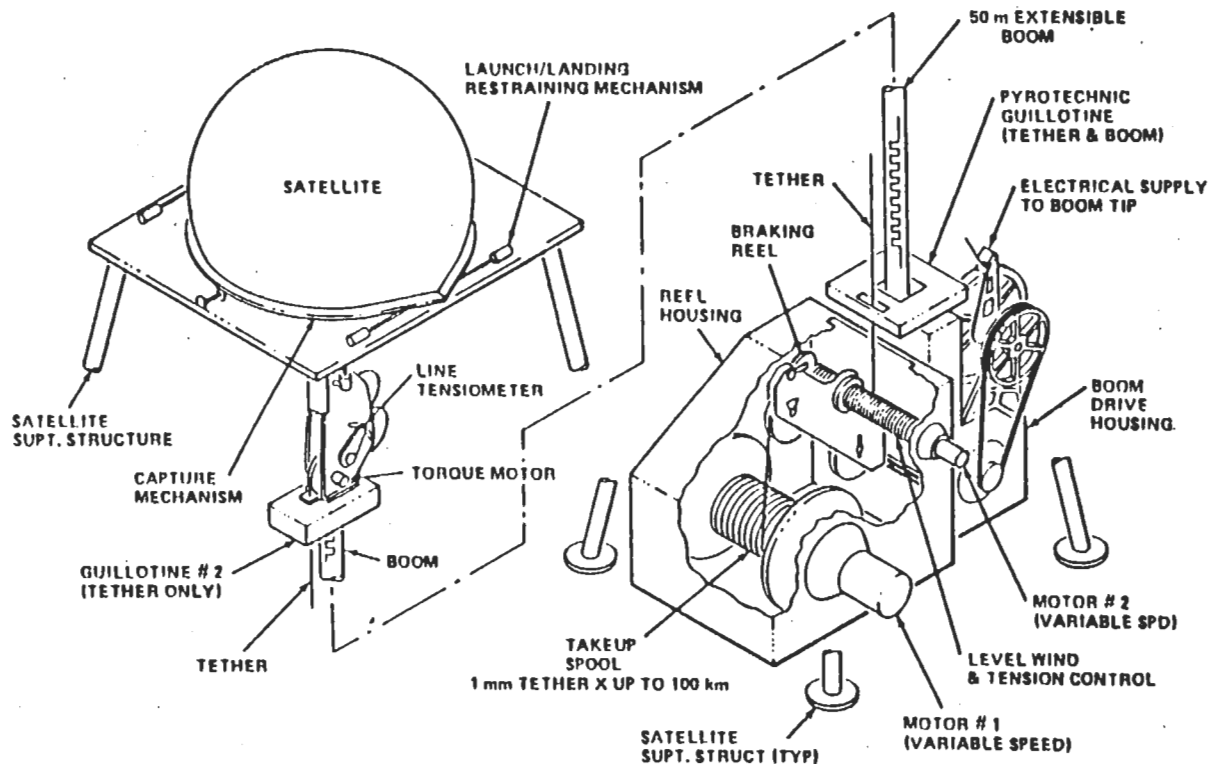


Fig. 2.8 TSS-1 Reel and Boom Mechanism[Ref. 6]

### III. PLASMA CONTACTOR HOLLOW CATHODES

Because of the ongoing need to understand the process of electrically connecting rockets and satellites with the ambient plasma, a concerted effort has been conducted by NASA/Lewis Research Center in coordinated laboratory and theoretical studies, along with analysis of existing flight data.

#### A. LABORATORY STUDIES

Much of the work done in this area has been conducted at Colorado State University, under the direction of Dr. Paul Wilbur. This work has been documented in annual reports as noted in the Reference. The CSU chamber is 1.2 m in diameter, and approximately 3.5 m of the axial length is utilized for the experiments described here. In the CSU work, hollow cathodes have been demonstrated to be effective electron sources at current levels of 1 A or more. Extraction voltages of a few tens of volts are generally required for such currents. Of greater concern is the matter of emitting a positive current.

Laboratory tests of hollow cathode systems as positive current sources (e.g. ion emission or electron absorption) have shown effects which are not totally understood, and may be important in space. Ion emission current levels of 10's of milliamperes are typically observed with hollow cathodes, and as much as 100 mA ion current is possible at high gas flow rates. If an "ambient" plasma exists, electron currents of 50–100 mA are collected at bias voltages of 20–100 V. Above these levels, recent laboratory results typically have shown an operating regime termed "ignited mode".[Ref. 37]

In this mode, a discharge is observed in the chamber, which appears to be associated with ionization of the neutral gas in the chamber. The ionization structure which results is a double layer, which allows a space-charge limited flow to occur. It is argued that the transition to the ignited mode results from plasma phenomena, and not from electron currents being drawn from the vacuum tank walls.[Ref. 38]

The observed luminosity is due to atomic or ionic excitation, implying that ionization is occurring and that it could be the cause of the improved contacting performance accompanying the transition to ignited mode electron collection. Figure 3.1 shows a typical comparison of the electron current collected by the contactor ( $J_{ce}$ ) compared to the electron emission current from the simulator ( $J_{se}$ ). Such plots were initially referenced to the tank. Figure 3.2 shows that a more natural dependent variable is the anode to ambient plasma potential difference. In both Figures, the transition to ignited mode represents a substantial increase in performance.

The most recent work by Wilbur has focused on understanding the potential distribution around the electron collecting cathode, in combination with modeling work described below. Figure 3.3 shows the plasma potential contours around a hollow cathode in electron collection mode (Wilbur, private communication, 1988). The high plateau (near anode potential) close in, and the 10–20 V drop are typical features found in this work. One relative weakness of the work so far is the relatively poor diagnostics of the plasma characteristics (density and temperature). Figure 3.4 shows the ignited mode configuration of hollow cathode by Wilbur.

Similar work is being conducted at NASA/Lewis Research Center (LeRC) by Mike Patterson in the 5 m × 19 m chamber used by the ion thruster group. Work in the facility has been focused on high current (1–10 A) collection, in an environment

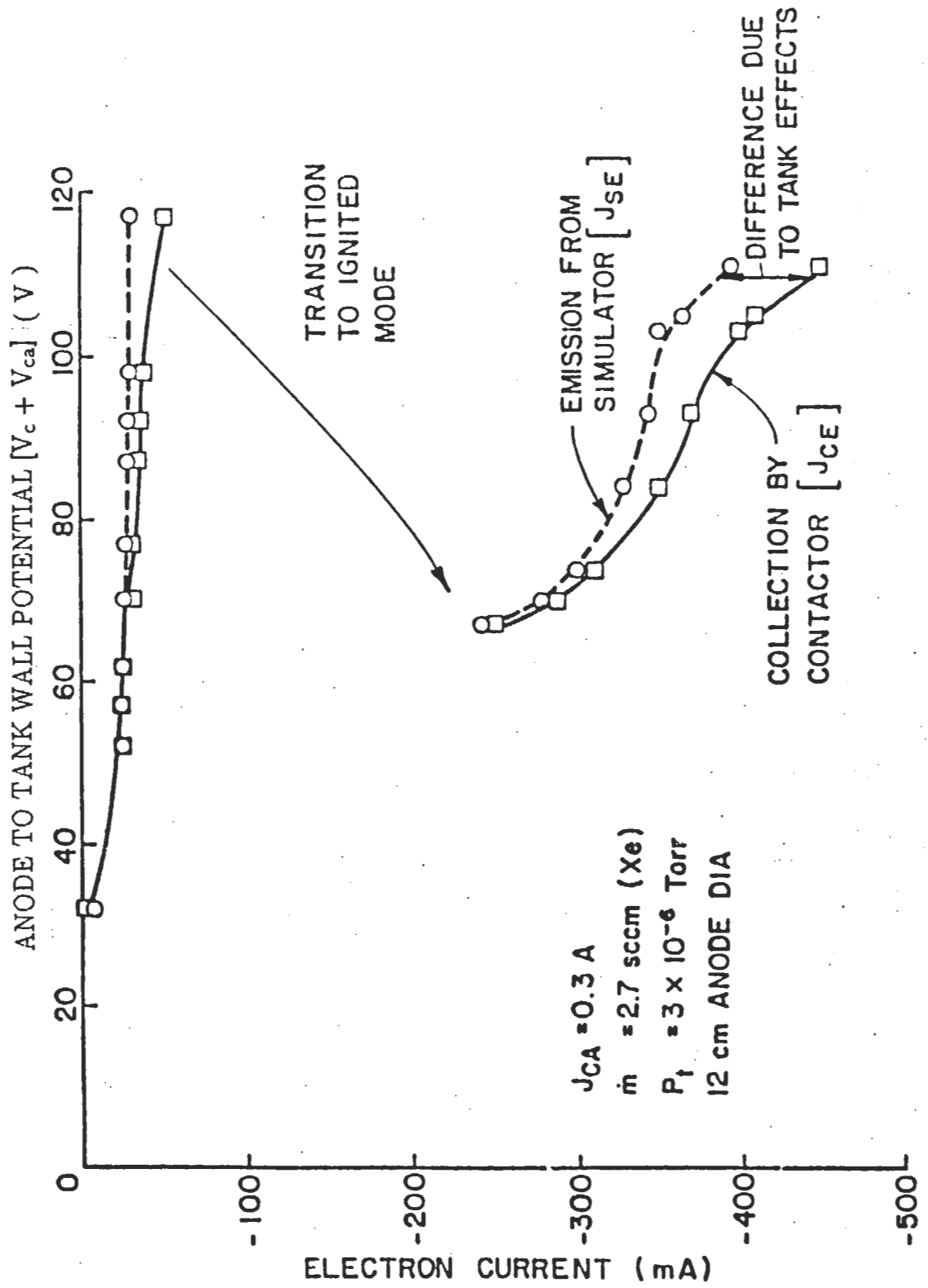


Fig. 3.1 Perturbing Effect of Vacuum Tank Wall [Ref. 37]

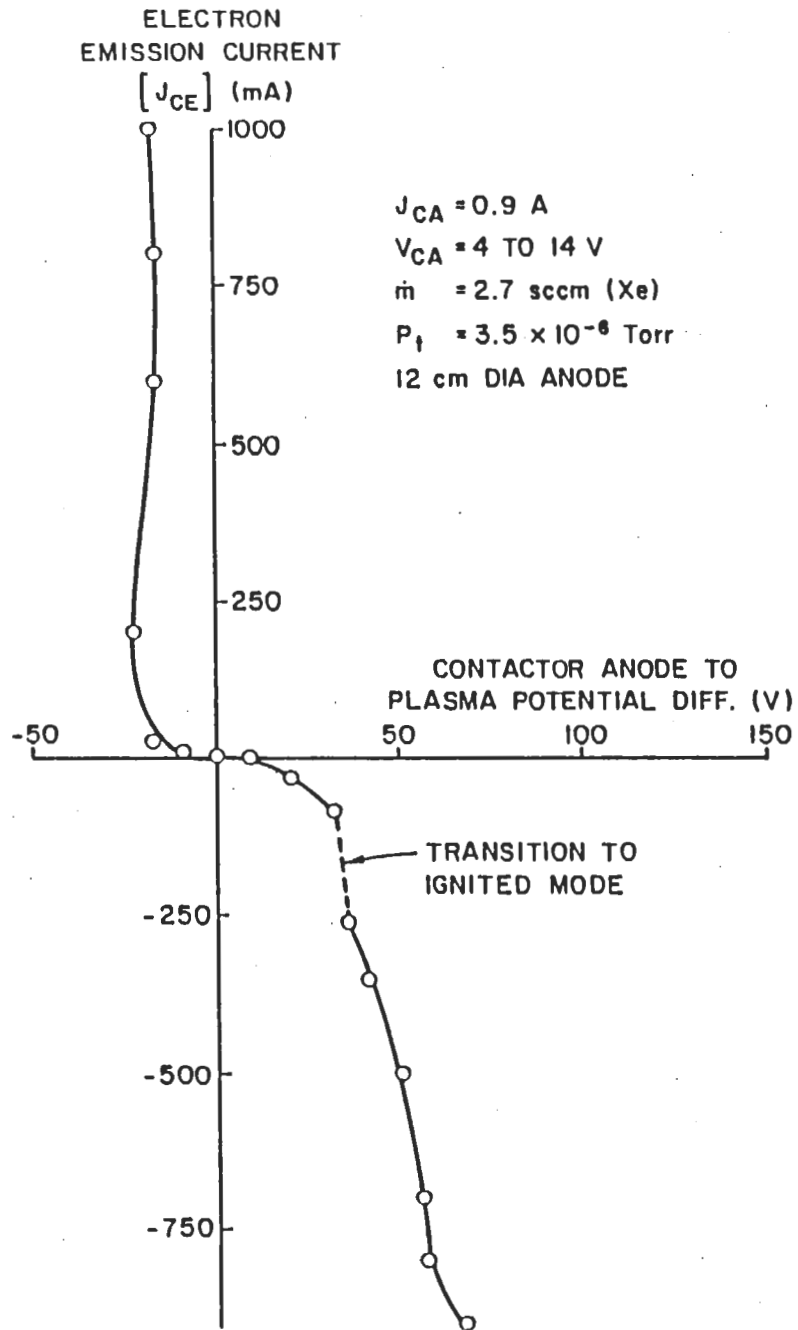
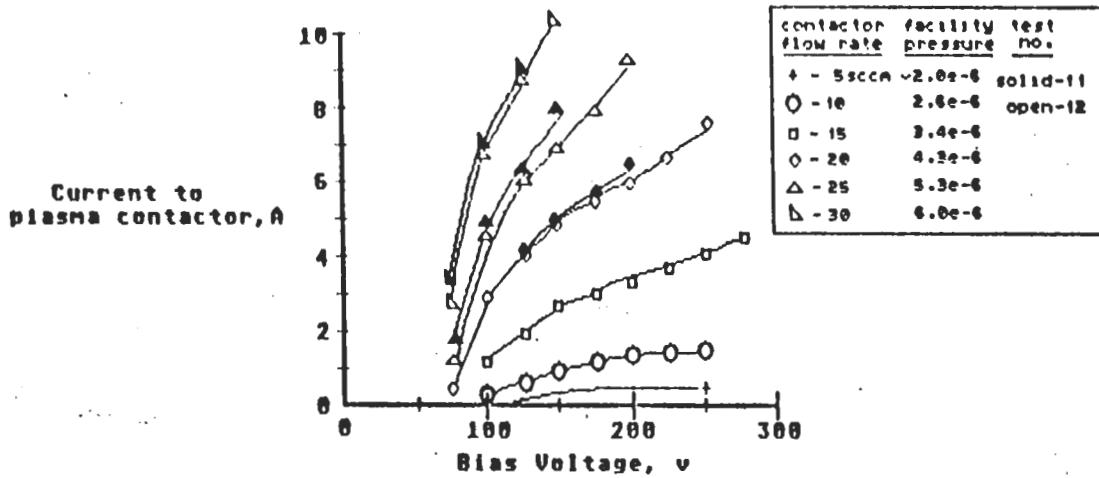


Fig. 3.2 Contactor Anode-to Ambient Plasma Potential Difference  
vs Electron Emission Current[Ref. 37]



Test no.	Space Plasma Simulator		Plasma Contactor			Simulator Reference	Contactor Bias Pt.
	Type	Expellant	Type	Expellant	Disch. Power		
11	1/4" hole cathode	Ar	30cm Ring-cusp Discharge w. Baffle	Xe	on (150w)	tank ground	Anode
12	"	"	"	Xe	off	"	"

Fig. 3.5 Current to Contactor vs Bias Voltages[Ref. 39]

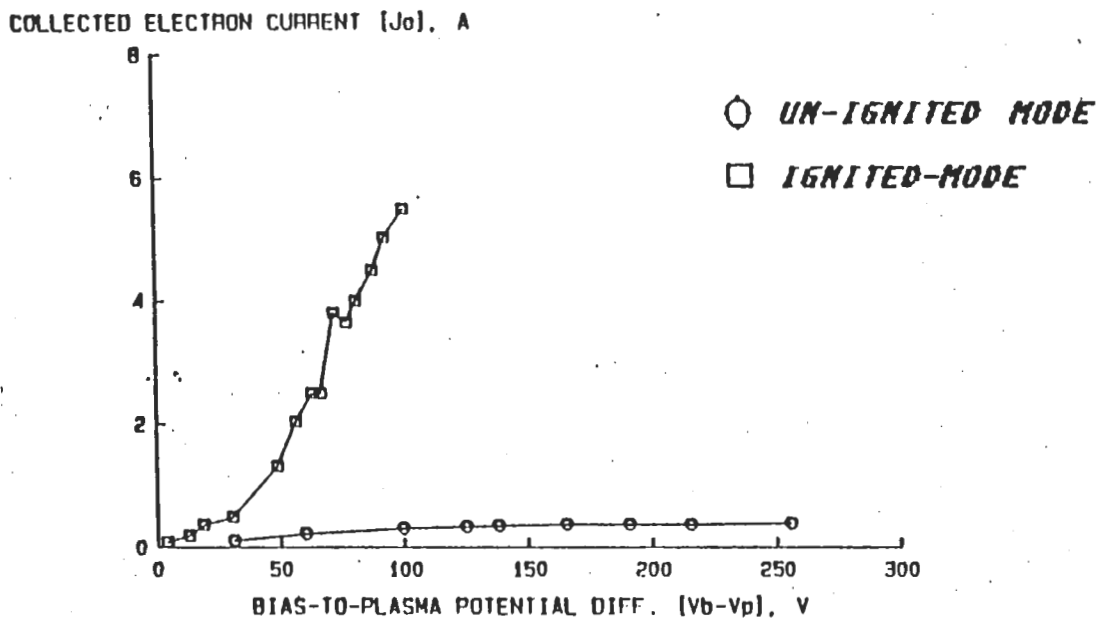


Fig. 3.6 Bias-to-Plasma Potential Difference[Ref. 39]

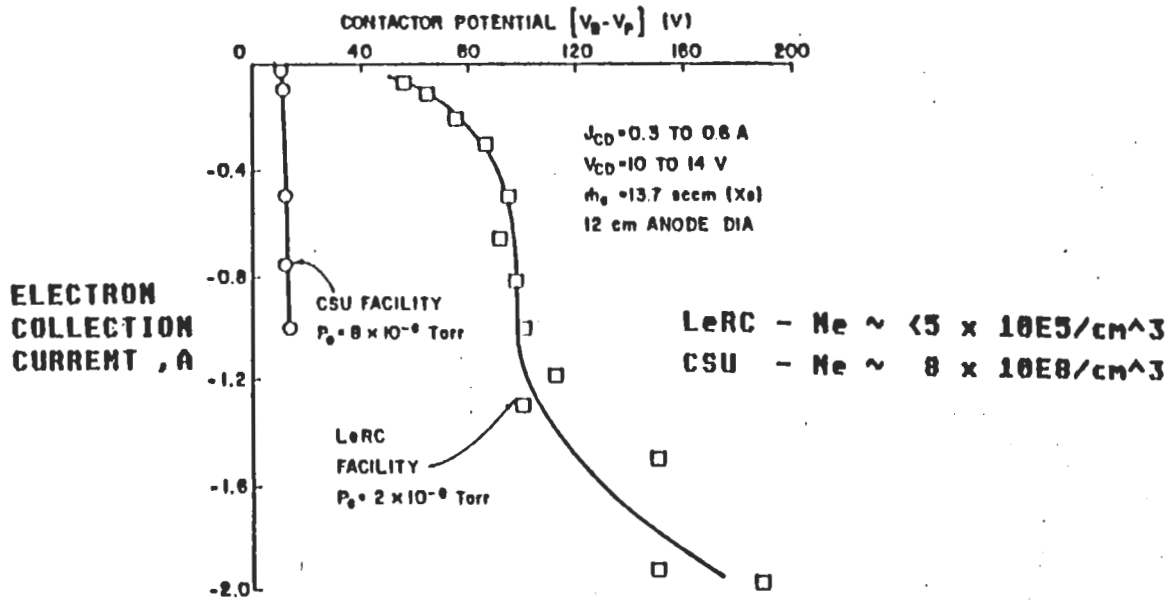


Fig. 3.7 Current vs Contactor Potential

chamber, even though the electron density (bias off) is substantially lower. This has been attributed to the enhanced area of chamber walls capable of emitting secondary electrons (Katz, private communication, 1988. Cohen, private communication, 1988). The work at CSU and LeRC is continuing. One element of the program proposed below is to conduct complementary experiments at Naval Postgraduate School.

## B. THEORETICAL STUDIES

Substantial theoretical work has been conducted under the NASA/LeRC program, particularly by Dr. Dan Hastings (MIT), and the S-cubed group. Hastings (1988) has addressed the plasma contactor problem at low earth orbit, as it might apply to tethered systems, from an analytic viewpoint. This work focuses on the micro-physical processes which will determine how well hollow cathode systems will

micro-physical processes which will determine how well hollow cathode systems will work at high current (1 A or more) levels.

An important conclusion from this work is that large amounts of turbulence ( $\nu_{\text{eff}} \sim 0.4\omega_{pe}$ ) are essential to effective operation of these devices. If such levels of turbulence can be achieved, a plasma contactor can exhibit gains of 2-6 for ion current in the Ampere level and for potential drops in the range 100-500 V. Here, gain is defined as the ratio of collected electron current to emitted ion current. The gain is a decreasing function of the total current, so high current devices are less efficient than lower-current device.

This suggests that plasma sources with low mass flow rate and high ionization fraction may be the most effective for use in plasma contactor. Of fundamental importance for collecting large currents is the level of turbulence established in the plasma, by the current flowing in the plasma. There are some indications in this work that multi-ampere systems will be ineffective, that is, excessively large potentials will develop because insufficient current can be collected.[Ref. 40]

This analytic work is complemented by numerical modeling efforts conducted at S-Cubed (a division of Maxwell Laboratories). This work has been focused on three-dimensional simulations of the hollow cathode, and of the overall systems response. This work has been successfully applied to interpretation of Wilbur's laboratory experiments. Figure 3.8 shows a 2 dimensional cut from an S-Cubed simulation of data similar to that shown in Figure 3.3 (Katz, private communication, 1988). Excellent agreement between theory and laboratory experiments is emerging from the NASA/LeRC effort.

The challenge will be to apply these models to space, and to validate the models for space by obtaining flight experiment data, and making comparisons.[Ref. 41]

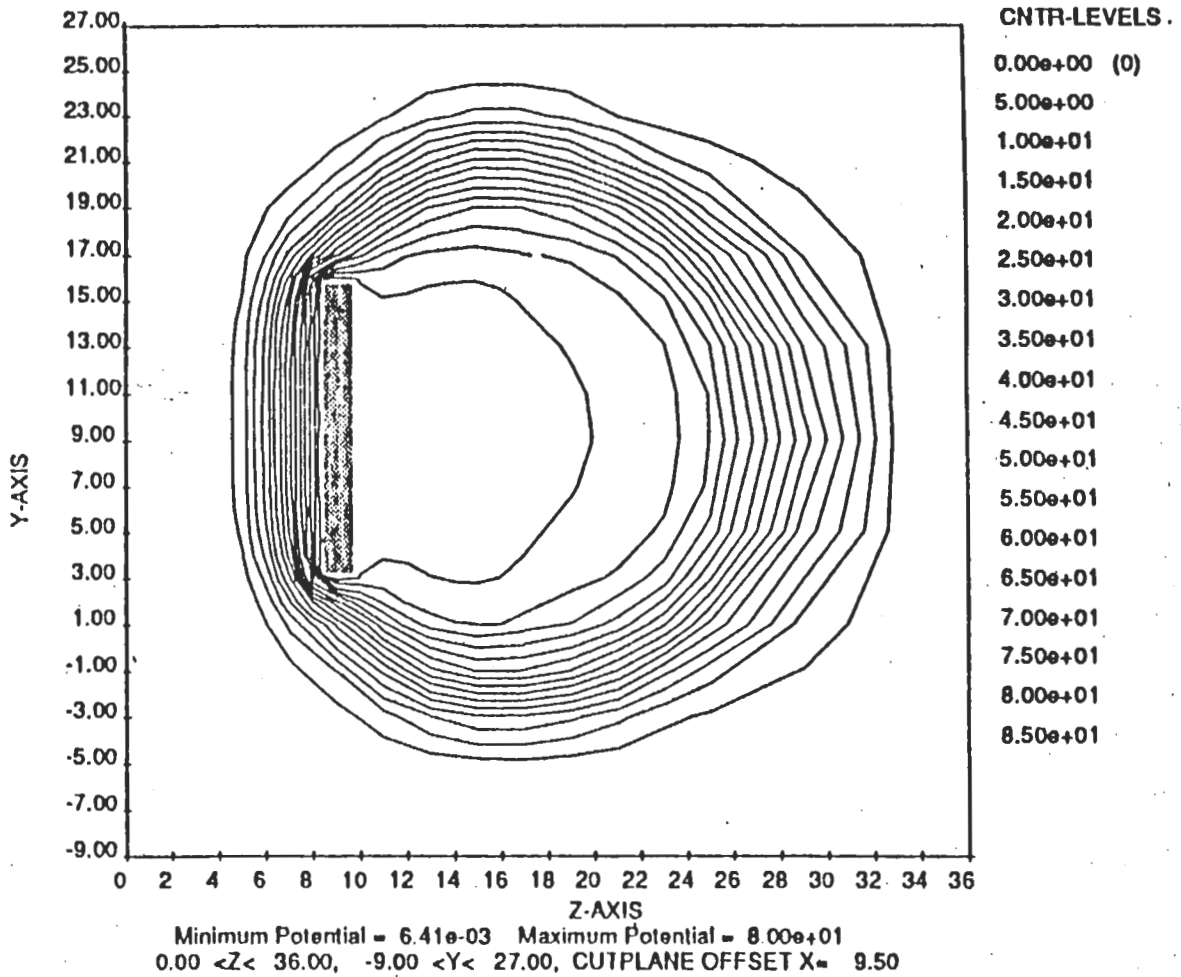


Fig. 3.8 2-Dimensional Cut[Ref. 41]

### C. FLIGHT EXPERIMENT DATA

Hollow cathode systems have been successfully operated in space for 2 decades. The SERT-II (1970-1979), ATS-6 (1974-1976), and SCATHA (1979-1983) missions all demonstrated success in their relative domains, as presented in a previous chapter. Under the NASA/LeRC program, data from the SCATHA satellite have been considered. Electron and ion gun experiments at the  $10 \mu\text{A} - 1 \text{ mA}$  level were conducted on SCATHA from 1979-1983. Particle and wave data were available for study. Electron gun experiments showed evidence that at current

levels above 10 – 100  $\mu\text{A}$  (roughly equal to the ambient thermal electron flux), the beam was disrupted by space charge effects.[Ref. 42]

Charged particle data showed that the beam was causing heating of the local electron population, and was failing to escape the satellite region. Recent studies have shown that electron cyclotron waves may be the mediating factor. The implications of this work are that electron beams are ineffective as "Plasma Contactor". This conclusion is partially supported by shuttle observations, though this remains somewhat controversial.[Ref. 43, 44]

Ion gun experiments on SCATHA showed a similar character, in that it was found that the beam rapidly became space charge limited when high current (1 mA) high voltage (1 kV) experiments were attempted. The satellite failed to charge to the beam energy, indicating only 1–10 % of the beam escaped the near satellite region. The ion gun was effective as a low energy plasma source, however, when operated in "trickle mode". In this mode, it operates without accelerator voltage, and resembles a large hollow cathode. In this mode, currents of 10's of  $\mu\text{A}$  could be emitted, at coupling voltages of less than 1 V.[Ref. 21]

These "Plasma Contactor" experiments, and the earlier ATS–6 and SERT–II data all indicate high levels of success with hollow cathode systems. There remains, however, a need to further test hollow cathode systems, particularly in the high current regime (Ampere level). From an operational point of view, the critical question remains: Can 1 ampere of positive current be emitted from a hollow cathode in space ?

## IV. EXPERIMENTAL FLIGHT PROGRAM

The natural extension of the ground-program conducted thus far is to conduct a flight experiment which will extend our understanding beyond the limits of the 10 m chamber at NASA/LeRC. We intend to test the hollow cathode for its viability as a plasma contactor with the specific application of a 1 A tether system.

This test will be a tethered, mother-daughter rocket payload, with hollow cathode plasma sources on both ends. The experiment has been dubbed "HOCAT". The payloads, as illustrated in Figure 2.2, would be instrumented in a way that would allow us to determine the nature of the coupling between the hollow cathodes and the ambient plasma, and the effects of driving positive and negative currents through the system.

The mother payload will be recovered, and could be reflown with alternate plasma contactor designs. Our goal at this time is to launch our first experiment in mid 1991. Subsequent flights could occur at 1 year intervals, at substantially reduced cost. In the following sections, the rocket, payload, and launch scenario for this experiment, are described.

### A. ENVIRONMENT

The plasma environment for the space shuttle and proposed space station is sub-auroral at altitudes from 250-500 km. This environment is a cold dense plasma, with temperatures of a few tenths of an electron volt (1000-3000 °K), and a plasma density which ranges from  $10^5$  particles/cm<sup>3</sup> in shadow to  $10^6$  particles/cm<sup>3</sup> in sunlight. The lower ambient plasma densities provide the most severe test of the

plasma contactor performance, and we wish to focus the experiment on that limit. The launch site would be Wallops Island, at the Wallops Flight Facility (WFF), in order to insure a quiet geomagnetic environment. This eliminates the need to disentangle artificial from natural processes, and provides access to substantial ground resources (particularly the Millstone Hill incoherent scatter radar facility).

For the experimental region, the electron densities of daytime and nighttime are shown in Figure 4.1 and 4.2. It is apparent from these two Figures that the lowest ambient plasma density  $N_e$  we are likely to encounter in the 1991–1992 period (solar maximum) is the  $10^5 / \text{cm}^3$  level found at night. The neutral density in this region is  $10^7 / \text{cm}^3$ , primarily Oxygen. This value can be compared to the neutral density of  $3.5 \times 10^{11} / \text{cm}^3$  found in the CSU and NASA/LeRC chambers at  $10^{-5} - 10^{-6}$  Torr. In the ionosphere, the neutral density is almost hundred times larger than the electron density.

The neutral gas environment for a sounding rocket has density  $N(\text{neutral}) > N(\text{ambient})$  because of rocket outgassing. Figure 4.3 shows neutral pressure data from SPEAR–1. Its apogee was 370 km and measured minimum payload pressure was about  $10^{-5}$  Torr. Until very late in the flight, outgassing dominates the local (rocket) environment.[Ref 45]

Typical electron temperature and thermal velocity profiles are shown in Figure 4.4. These are important for determining the ambient electron current. Ion temperature, average mass, thermal velocity are shown in Figure 4.5. These values result in a Debye–length illustrated in Figure 4.6, and electron collision frequencies and mean free paths as shown in Figure 4.7. These are important for determining the potential distribution and collected currents. Expected values at solar maximum, night, 500 km altitude, are a Debye length of 0.3 cm, mean free path of about 600 m, and collision frequency of about 350 Hz.[Ref. 46]

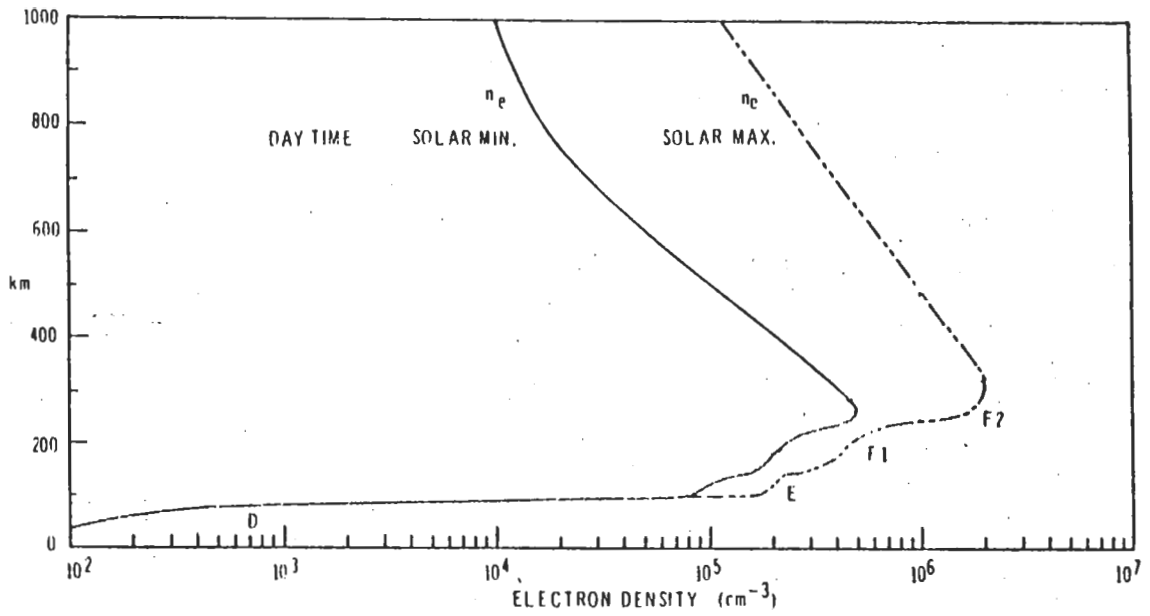


Fig. 4.1 Ionospheric Electron Density (daytime)[Ref. 46]

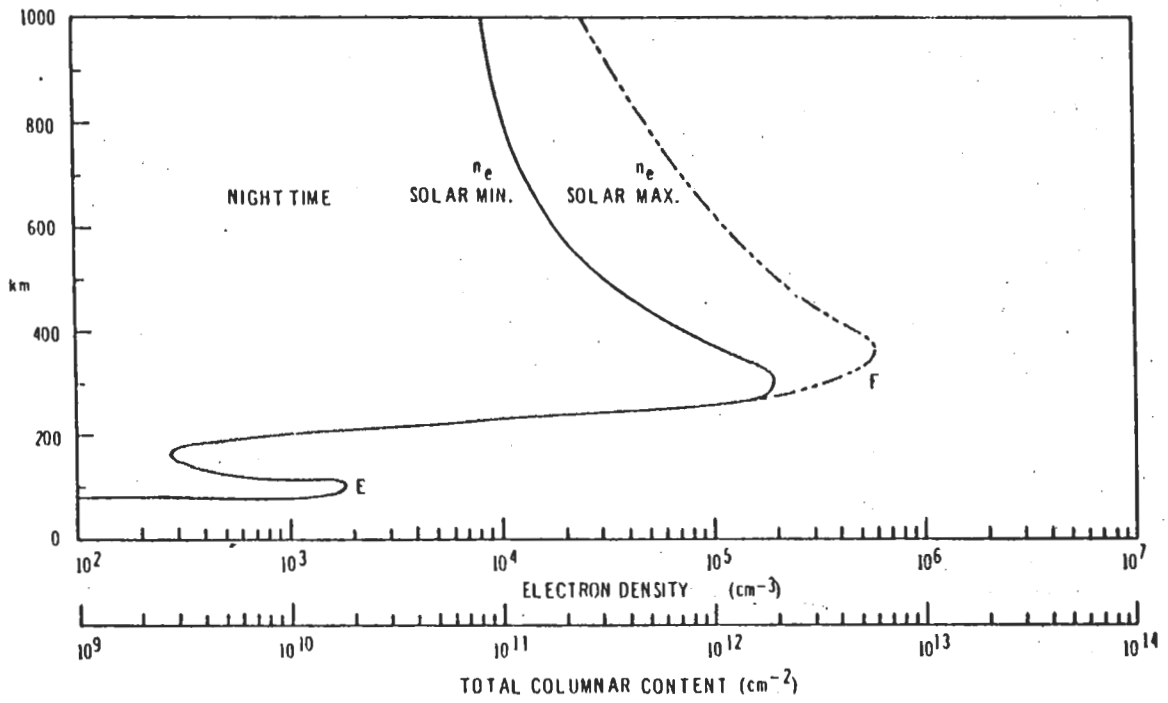


Fig. 4.2 Ionospheric Electron Density (nighttime)[Ref. 46]

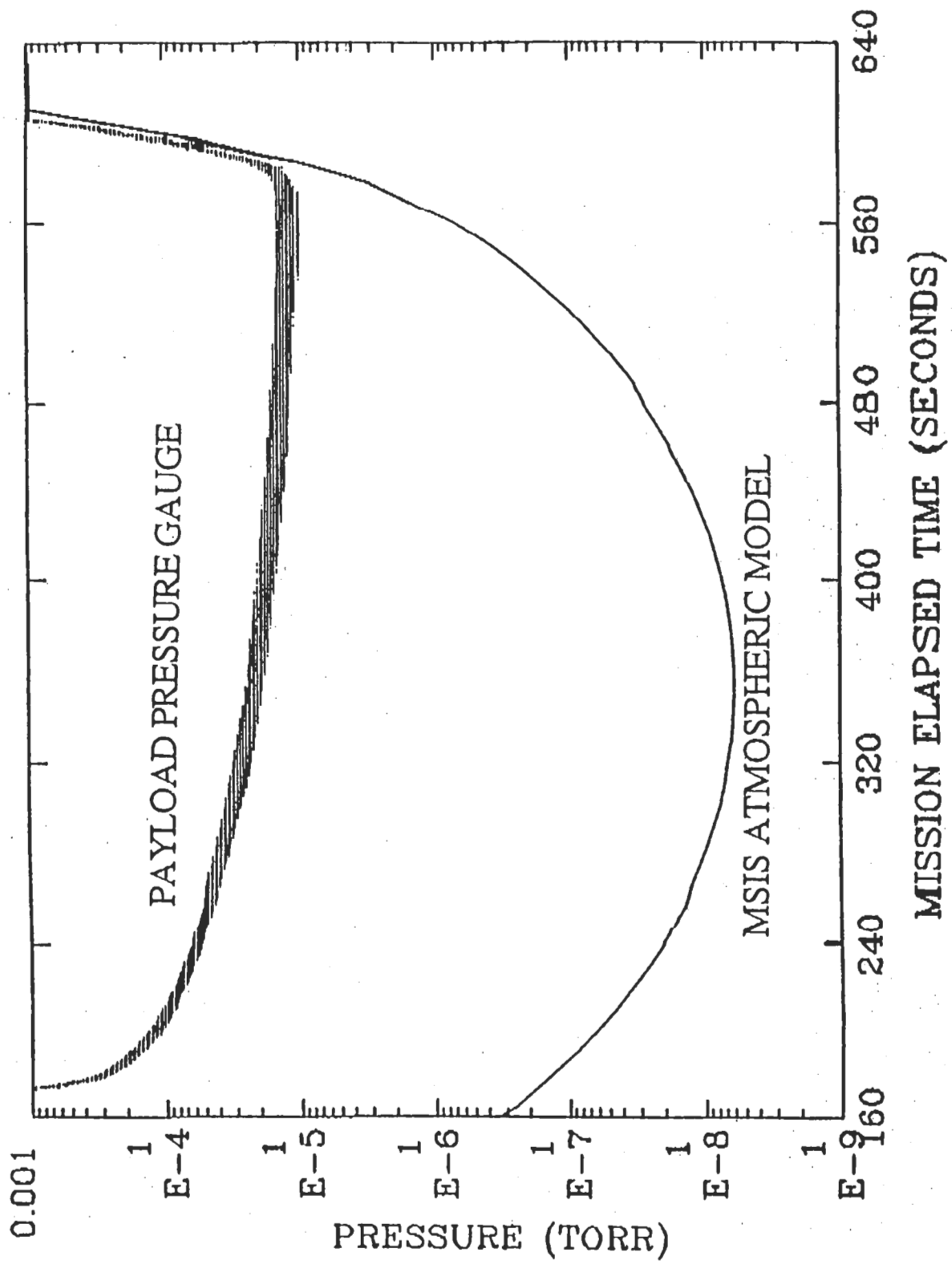


Fig. 4.3 SPEAR-1 Neutral Pressure Data[Ref. 45]

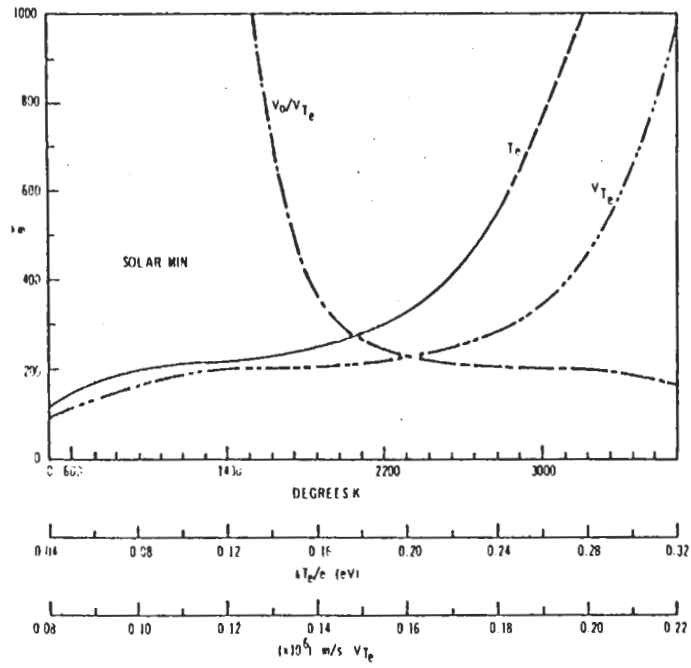


Fig. 4.4 Electron Temperature and Thermal Velocity [Ref. 46]

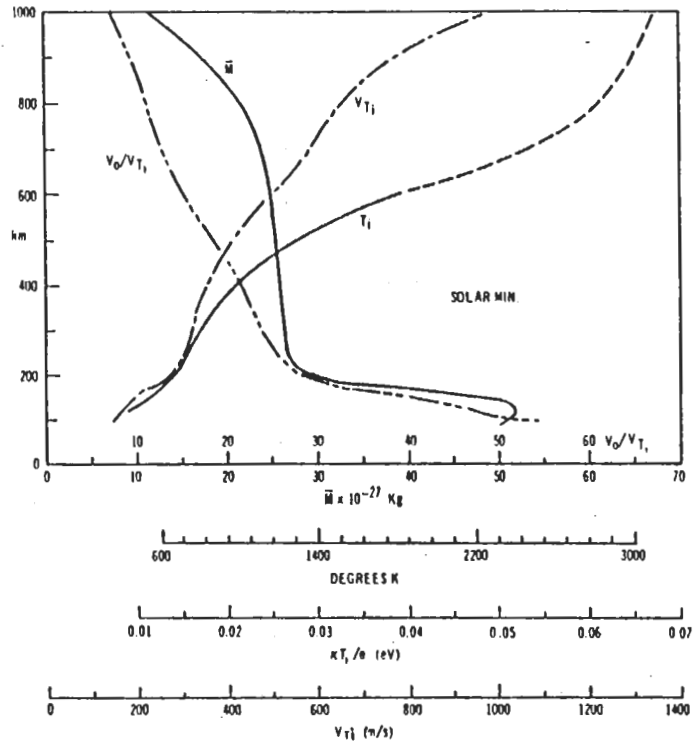


Fig. 4.5 Ion Temperature, Mass and Thermal Velocity [Ref. 46]

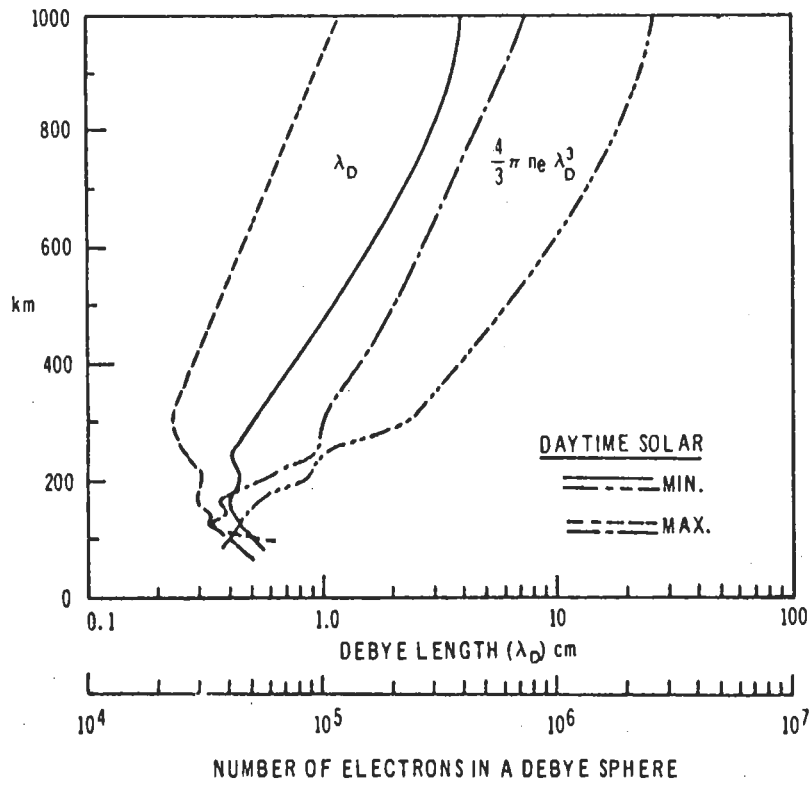


Fig. 4.6 Debye Length[Ref. 46]

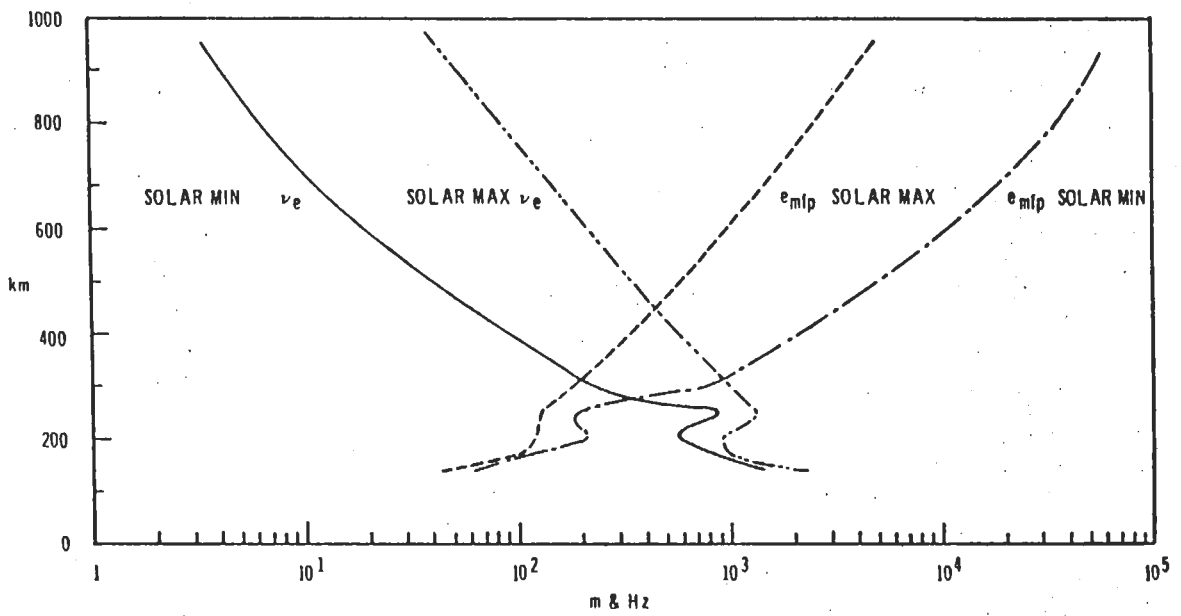


Fig. 4.7 Electron Collision Frequency and Mean Free Path[Ref. 46]

## B. LAUNCH VEHICLE

A Black Brant X has been selected as the appropriate vehicle for launching the HOCAT experiment. This decision is based on the desire to reach 500 km altitude, with an estimated payload of 610 lb. Table 1 shows the rough allocation of weight to payload components based on previous experience with the UAH-CRIT 1 experiment. As illustrated in Figure 4.8, this gives us a weight growth margin of 60–70 lb (e.g. 10 %). The Black Brant X outer diameter is 17.25 inches and length is about 10 feet. The configuration of the Black Brant X payload is shown in Figure 4.9.

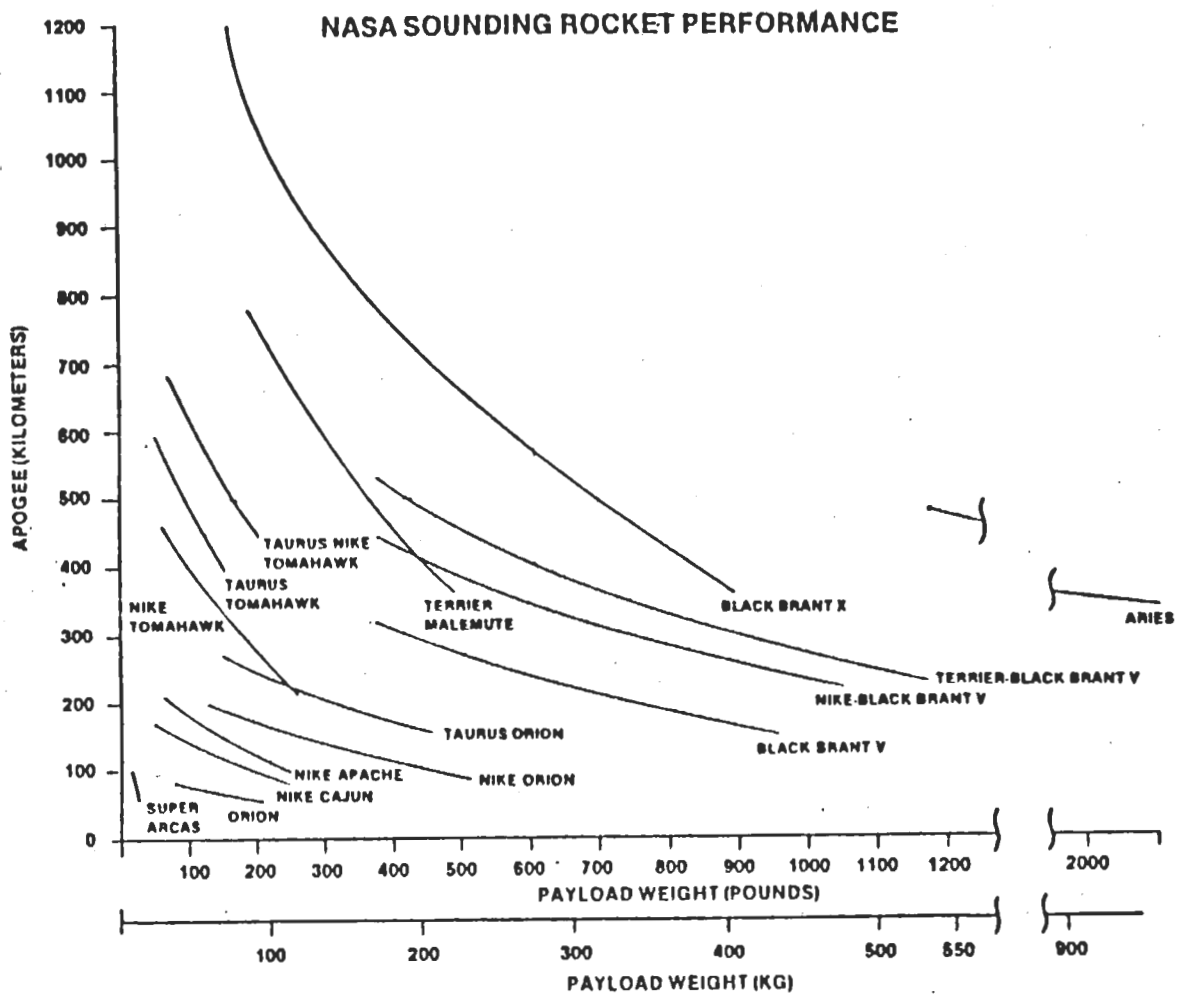


Fig. 4.8 NASA Sounding Rocket Performance

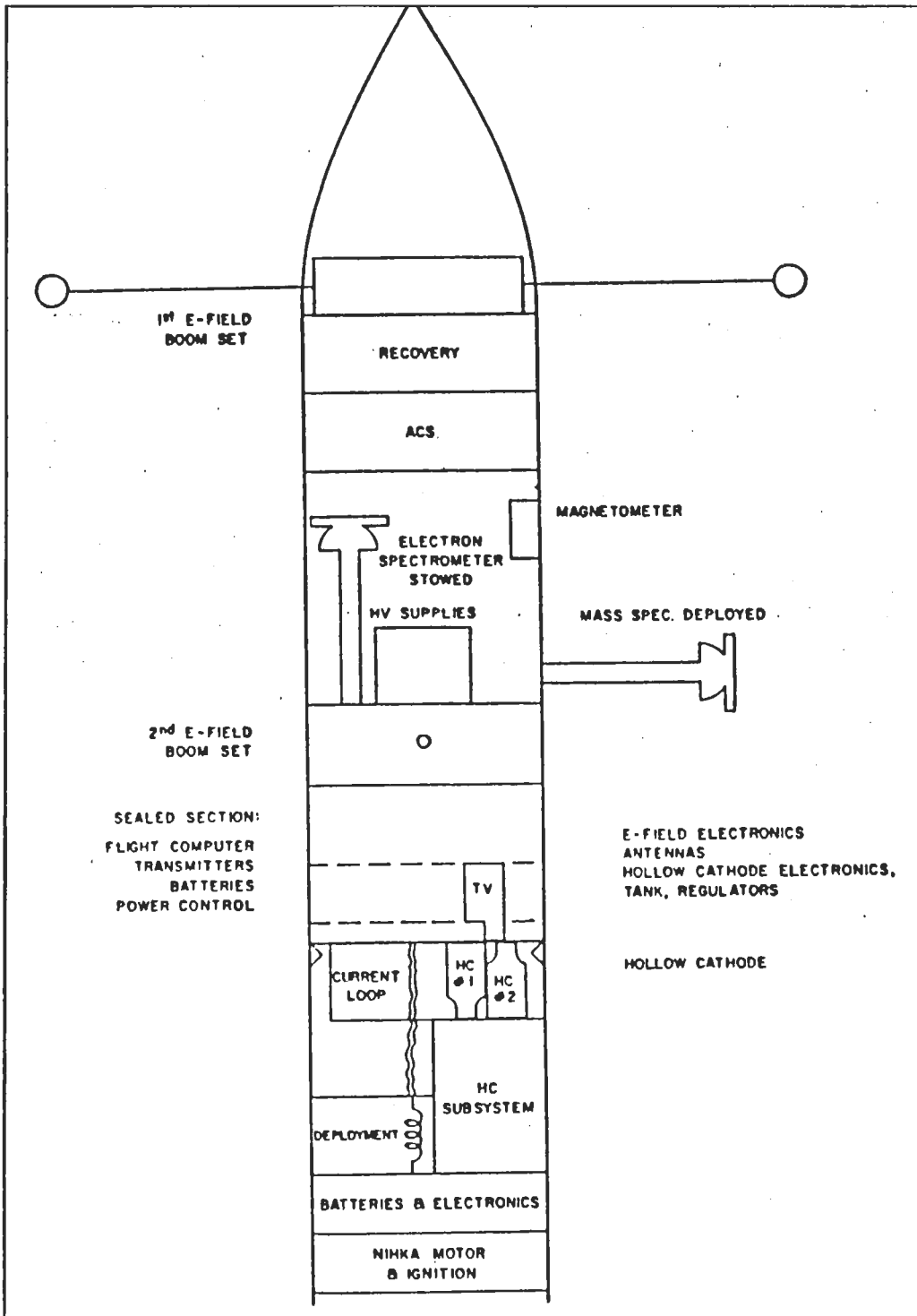


Fig. 4.9 HOCAT Black Brant X Payload

TABLE 1 ALLOCATION OF WEIGHT AND POWER

Weight and Power

Section	Weight(Pounds)	Power(Watts @28 VDC)
Nose Cone	20.	0.
Boom Set #1	12.	0.
Recovery	89.	0.(self)
RCS	72.	0.(self)
Magnetometer	1.	1.4
Plasma Analyzers	18.	2.4
Scaled Section		
Flight Computer	12.	18.
Transmitters(2)	4.	112.
Transponders	2.	12.
TV Camera	1.	20.
E field electronics	6.	5.
Power Control	4.	1.
Batteries	12.	0.
Hollow Cathode # 1 electronics & plumbing	21.	25.
Altitude Switches (G-switch, relays, timers)	10.	8.4
Hollow Cathode # 1	1.	0.
Current Loop	8.	4.
Structure, Cabling	225.	0.
Hollow Cathode # 2	22.	25.
Batteries & Power system	8.	2.
Deployment Mechanism	20.	0.
Nihka ignition & sep	43.	0.
Total	610.	244.

C. DEPLOYMENT SYSTEM

For the HOCAT experiment, the Canadian OEDIPUS Canadian deployment system has been adopted as nearly ideal for our purposes. An initial separation velocity of 1 m/s can be obtained by firing a gas jet for 10 seconds. The maximum

separation will be 100 m at about 500 km apogee. This is a reasonable separation distance in the available time.

#### D. FLIGHT SCENARIO

This rocket flight should provide about 11 minutes of flight time. The Nihka motor burnout occurs at 100 second, as the 100 km mark is passed. Our operations would begin at this point, with deployment of the booms, and the beginning of the tether deployment. The Nihka motor will be jettisoned to reduce neutral gas contamination.

We have tentatively selected a goal of reaching maximum extension of about 100 m at apogee, at about 8 minutes into the flight. On the downward leg, there would then be 6 minutes of data before crossing the 100 m altitude mark, at which time the tether would be jettisoned, and the recovery effort (for the mother payload) would begin. During the operation period, the currents to each satellite would be determined, both for passive conditions, and with the packages actively biased with respect to each other. The attitude of the tether line with respect to the magnetic field will, of course, vary with time. Rotation of the tethered pair about their center of mass will allow studies of current collection parallel and perpendicular to the magnetic field line.

#### E. PAYLOAD

The proposed payload, and satellite, would largely be built and integrated at UAH, with assistance from WFF in key areas (In particular, machining deck plates, and acquiring standard WFF flight hardware such as transmitters). The main satellite provides power, a basic telemetry system (i.e. transmitters and receivers),

attitude control, and a magnetometer. Basic WFF services include environmental tests, launch, recovery, and ground telemetry.

1. Hollow Cathode

The core of the experiment is of course, the plasma source. We propose to use the standard hollow cathode geometry, used previously on the SERT II and ATS-6 ion engine experiments. Figure 4.10 and 4.11 illustrates the standard features and size of the Hollow cathode respectively. Gas (we will use Xenon) is fed

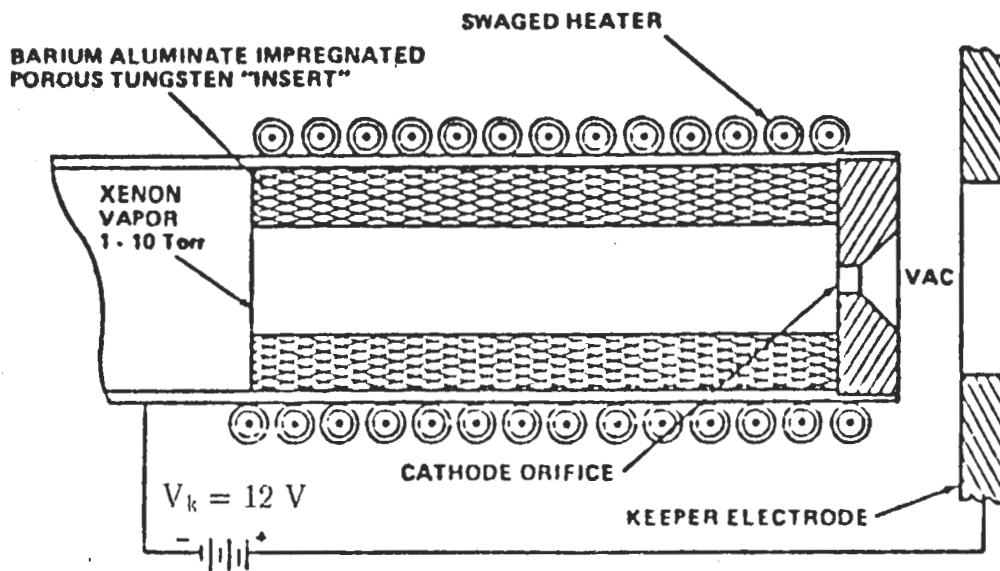


Fig. 4.10 Hollow Cathode Design

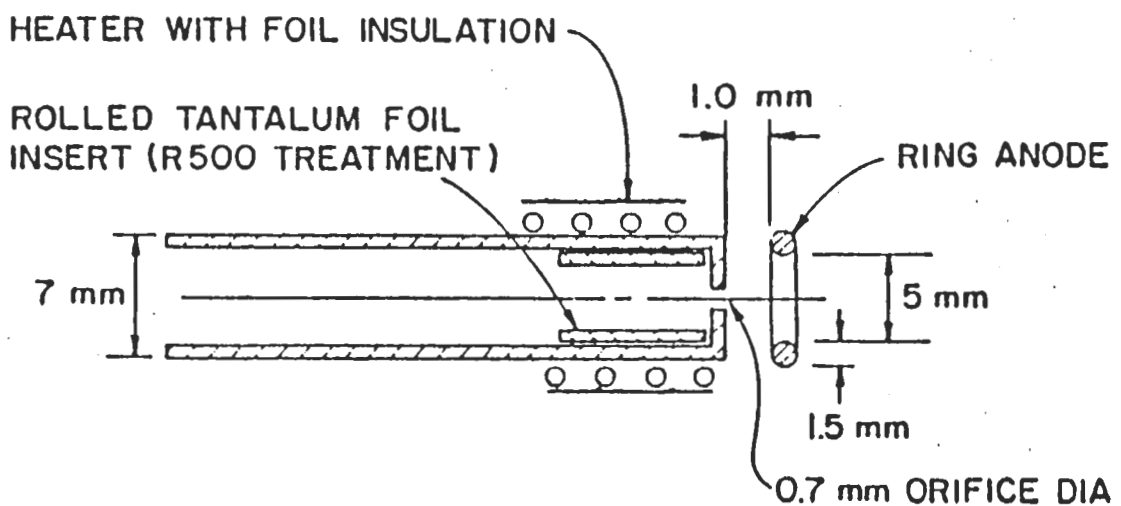


Fig. 4.11 Dimensions of Hollow Cathode

through the end of the cathode, passing through the cylindrical device, with an arc struck at the exit aperture. The porous tungsten insert provides a low work function electron emitting surface, which is typically operated at about 1000 °C, with heat supplied by an external heater. A typical cathode is 1/4" in diameter, and a few inches long. One problem with hollow cathode systems is contamination of the barium insert by ambient atmosphere, and long startup sequences.

This problem is resolved by a vacuum enclosure around the cathode, which is blown off after launch. Two designs have been considered for plasma source. The first of the Hughes Research Laboratory design recently implemented for the AF/Flight Model Discharge System (FMDS). This design is derived from the successful SPIBS design flown on the SCATHA satellite. The second possible supplier is SRS Inc, which provided a cathode system for the recent SPEAR-1 sounding rocket experiment.

## 2. Experiment Control and PCM Encoder

The encoder system developed at UAH provides the facility not only to collect and encode all data (analog and digital) into a high bit rate stream (750 kbps), but also to intelligently control complex experiments, to store the data at even higher bit rates (up to 12 Mbps) and to telemetry it back down to the ground during less interesting intervals. Significant processing power exists within this system (about 50 % of a VAX 780) so that on-board processing is convenient.

Instrument power at 28, +/-15, and +/-5 volts is provided. The output of the encoder directly drives NASA standard S-band transmitters and is compatible with all Wallops ground facilities. This system has now completed three successful space flights, the last being the CRIT I campaign which was one of the most complex that Wallops has yet flown.

A particularly valuable aspect of the fast-event-analyzer (Figure 4.12) is the "burst mode" capability—the ability to sample instruments at rates greater than 10 Mhz for 1–2 seconds. This will be particularly useful for studying the transient response of the system to changes in the bias voltage on the tether wire.

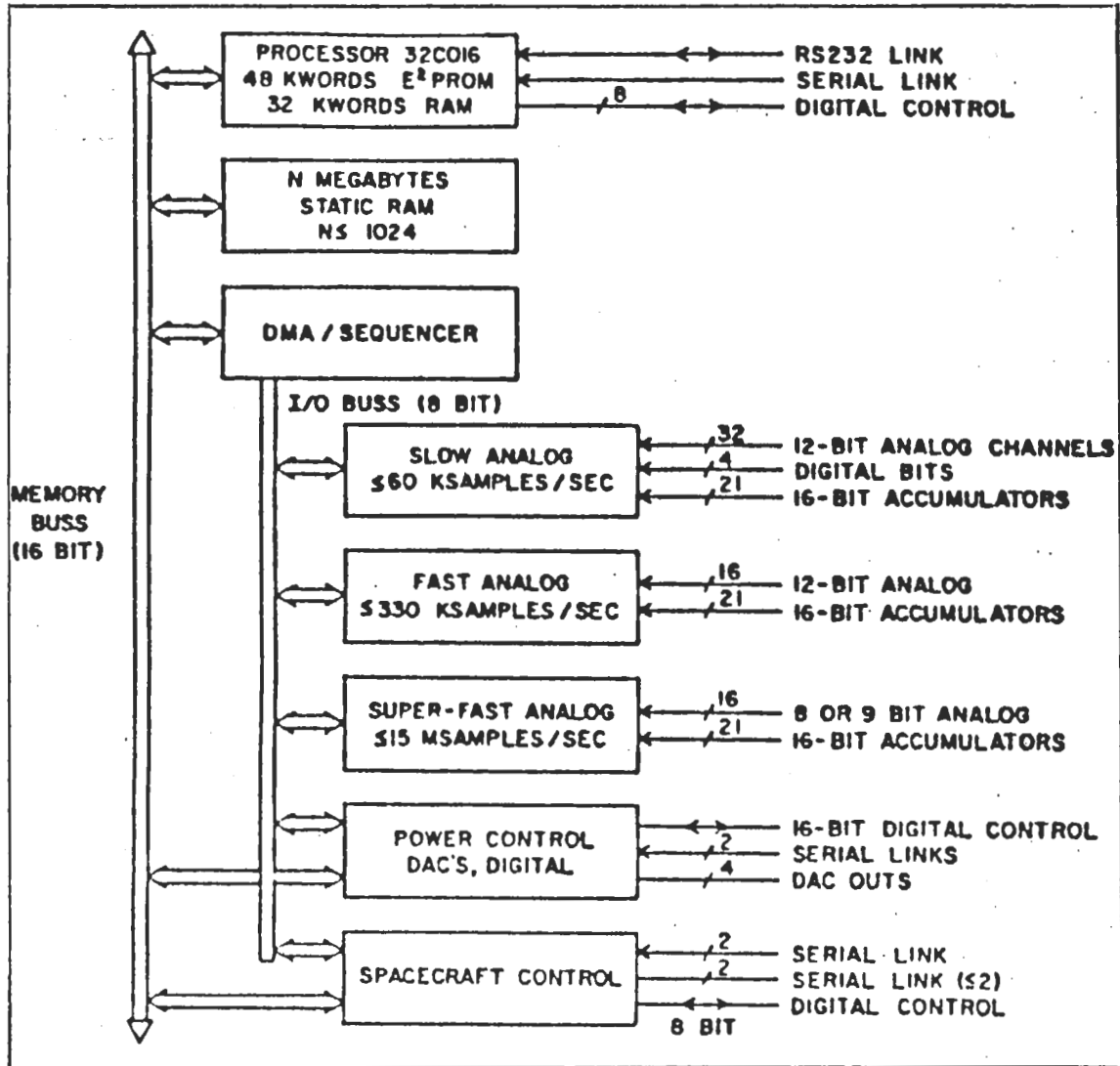


Fig. 4.12 UAH Fast Event System

### 3. Electric Field Instruments

The electric field instrument consists of a pair of spherical double probes on 3 m boom. The objectives of this experiment are to measure thermal electron density and temperature, the plasma wave spectrum, electric fields, and to provide a

reference point indicating payload potential. Two pairs of booms will be flown, placed as far apart as practical on the main payload, oriented orthogonally. This experiment design has been successfully used on numerous rocket experiments over the last decade. When the instrument is operated in the Langmuir probe mode, the spherical sensors are biased at fixed potentials relative to the plasma and the current collected by the spheres is measured.

By allowing the probes to float with respect to the vehicle, information about the payload potential can be obtained, and local electric fields can be measured. High speed sampling of the electric field data (using the super-fast channels of the flight computer) allow measurements at frequencies from 15 kHz to 10 MHz, allowing us to watch for high frequency waves (e.g. electron plasma waves). The low frequency waves (0–15 kHz) for electric fields or  $\delta n/n$  measurements will be sampled directly, allowing for observations of turbulence in the plasma, and key signals such as the lower hybrid resonance. One telemetry transmitter would be dedicated to these "wideband" measurements.

Electric field and density data from a recent flight from Sondre Stromfjord, Greenland is shown in Figure 4.13. As can be seen, the plasma density ranges from  $2 \cdot 10^5$  to about  $10^4$  on a typical flight to 500 km apogee.

#### 4. Thermal Plasma Analyzer (Ions and Electrons)

The objective of this pair of instruments is to obtain measurements of the distribution function of plasma ion components and electrons in as much detail as practicable. This will require the use of instruments having differential response in angle and energy, with energy coverage from a few eV to keV. The instruments primary tasks are to determine the satellite potential accurately, and to watch for nonthermal characteristics of the local plasma which indicate heating, or other interesting plasma interactions. The detectors can characterize the density, and

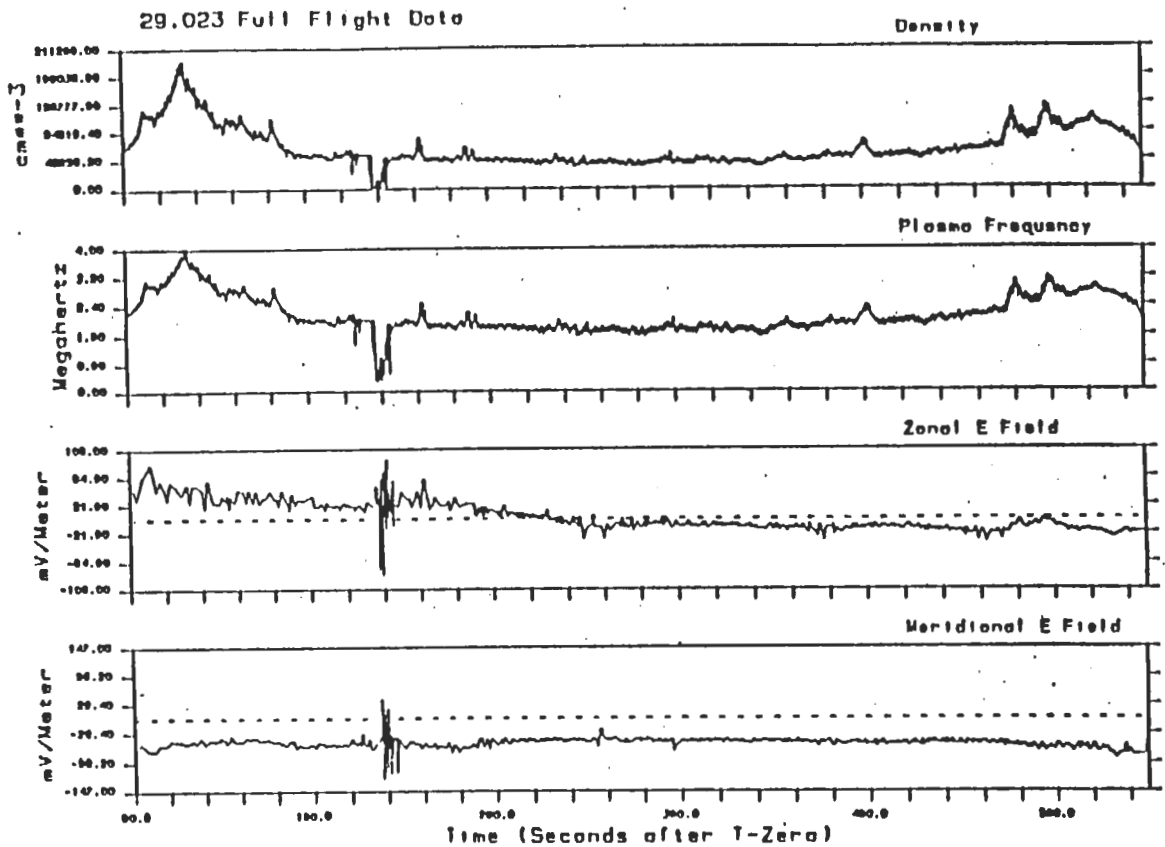


Fig. 4.13 Electric Field and Density Data

temperature of the low energy core of the electrons and ions, and also the supra-thermal features such as anisotropic heating or acceleration and conical angular distributions which may arise.

The electron detector (Figure 4.14) is an electrostatic analyzer (ESA) which the UAH group has successfully used on several rocket campaigns. It is a 2-D imaging spectrometer, covering the energy range from near zero to 3 keV, with 10 % energy resolution over that range. The ion detector is based on a modification of the ESA, in order to include mass resolution (Figure 4.15). This is done by adding a toroidal magnet at the exit aperture of the ESA. It will have sufficient mass resolution to separate  $H^+$ ,  $O^+$ , and  $Xe^+$ .

axis is detector rotation angle on the 3-axis-stabilized spacecraft, and the vertical axis is ion kinetic energy. The third axis, flux, is presented as shades of grey, with black corresponding to zero, or low counts. White, or light grey shades correspond to high flux. This is seen at high energies (10–80 keV), and in the lower left hand corner (–20° to +20°, 0 to 10 eV). This demonstrates the separation of local and distant plasma by energy and arrival direction. Ions from the ion engine (charge exchange) are found in the lower left hand corner.[Ref. 36]

Spectrometer results from the SPEAR–1 experiment using the basic (no mass analysis) design are illustrated in Figure 4.17. The data are from a period where a small sphere deployed on a boom was biased 15 kV with respect to the sounding rocket body. As a result, the rocket body was pushed 5 to 10 kV negative.

One-half second later, the data from Figure 4.17 are found. The peak in the ion flux from 3 to 4 keV indicate the detector (and rocket body) are charged to –3 to –4 kV. These data illustrate how the ESA design can be used to infer satellite potentials – a fundamental element of the mission.[Ref. 47]

## 5. Direct Current Measurements (Current Loop)

A major question to be addressed with this experiment is the question of how the currents flow from the satellite, and parallel and perpendicular to the magnetic field lines. Traditionally, currents are measured by using the observed ambient particle distributions. We will be making such measurements.

Generally, however, important portions of the ambient distribution function are easily missed, either due to satellite charging, or gaps on the angular coverage. Hence energy and angle space are inadequately covered. In the proposed mission, it would be highly desirable to have a direct measurement of current density, several meters from the satellite. A new technique for making such measurements has been developed at UAH. The principle of the current loop

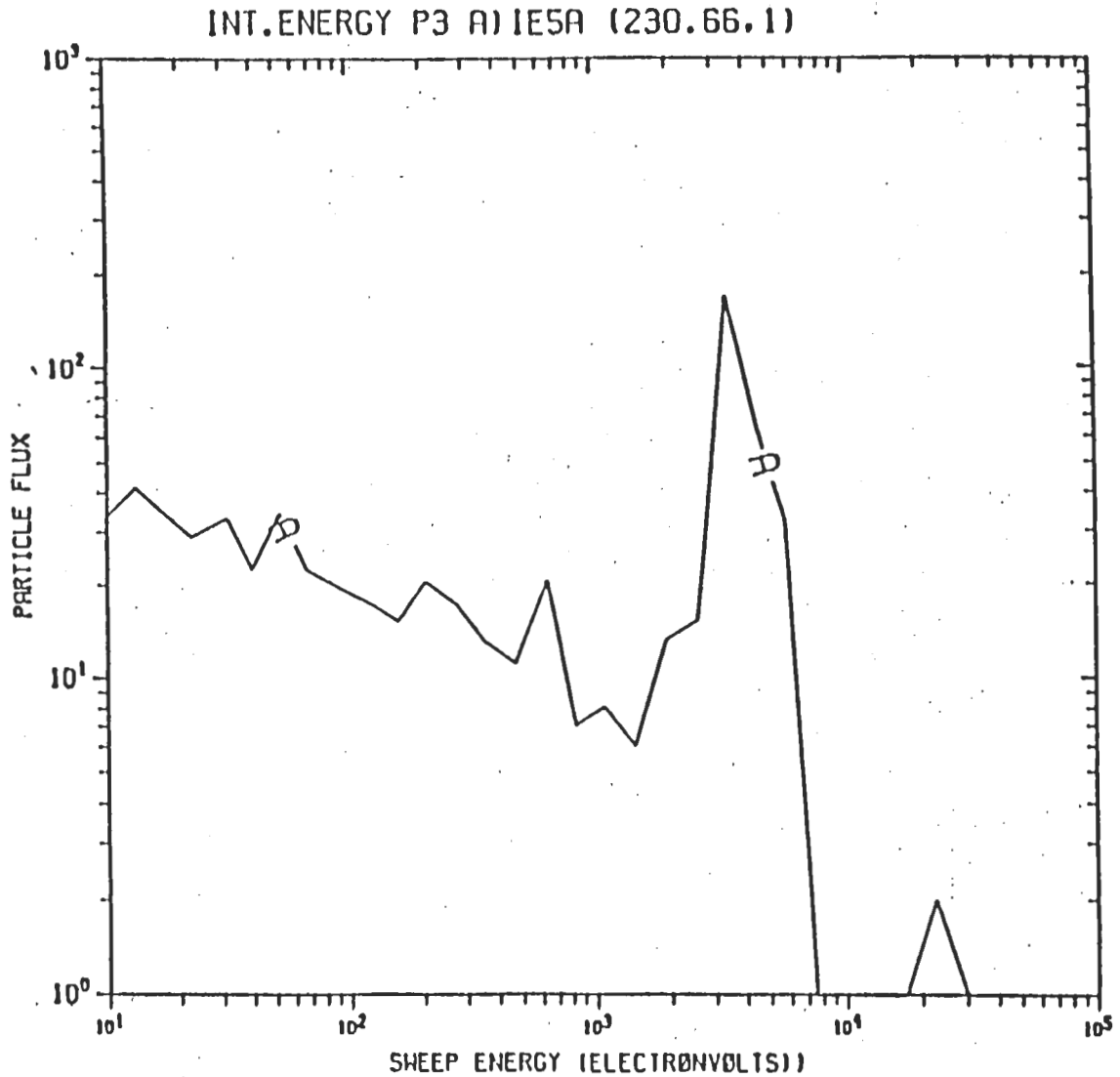


Fig. 4.17 Spectrometer Results from SPEAR-1

measurement, illustrated in Figure 4.18, determines the current through a loop of optical fiber by measuring the Faraday rotation of polarized light propagating around the fiber.

This technique allows measurement of currents at frequencies up to a few kilohertz and a sensitivity of a few microamps per square meter. It is impervious to electromagnetic interference from the spacecraft, and measures the entire current independent of the characteristics of the distribution function or the species that are

carrying it, and is relatively lightweight and rugged. The current loop will be deployed approximately 1-m from the mother payload.

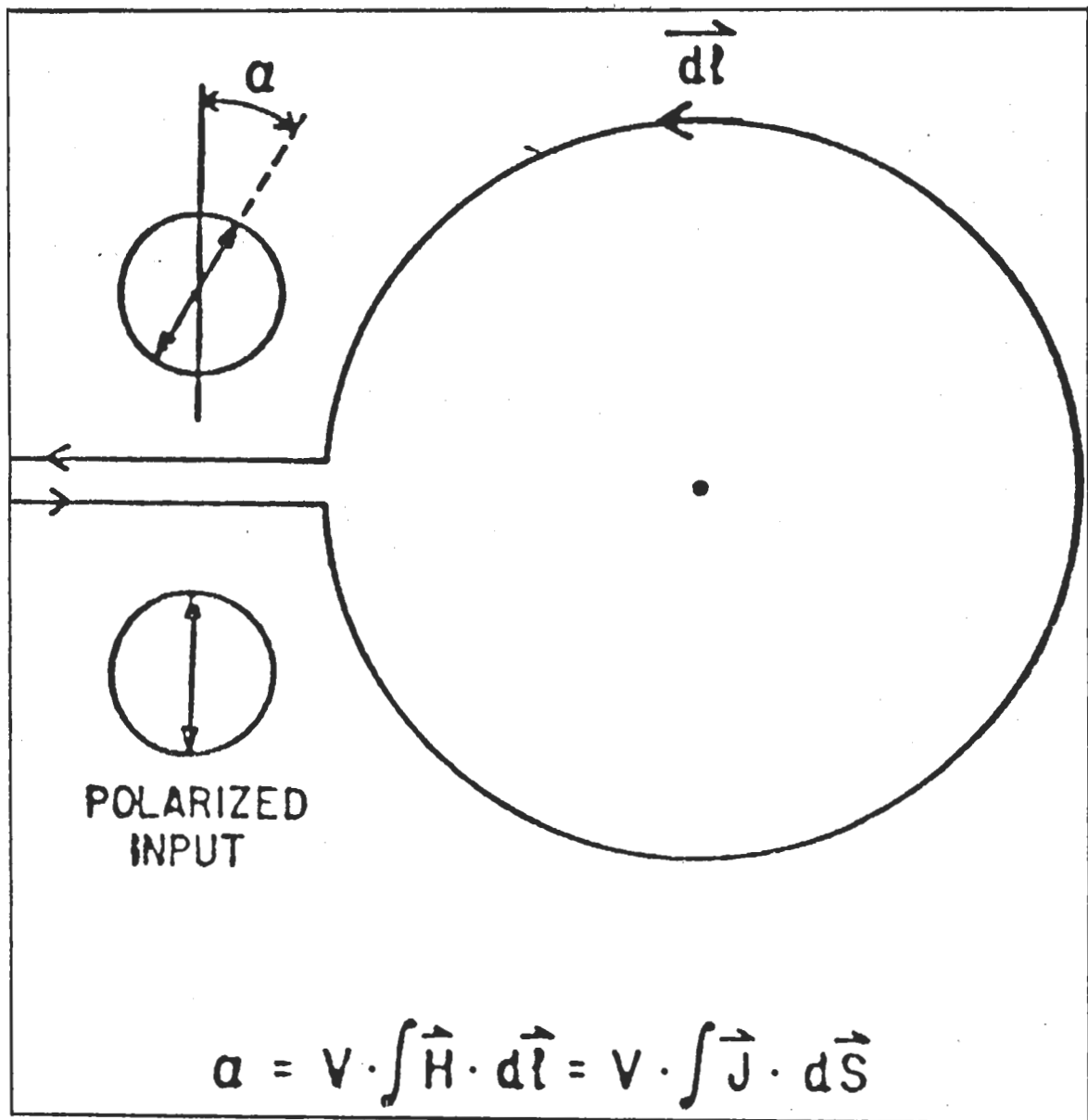


Fig. 4.18 Principle of the Current Loop Measurement

6. TV Camera

A low-light level television camera has been included in the design for two reasons. The primary reason is to watch for visual aspects of the "ignited

mode", and to determine the extent of the discharge region around the electron collecting subsatellite. The second reason is to verify deployment, and provide a secondary means of measuring the rocket-satellite separation. A standard "off-the-shelf" camera has been specified. The size is 160 mm x 47.5 mm x 50 mm and weight is 410 grams without lens. The supplier will be EEV, Inc.

#### 7. Magnetometer

Wallops Flight Facility will provide a flux-gate magnetometer with a resolution of about 100 nT that can be directly sampled on three-axes by the UAH telemetry system. This should be sufficient for attitude determination and the detection of any large magnetic disturbances.

## V. MODEL OF SYSTEM ELECTRODYNAMIC BEHAVIOR

### A. PROBE THEORY

The design and operation of the system described thus far depends on the currents and potentials that will be developed. These parameters are addressed in the following sections, beginning with elementary probe theory. The plasma consists of electrons, and ions, with, in our case, a substantial background. The interesting quantities to be determined using a probe are the particle temperatures, particle densities, and random current densities. These are the quantities that determine the current flow through the contactors and the tether wire, which is the main theme of this study.

Langmuir and Mott–Smith showed that a small metal electrode or "probe" inserted into the plasma can be used to determine some of these quantities experimentally, by applying various potentials and measuring the corresponding collected currents. We apply this basic probe theory to the HOCAT system, ignoring for now the extent of the Debye sheath.[Ref. 48]

When a probe is at plasma potential, it collects both the random electron and the random ion current. The electron current is much greater than the ion current because the electrons have much larger average velocities. If the electron distribution is characterized by a temperature  $T_e$ , then according to the kinetic theory, the random electron current density is:

$$J_e = N_o e V_{\text{random}} = N_o e \sqrt{\frac{KT_e}{2\pi m_e}} \quad (8)$$

where  $N_o$  is density,  $e$  is electron charge, and  $v_{th}$  is the average thermal velocity of the electrons. Typical ionosphere values give  $J = 1 \text{ mA/m}^2$  so to collect 1 A (electron) current requires a conducting balloon whose radius is 12.6 m.

If we ignore the effect of the potential on the ambient plasma distribution (e.g. Debye shielding), we can determine how the particle flux varies with potential. For a negatively charged body, flux for the repelled electrons can be expressed as follows:

$$\text{Flux} = N_o \sqrt{\frac{KT_e}{2\pi m_e}} e^{-\left(\frac{e\phi}{KT_e}\right)} = N_o \sqrt{\frac{KT_e}{2\pi m_e}} \left(1 - \frac{e\phi}{KT_e}\right) \quad (9)$$

where  $e\phi > 0$ . The flux of electrons for an attractive potential can be expressed as follows:

$$\text{Flux} = N_o \sqrt{\frac{KT_e}{2\pi m_e}} e^{-\left(\frac{e\phi}{KT_e}\right)} = N_o \sqrt{\frac{KT_e}{2\pi m_e}} \left(1 + \frac{e\phi}{KT_e}\right) \quad (10)$$

where  $e\phi > 0$ . This expression for a collector with spherical geometry can be expressed as follows:

$$J_e = N e v_{th} \left(1 + \frac{e\phi}{KT_e}\right) \quad (11)$$

where  $J_e$  is current density,  $e$  is electron charge,  $v_{th}$  is the average thermal velocity,  $\phi$  is spacecraft potential,  $K$  is Boltzmann constant, and  $T_e$  is electron temperature. The total current collected to the outer surface of spacecraft is just  $I = J_e \cdot \text{Area}$ . This would be the main term for the positive end of the tether system, excluding plasma contactor operations. Figure 5.1 shows a plot of the electron current density

which would be collected at the positive end of a tether, in the absence of a plasma source device, at three different altitudes. The model ionosphere values previously illustrated were used here.

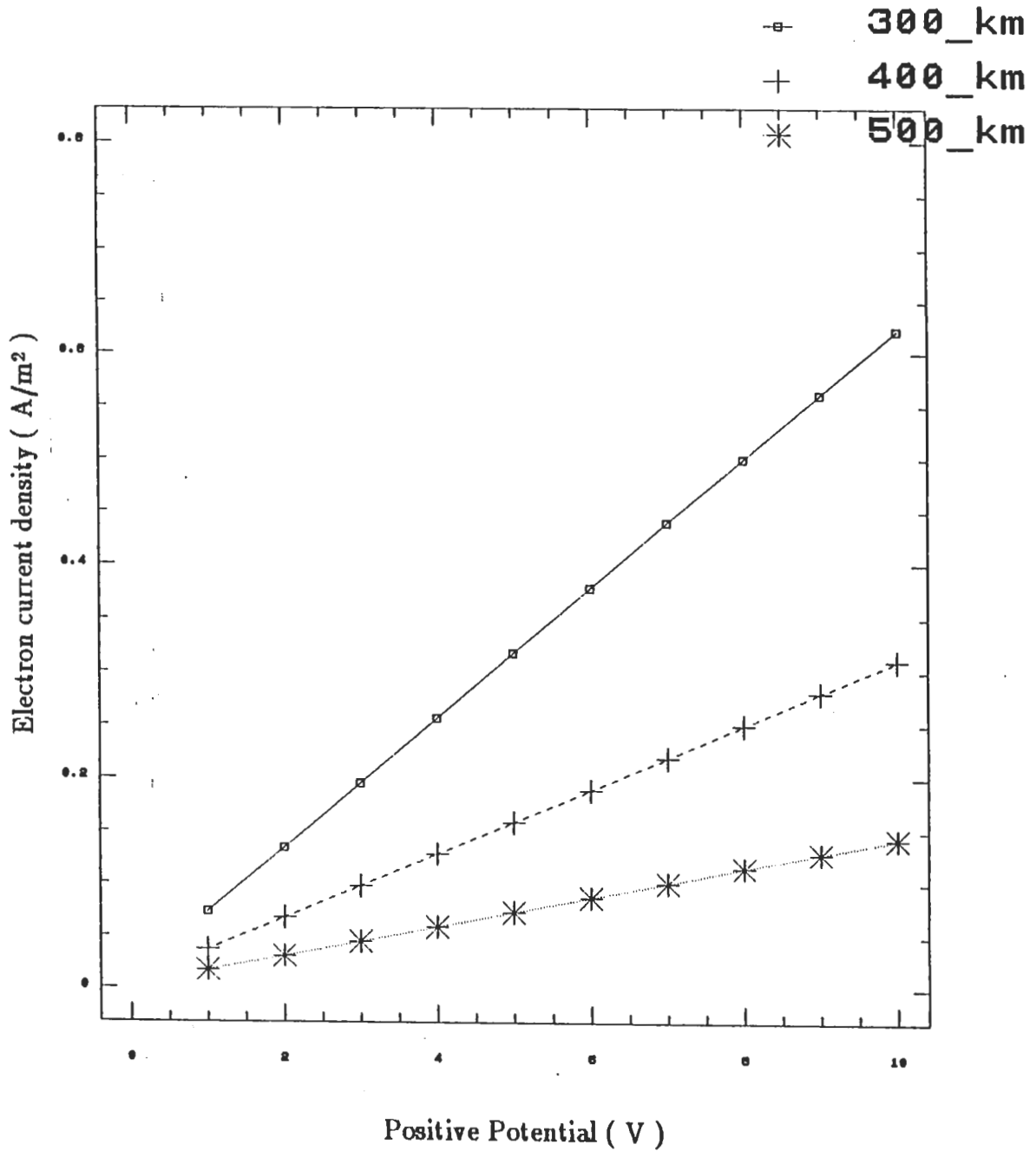


Fig. 5.1 Plot of Electron Current Density vs Positive Potential

Ion collection at the negative end of the tether system has a similar functional form. For the ion collector, the equation can be expressed as follow:

$$J_i = N q V_i \left( 1 - \frac{q \phi}{K T_i} \right) \quad (12)$$

where  $V_i = \sqrt{K T_i / M}$ ,  $M$  is ion mass. The ion current is much smaller than the electron current because of the greater mass. Figure 5.2 shows the plot of the ion current density versus negative tether end potential.

If we specify the collected current, we can determine  $\phi_+$ ,  $\phi_-$ , and hence the necessary bias voltage to be applied. Equilibrium requires that the collected electron current equal to the collected ion current for the system. If we assume for the moment that collecting areas are equal – system equilibrium should be relatively small positive potential at one end, relatively large negative potential at the opposite end (e.g.  $|\phi_+| \ll |\phi_-|$ ). If we assume that the current density is 0.2 A/m<sup>2</sup>, the potential is about 3, 6, and 15 V for the three different altitudes. This current density is applied to the ion collection for equilibrium condition. Potential difference between the electron collection and ion collection is bias potential. Figure 5.3 shows plot of current density versus bias potential for those altitudes.

Up to this point, we have ignored the Debye shielding effect and collisions. If we assume Debye approximations can be applied, we can obtain an opposite limit on the required bias potential. There is a practical limit to the collected current for large potentials. This can be estimated by considering the current collected at the edge of the Debye sheath. If we use the Debye lengths inferred in previous sections, and assume cylindrical geometry, the total collected current can be expressed as:

$$I = J_{\text{thermal}} \cdot 2 \pi r^2 \quad (13)$$

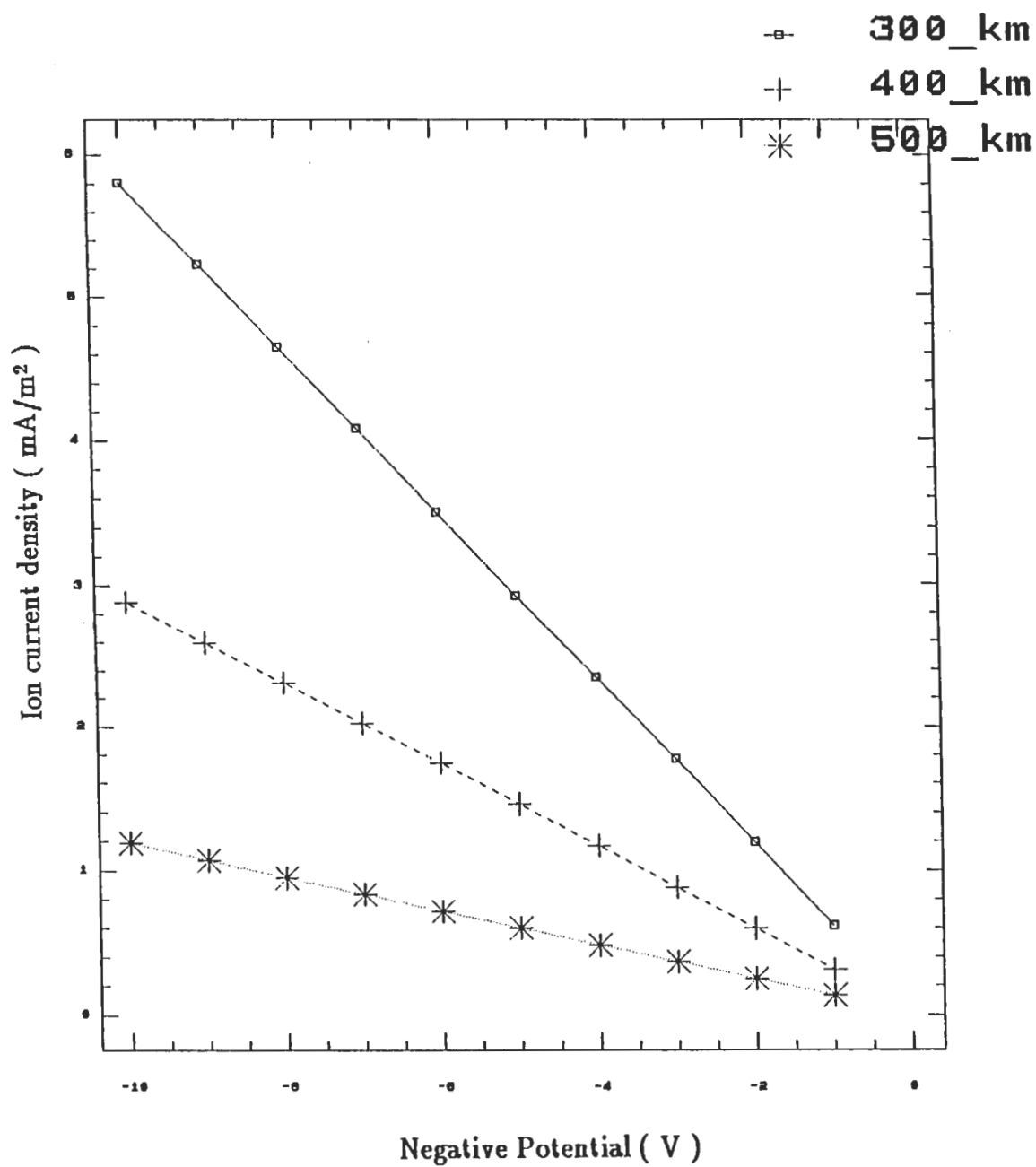


Fig. 5.2 Plot of Ion Current Density vs Negative Potential

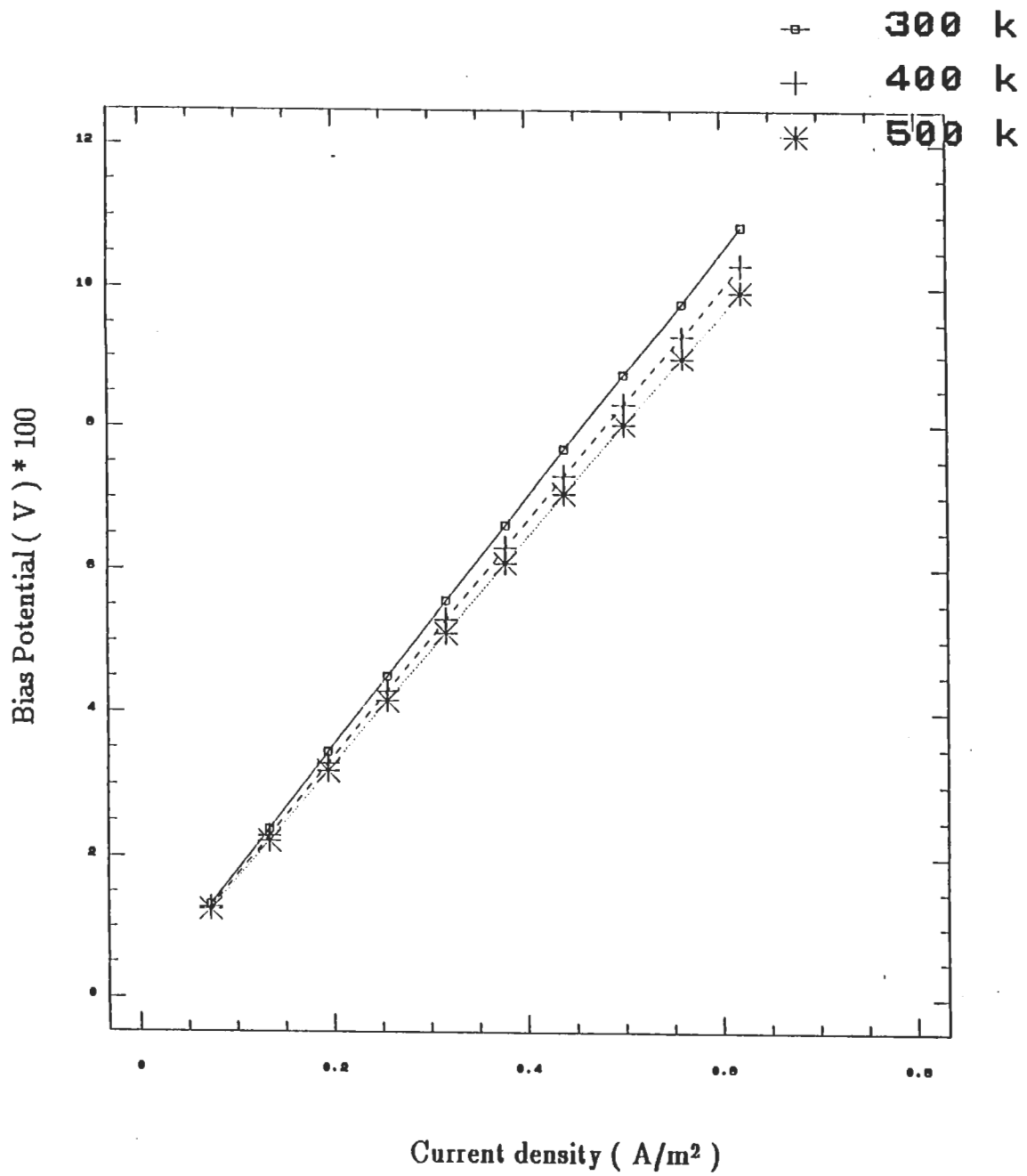


Fig. 5.3 Plot of Bias Potential vs Current Density

where  $r$  is Debye length for large Debye length, or  $r$  is sum of the radius of spacecraft and Debye length for small Debye length. Debye lengths are 0.52, 0.75, and 1.1 cm at altitudes 300, 400, and 500 km which are much smaller than diameter of the rocket. Hence the Debye effect limits the collected current to the thermal values. The thermal current density  $J_{\text{thermal}}$  is 4.7, 2.6, and 1.3 mA/m<sup>2</sup>. Using equation (13), the maximum current that can be collected in a collisionless plasma is 1.4, 0.78, and 0.39 mA to the surface perpendicular to the magnetic field line (e.g. saturation current ignoring conductivity—but with turbulence to enhance transport when there is a magnetic field).

Obviously, these extremes do not adequately define the problem. For our case of  $J \gg J_{\text{th}}$ ,  $\phi \gg KT$ , alternate approaches must be found. Theories developed by Beard and Johnson, Parker and Murphy, and Linson can be applied. These works, summarized by Linson, estimate the current collection to a highly charged body in the ionosphere. They differ mainly in their approach to dealing with magnetic fields. Ignoring magnetic effects, the vehicle as cylinder along magnetic field with radius 'a' meters, and a collecting area of radius 'b' which is perpendicular to the magnetic field. Figure 5.4 shows the schematic diagram of physical system.[Ref. 49]

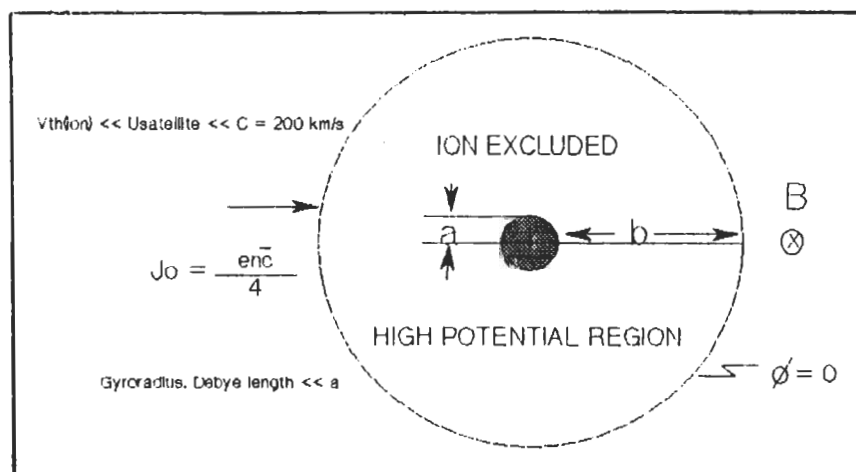


Fig. 5.4 Schematic Diagram of System

The ratio between I and I<sub>0</sub> can be expressed in terms of the ratio between the radius of the collecting area and the radius of the rocket as follows:

$$\frac{I}{I_0} = \left(\frac{b}{a}\right)^2 \quad (14)$$

where I<sub>0</sub> is thermal current, and I is collected current which is 1 A for this experiment. The potential can be calculated in terms of  $\frac{I}{I_0}$  for the cases of spherical space charge limit by equation (15) as follows:

$$\phi = 34 a^{\frac{4}{3}} \left(\frac{I}{I_0}\right)^{\frac{7}{6}} \quad (15)$$

Figure 5.5 shows the measured data from the SPEAR-1 experiment. This ionosphere experiment shows the relationship between bias voltage and sphere current, up to 40 kV, 0.2 A. The (positive) sphere potential is about 75 % of the bias, the rocket body is about  $-0.25V_{\text{bias}}$ . These data suggest that the (approximately) linear relationship of equation (15) can be applied to ionospheric current collection.

If the magnetic field effects are partially included, as developed by Parker and Murphy, the ratio  $\frac{I}{I_0}$  can be expressed by equation (16), which gives rise to a "dynamic upper limit", as follows:

$$\frac{I}{I_0} \leq 1 + \left(\frac{4\phi}{\phi_0}\right)^{\frac{1}{2}} \quad (16)$$

where  $\phi_0 = 178*a^2$  for a typical magnetic field strength of 0.45 Gauss. To bridge the gap between the magnetic field limited collection and space charge limited

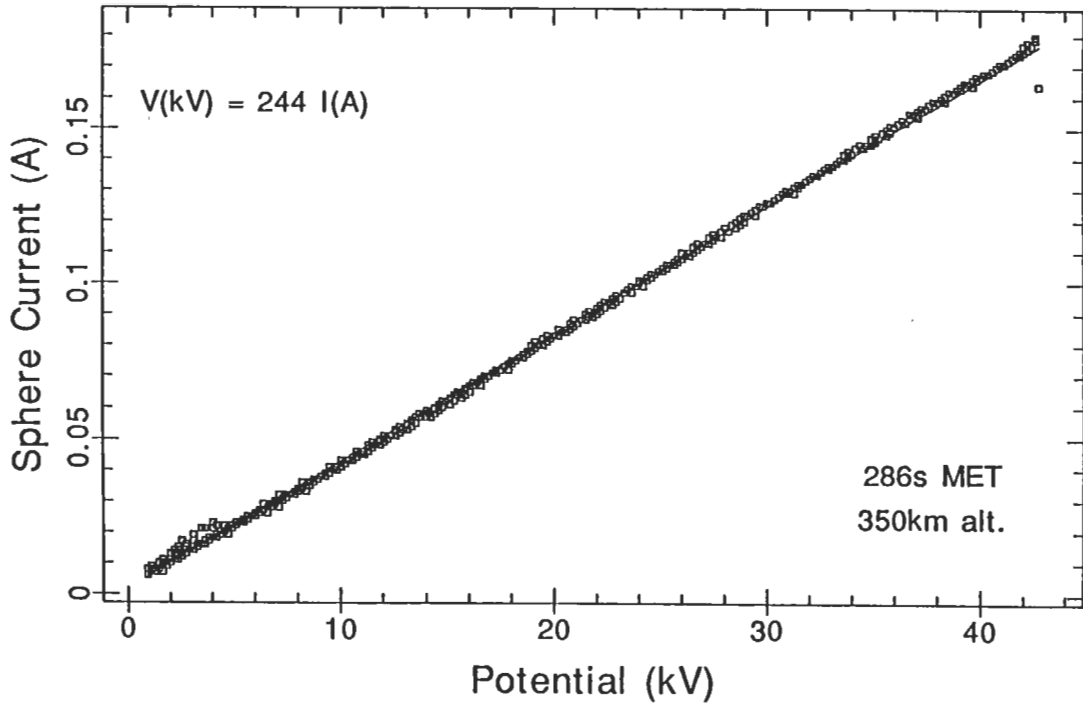


Fig. 5.5 Sphere Current Data from SPEAR-1

collection, Linson has developed a theory which deals with the magnetic field. The ratio  $\frac{I}{I_0}$  can be expressed in terms of the potential by equation (17).

$$\frac{I}{I_0} \approx \frac{2\phi_0}{q_c\phi_0[\ln(2\phi/q_c\phi_0) - 1]} \quad (17)$$

where  $q_c$  is  $1/4 - 1$ . Figure 5.6 shows the plot of  $\frac{I}{I_0}$  versus bias potential for spherical space charge limit, dynamic upper limit, and the cylindrical model with magnetic field. The radius 'b' of the collecting area is 5.8, 7.8, and 11 m for three different altitudes above. Figure 5.6 shows the relation between radius and bias potential so that the radius can be expressed as a function of potential. If we assume that the potential is 100 – 200 V, the radius is 3.5 – 5.7 m.

For ion collection, first, the space charge limited current problem is similar so that the area must be much larger. The radius is 45 m at 400 km altitude, which in

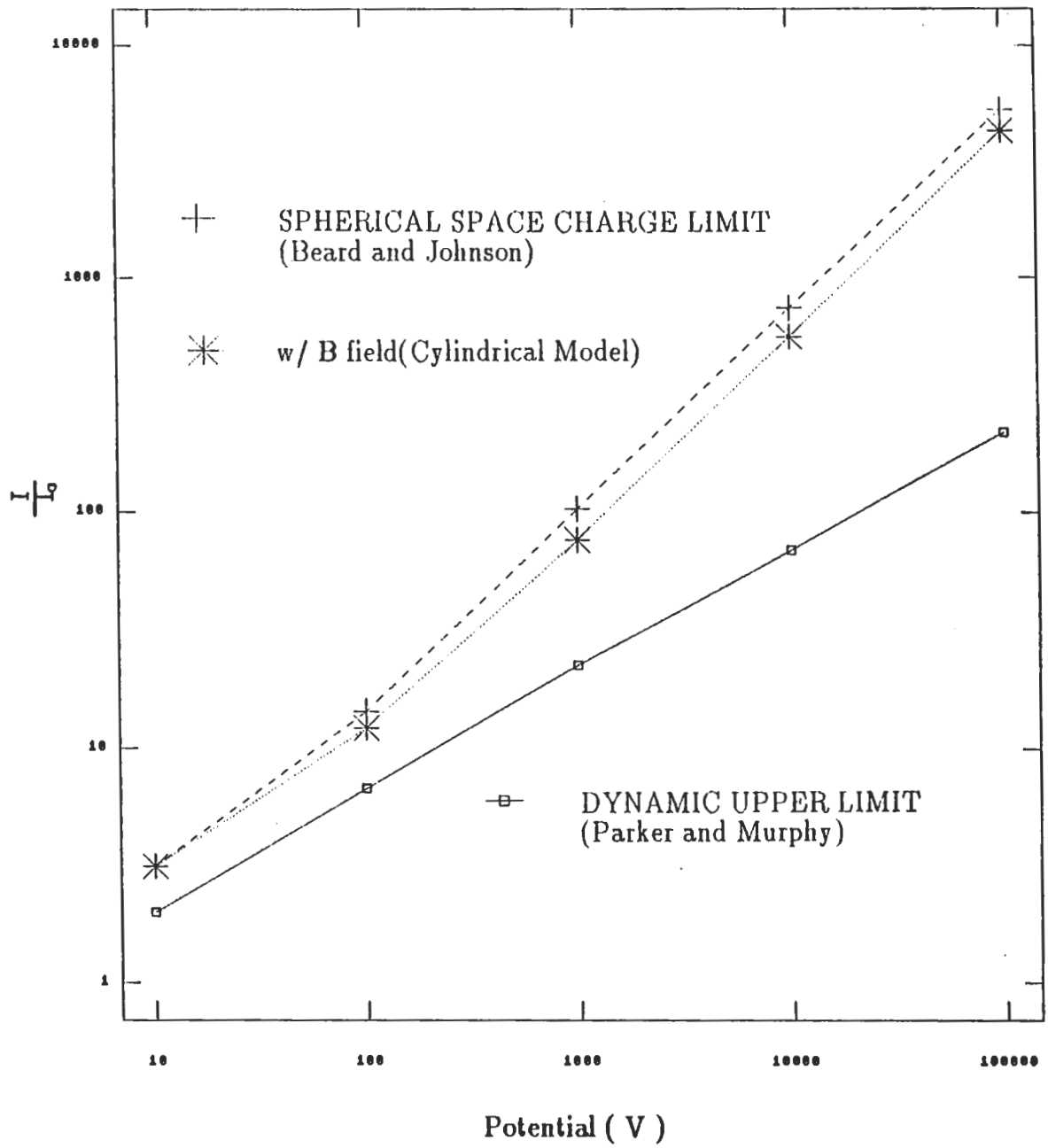
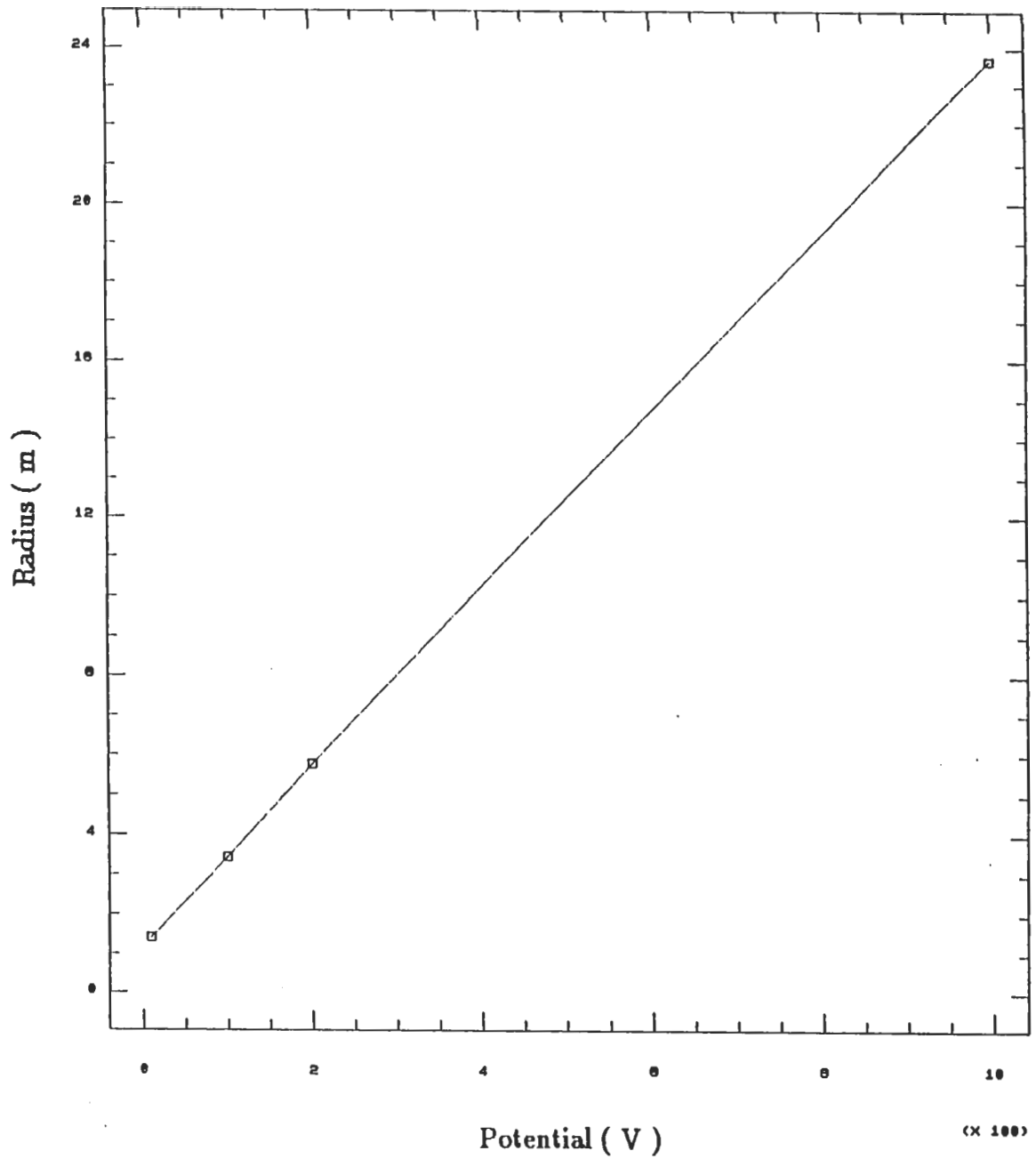


Fig. 5.6 Plot of  $\frac{I}{I_0}$  vs Positive potential



$$\text{Radius} = 2.253 \cdot 10^{-2} \cdot (\text{Bias Potential}) + 1.173$$

Fig. 5.7 Plot of Radius vs Bias Potential

turn gives a higher potential of about 8 kV. This does not include the important effect of electron emission from rocket surfaces, due to secondary electron production from the surface or nearby neutral gas (outgassing). This leads to greatly reduced potentials. For the SPEAR-1 experiment, the illustrated bias potential was 40 kV and the reduced potentials  $\phi_+$ ,  $\phi_-$  were  $\pm 10$  kV.

## B. MODIFICATIONS DUE TO PLASMA CONTACTOR

The introduction of the plasma contactor has two effects. First, it is an effective electron emitter. Therefore, the ion collection problem is eliminated. By comparison with Wilbur's data (presented earlier), potentials of less than 100 V are needed to extract Amperes of electrons. Second, the electron collection process is enhanced. For the tethered satellite system, the potential difference between the electron collector and electron emitter will be the potential that we have to apply through the tether for the tethered rocket system.

### 1. Electron Emission

The theory for electron transport has been applied in simplified form to electron emission to the space plasma. When the hollow cathode is used as an electron emitter, the plasma density at distance  $R$  from the orifice can be expressed as equation (18):[Ref. 50]

$$R = r_o \left( \frac{n_o}{n_{amb}} \right)^{\frac{1}{2}} \quad (18)$$

where  $n_o$  is produced electron density (about  $10^{12}/\text{cm}^3$ ),  $r_o$  is distance from the orifice about 1 cm, and  $n_{amb}$  is  $10^6/\text{cm}^3$ . For the collisionless plasma, there is an effective collision frequency which determines the potential-current relation. It can be expressed as follow:

$$\nu = \alpha \omega_p \quad (19)$$

where  $\alpha$  is about 0.1,  $\omega_p$  is the plasma frequency ( $\sqrt{4\pi n_e^2/m}$ ). The potential can then be expressed in terms of known parameters as function of  $r_o$ :

$$\phi_o(r_o) = KTe \ln\left(\frac{n_o}{n_{amb}}\right) + 9 \times 10^{10} \frac{\alpha I_{amp}}{r_o \omega_p(r_o)} \frac{1}{2} \ln\left(\frac{n_o}{n_{amb}}\right) \quad (20)$$

A hollow cathode operating in the spot mode at a flow rate of 100 mA equivalent, produces an electron density of about  $10^{12}/\text{cm}^3$  at about 1 cm from the orifice. For those values, the impedance is 23  $\Omega$ . Therefore, the potential drop is 23 V for a 1 Ampere system.

## 2. Electron Collection

Electron collection can again be considered as a problem of establishing a conducting plasma cloud, of sufficient radius to collect the required current. Figure 5.8 shows the plasma cloud expansion model. The three density regions are defined here as the inner, collisional, high density region (a few cm), a transition region (a few m in radius), and "ambient" low density collisionless plasma. The diameter of the collecting cloud is not changed from our previous discussion – only the necessary potentials. The space charge limited condition has been relaxed by the addition of positive space charge from the contactors.[Ref. 51]

The current potential relation can be estimated if we assume that there is no magnetic effect, and the system is operating at constant current. The plasma ions stream out across the sheath, canceling a portion of the electron space charge, which is formed by the inward streaming electrons. The ratio of the thermal fluxes in this case is just that due to the relative mobility.

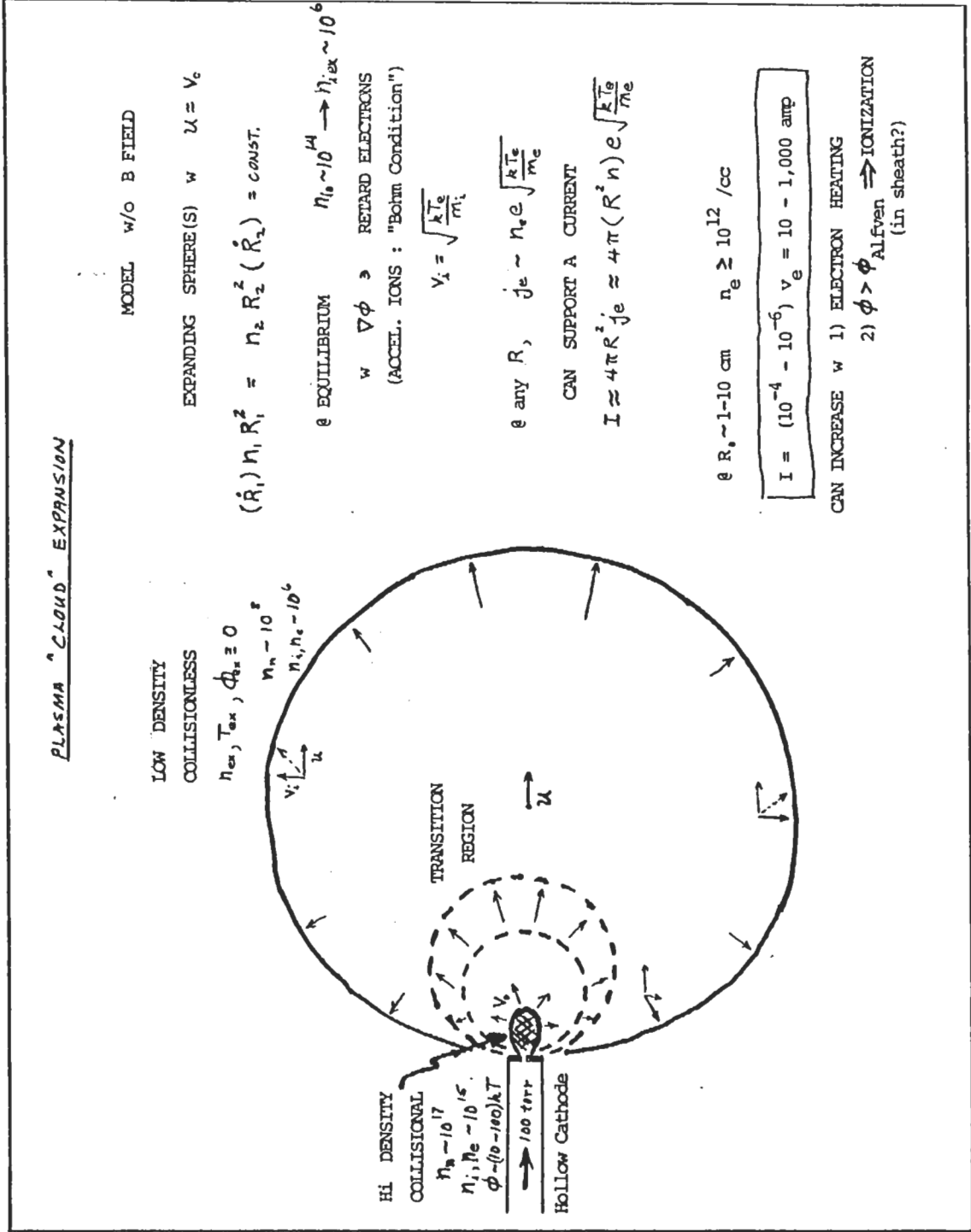


Fig. 5.8 Plasma Cloud Expansion Model[Ref. 51]

$$J_i = \sqrt{\frac{M_e}{M_i}} J_e \quad (21)$$

This relation is known as the "Langmuir condition" which is the basic stability condition for a strong plasma double layer. At this ion current, the voltage required to sustain a fixed electron current is reduced by one-third. If the "Langmuir condition" ion current is exceeded where  $\sqrt{m/M} I_e < I_p < I_e$ , the generated plasma remains quasineutral and the ions expand hydrodynamically. This will lead to substantially reduced potentials. Theories developed by Parks and Katz and Hastings indicate potentials of about 20–30 V for  $\alpha$  of 0.2 are necessary to draw 1 Ampere current. Theoretical works by Dr. D Hastings have been investigating the radius and gain for the ambient plasma to develop the function  $R = R(\phi)$ . [Ref40]

### C. SUMMARY

Relatively large (kilovolts) potentials are developed in ionospheric systems driven to the Ampere level. For both the electron emitting and electron collecting ends of the tethered satellite system, locally generated plasmas eliminate the space charge sheath. The high voltages necessary to transport charge across a space charge sheath makes the sheath regions the highest impedance portions of the tether system. Reducing this impedance by local plasma sources will greatly enhance the effectiveness of a tethered satellite system. Systems with hollow cathodes are predicted to develop potentials of the order 10 V. This value is in contrast to laboratory results which indicate that potentials of order 100 V were needed to collect 1 Ampere electron current. The conclusion which results from these estimates is that the primary energy range that the particle detectors should be designed for is the 1 – 100's of eV range, with at least some capability in the kilovolts range.

## VI. CONCLUSIONS AND RECOMMENDATIONS

This study has defined the the Hollow Cathode sounding rocket experiment (HOCAT). The purpose of this experiment is to measure the coupling of large currents (up to 1 A) from a satellite into the ambient plasma, and the nature of the return path through the plasma. Two bodies will be deployed to approximately 100 m separation with Hollow Cathode subsystems mounted at both ends. The system will be aligned along the geomagnetic field line during the initial deployment. The practical deployment system for this rocket payload will be based on Canadian OEDIPUS deployment system.

Laboratory and theoretical studies of Hollow Cathode performance have been reviewed. Analysis suggests that for the HOCAT system to derive 1 A current, a bias potential of about 30 V will be required. This bias estimate should be within a factor of 3 of being correct. Hence, power system should designed to cycle the bias from 1 to 100 V. Once the current reaches 1 A, the bias potential will be constant (e.g. current limited operation).

Instrumentation will include particle detectors with with coverage up to 1 – 2 keV, and mass analysis for  $H^+$ ,  $O^+$ , and  $Xe^+$ . Hence, it will be possible to infer negative potentials, and the nature of local plasmas accurately. Direct current measurement can be made through the current loop of optical fiber by measuring Faraday rotation of polarized light propagating around the fiber. This allows measurement of currents at frequencies up to a few kilohertz and a sensitivity of a few microamps per square meter. The langmuir probe will provide us with measurements of thermal electron density and temperature, the plasma wave

spectrum, electric fields, and a reference point indicating payload potential. The wave data will make possible to search for turbulence, and plasma heating signatures in the VLF and HF frequency range.

The results of this experiment will enable us to understand how the the Hollow Cathode works as a current source and sink. If we succeed in emitting/collecting 1 A current, such subsystems can be applied to long tether systems which can produce power up to MW level. Similarly, they can be employed for experiments with large electron guns which require current balance. This experiment should demonstrate the validity of theories previously developed for laboratory work, or indicate which new physical processes must be included to properly model charged particle beam and electrodynamic tether system.

## LIST OF REFERENCES

1. **Stuart, D. G.**, *A Guidance Algorithm for Cooperative Tether-Mediated Orbital Rendezvous*, pp. 31–45, MIT, 1987.
2. **Grossi, M. D.**, "Historical Background Leading to the Tethered Satellite System (TSS)" *AIAA 24th Aerospace Sciences Meeting*, Reno. 6–9 January, 1986.
3. **Lang, D. L., and Nolting, R. K.**, *Operation with Tethered Space Vehicles* Gemini Summary Conference, Manned Spacecraft Center, NASA SP-138, 1967.
4. **Piland, R. O., and Penrod, P. R.**, *Summary of the Gemini Program and Its Effect on Manned Space Science*, The seventh International Symposium on Space Technology and Science, Tokyo, pp. 27–53, AGNE Publishing Inc., 1967.
5. General Research Corporation Report 1545-03-88-TGM, *Spring Electrodynamic Tether Workshop*, by **K. Kolecki**, Section No. 2, 18–19 May, 1988.
6. Facility Definition Team, Utah State University, Report NASA Contract NAS8-33383, *The Tethered Satellite System*, by **P. M. Banks**, pp. 7–75, 23 April, 1980.
7. **Sasaki, S., Oyama, K. I., Kawashima, N., Hirao, K., Obayashi, T., Raitt, W. J., Williamson, P. R., Banks, P. M., and Sharp, W. F.**, "Results from a Series of US/Japan Tethered Rocket Experiments", *NASA/AIAA/PSN International Conference on Tethers in Space*, 1986.
8. **Maehlum, B. N., Denig, W. F., Egeland, A. A., Friedrich, M., Hansen, T., Holmgren, G. J., Maseide, M., Maynard, N. C., Narheim, B. T., Svenes, K., Torkar, K., Troim, J., and Wingham, J. D.**, "A High Current Electron Beam Experiment on a Sounding Rocket from Andoya Rocket Range", *The 8th ESA symposium on European Rocket and Balloon Programs and Related Research*, (EAS SP-270) SWEDEN, 17–23 May, 1987.
9. **Obayashi, T., Kawashima, N., Kuriki, K., Nagatomo, M., Ninomiyo, K., Sasaki, S., Yanagisawa, M., Kudo, I., Ejiri, M., Roberts, W. T., Chappell, C. R., Reasoner, D. L., Burch, J. L., Taylor, W. L., Banks, P. M., Williamson, R.R., and Garriott, P. M.**, "Space Experiments with Particle Accelerators", *Science*, Vol. 225, pp. 195–196, 1984.

10. **Riedler, W.**, "Proposal for an Active Space Potential Control Experiment for the STSP CLUSTER Mission Part 1: Scientific/Technical Plan", IWF, Austira, July 1987.
11. **Hess, W. N., Trichel, M. C., Davis, T. N., William, C., Geggs, G. E., Kraft, E. S., Stassinopoulos, E., and Maier, E. J.**, "Artificial Aurora Experiment and Principle Results" *Journal of Geophysical Research*, Vol. 76, No. 25, 1971.
12. **Winckler, J. R.**, "An Investigation of Wave Particle Interactions and Particle Dynamics Using Electron Beams Injection from Sounding Rockets", *Space Science Reviews* 15 (1974), pp. 751–780, 1974.
13. **Winckler, J. R.**, "A Summary of Recent Results under the ECHO Program for the Study of the Magnetosphere by Artificial Electron Beams", *Comic Physics Technical Report* 168, 1 September, 1976.
14. **Sasaki, S., Kawashima, N., Kuriki, K., Yanagisawa, M., and Obayashi, T.**, "Vehicle Charging Observed in SEPAC Spacelab-1 Experiment", *Journal of Spacecraft*, Vol. 23, No. 2, 1985.
15. **Beghin, C.**, "Phenomena Induced by Charged Particle Beams", *Science*, Vol. 225, pp. 188, July 1984.
16. **Olsen, R. C.**, "Experiments in Charge Control at Geosynchronous Orbit-ATS-5 and ATS-6", *Journal of Spacecraft and Rocket*, 1985
17. **Getty, W. D., and Smullin, L. D.**, "Beam-Plasma Discharge: Buildup of Oscillations", *Journal of Applied Physics*, Vol. 34, pp. 3421, 1963.
18. **Israelson, G. A., and Winckler, J. R.**, "Effect of a Neutral N<sub>2</sub> Cloud on the Electrical Charging of an Electron Beam-Emitting Rocket in the Ionosphere: ECHO IV", *Journal of Geophysical Research*, Vol. 84, No. A4, 1 April, 1979.
19. **Grandal, B.**, "*Artificial Particle Beam in Space Plasma Studies*", pp. 3–33, Plenum Press., 1982.
20. **Burch, J. L.**, "Space Plasma Physics Results from Spacelab-1", *Journal of Spacecraft*, Vol. 23, No. 3, May-June 1986.
21. **Watermann, J., and Wilhelm, K.**, "Space Shuttle Charging or Beam-Plasma Discharge: What Can Electron Spectrometer Observations Contribute to Solving the Questions ?", *Journal of Geophysical Research*, Vol. 93. No. A5. pp. 4134–4140, May 1988.
22. **Kaufmann, R. L., Arnoldy, R. L., Moore, T. E., Kintner, P. M., Cahill Jr, L. J., and Walker, D. N.**, "Heavy Ion Beam-Ionosphere Interactions: Electron Acceleration", *Journal of Geophysical Research*, Vol. 90, No. A10, pp. 9595–9614, October 1985.

23. Moore, T. E., Arnoldy, R. L., Kaufmann, R. L., Cahill Jr, L. J., Kintner, P. M., and Walker, D. N., "Anomalous Auroral Electron Distribution Due to an Artificial Ion Beam in the Ionosphere", *Journal of Geophysical Research*, Vol. 87, No. A9, pp, 7569–7579, September 1982.
24. STAR Laboratory, Stanford University, Report D131–1, *New Concepts in Ionospheric Modification* by Storey, L. R. O., Bank, P. M., Fraser–Smith, A. C., Gilchrist, B. E., Harker, K. J., and Williamson, P. R., pp. 83–133, 1987.
25. Häusler, B., Treumann, R. A., Bauer, O. H., Haerendel, G., Bush, R., Carlson, C. W., Theile, B., Kelley, M. C., Dokukin, V. S., and Ruzhin, Yu. Ya., "Observations of the Artificially Injected Porcupine Xenon Ion Beam in the Ionosphere", *Journal of Geophysical Research*, Vol. 91, No. A1, pp. 287–303, 1 January, 1986.
26. Hunter, R. E., and Bartlett, R. O., "Cesium Contact Ion Microthruster Experiment aboard Applications Technology Satellite (ATS–IV)", *Journal of Spacecraft and Rockets*, Vol. 6, 1969.
27. Gavrilov, F. V., Myasnikov, A. S., Zhadan, G. G., Orlova, G. S., and Strokin, M. V., "Some Results of Flight Tests of an Ion–Engine Model Using Surface Ionization of Cesium on Tungsten", *Kosmicheskie Issledovaniya*, Vol. 11, No. 1, pp. 140–144, January–February 1973.
28. Byers, D. C., and Staggs, J. F., "SERT–II Thruster System Ground Testing", *AIAA 7th Electric Propulsion Conference*, Paper 69–235, 3–5 March, 1969.
29. Kerslake, W. R., Goldman, R. G., and Neiberding, W. C., "SERT–II Mission, Thruster Performance, and In–Flight Thrust Measurements", *AIAA 8th Electric Propulsion Conference*, Paper 70–1125, 31 August–2 September, 1970.
30. Jones, S. G., Staskus, J. V., and Byers, D. C., "Preliminary Results of SERT–II Spacecraft Potential Measurements Using Hot Wire Emission Probe", NASA TM X–2083 1970.
31. Kerslake, W. R., and Finke, R. C., "SERT–II Hollow Cathode Multiple Restarts in Space", *AIAA 10th Electric Propulsion Conference*, 31 October–2 November, 1973.
32. Kerslake, W. R., and Finke, R. C., "SERT–II Thruster Space Restart", *AIAA 11th Electric Propulsion Conference*, 19–21 March, 1975.
33. Kerslake, W. R., and Domitz, S., "Neutralization Tests on the SERT–II Spacecraft", *AIAA 14th International Electric Propulsion Conference*, Princeton, N. J. AIAA paper 79–2064, 30 October–1 November, 1979.

34. Kaufman, H. R., "Plasma Physics Analysis of SERT-II Operation", NASA CR-159814, January, 1980.
35. Sasaki, S., Kawashima, N., Kuriki, K., Yanagisawa, M., and Obayashi, T., "Neutralization of Beam-Emitting Spacecraft by Plasma Injection", *Journal of Spacecraft*, Vol. 24, No. 3, May-June, 1986.
36. Olsen, R. C., "Modification of Spacecraft Potential by Plasma Emission", *Journal of Spacecraft and Rockets*, Vol. 18, pp. 462, 1981.
37. Lewis Research Center Annual Report, *Advanced Electric Propulsion and Space Plasma Contactor Research*, by P. J. Wilbur, Colorado State University, NASA CR 175119, January, 1986.
38. Wei, R., and Wilbur, P. J., "Space-Charge-Limited Current Flow in a Spherical Double Sheath", *Journal of Applied Physics*, Vol. 60, pp. 2280, 1986.
39. Patterson, M. J., "Plasma Contactor Laboratory Characterization", *Electrodynamic Tether Meeting*, General Research Corporation, 18 May, 1988.
40. Hastings, D. E., "The Theory of Plasma Contactors Used in the Ionosphere", *Journal of Spacecraft and Rockets*, in press, 1988.
41. Davis, V. A., Katz, I., Mandell, M. J., and Parls, D. E., "Three-Dimensional Simulation of the Operation of a Hollow Cathode Electron Emitter on the Shuttle Orbiter", *NASA/AII/PSN International Conference on Tethers in Space* 17-19 September, 1986.
42. Olsen, R. C., "Electron Beam Experiments at High Altudes", *Journal of Electrostatics*, Vol. 20, pp. 43-57, 1987.
43. McPherson, D. A., and Schober, W. R., "Spacecraft Charging at High Altudes: The SCATHA Satellite Progrm", *Progress in Astronautics and Astronautics*, Vol. 47, "Spacecraft Charging by Magnetospheric Plasma", edited by A. Rosen, pp. 15-30, AAIA, NY, NY, 1976.
44. Katz, I., Jongeward, G. A., Parks, D. E., Reasoner, D. L., and Purvis, C. K., "Energy Broadening Due to Spacecharge Oscillations in High Current Electron Beams", *Geophysical Research Letter*, Vol. 12, pp. 64, 1986.
45. Raitt, W. J., Burt, D. A., Berkey, F. T., Jost, J., Kelley, M. C., Pickett, J., Torbert, R., "A Sounding Rocket Payload to Study High Voltage Current Collection from the Ionosphere at Low Earth Orbit (LEO) Altitude", *AAIA 26th Aerospace Sciences Meeting*, 13 January, 1988.
46. Michael, Kasha., *Ionosphere and Its Interaction with Satellites*, Gordon and Breach, pp. 7-71, 1969

47. **Foley, T. M.**, "SDI Suborbital Launch Yields Data for High-power Platform Design", *Aviation Week and Space Technology*, 1987
48. **Reitz, J. R., Milford, F. J., and Christy, R. W.**, *Foundations of Electromagnetic Theory*, Addison-Wesley Series in Physics, June 1980.
49. **Linson, L. M.**, "Current-Voltage Characteristics of an Electron-Emitting Satellite in the Ionosphere", *Journal of Geophysical Research, Space Physics* Vol. 74, No. 9, 1 May, 1969.
50. **Parks, D. E., and Katz, I.**, Theory of Plasma Contactors for Electrodynamic Tethered Satellite Systems", *Journal of Spacecraft*, Vol. 24, No. 3, May-June 1984.
51. **McCoy, J. E.**, "Plasma Motor/Generator Reference System Designs for Power and Propulsion", *NASA/AIAA/PSN International Conference on Tethers in Space*, 18, September 1986.

## INITIAL DISTRIBUTION LIST

	No. Copies
1. Defense Technical Information Center Cameron Station Alexandria, VA 22304-6145	2
2. Library, Code 0142 Naval Postgraduate School Monterey, CA 93943-5002	2
3. Physics Library Code 61 Department of Physics Naval Postgraduate School Monterey, CA 93943-5000	1
4. Department Chairman, Code 61 WH Department of Physics Naval Postgraduate School Monterey, CA 93943-5000	1
4. Professor R. C. Olsen Code 61 OS Department of Physics Naval Postgraduate School Monterey, CA 93943-5000	10
5. Professor S. Gnanalingum Code 61 GM Department of Physics Naval Postgraduate School Monterey, CA 93943-5000	1
6. Maj. Yoon, Sang Il Postal Code 138-150 Gangdong Gu, Bang-i Dong, Samik APT 201-1103 Seoul, Republic of Korea	2
7. Maj. Han, Hwang Jin SMC 2402 Naval Postgraduate School Monterey, CA 93943-5000	1
8. Maj. Kim, Jong Ryul SMC 1659 Naval Postgraduate School Monterey, CA 93943-5000	1

9. LT. Commander. Youn, Duk Sang 1  
SMC 1254  
Naval Postgraduate School  
Monterey CA 93943-5000
10. Lee, Yong Moon 1  
Ma-Po Gu, Yun-Nam Dong, 382-17  
Seoul, Republic of Korea
11. Cpt. Song, Tae Ik 1  
SMC 2686  
Naval Postgraduate School  
Monterey, CA 93943-5000
12. Mr. Joe Kolecki 2  
NASA/Lewis Research Center  
MS 302-1  
21000 Brookpark Rd  
Cleveland, OH 44135
13. Dr. Roy Torbert 2  
Physics Department  
University of Alabama  
Huntsville, AL 35899
14. Cpt. Ryu, Jong Su 1  
SMC 2039  
Naval Postgraduate School  
Monterey, CA 93943-5000
15. Library, P.O Box 2 1  
Korea Military Academy  
Postal Code 130-09  
Gong-neung Dong, 556-21 Dobong Gu  
Seoul, Republic of Korea
16. Library, P.O Box 2 1  
Postal Code 140-01  
Yongsan Gu, Yongsan Dong  
Seoul, Republic of Korea





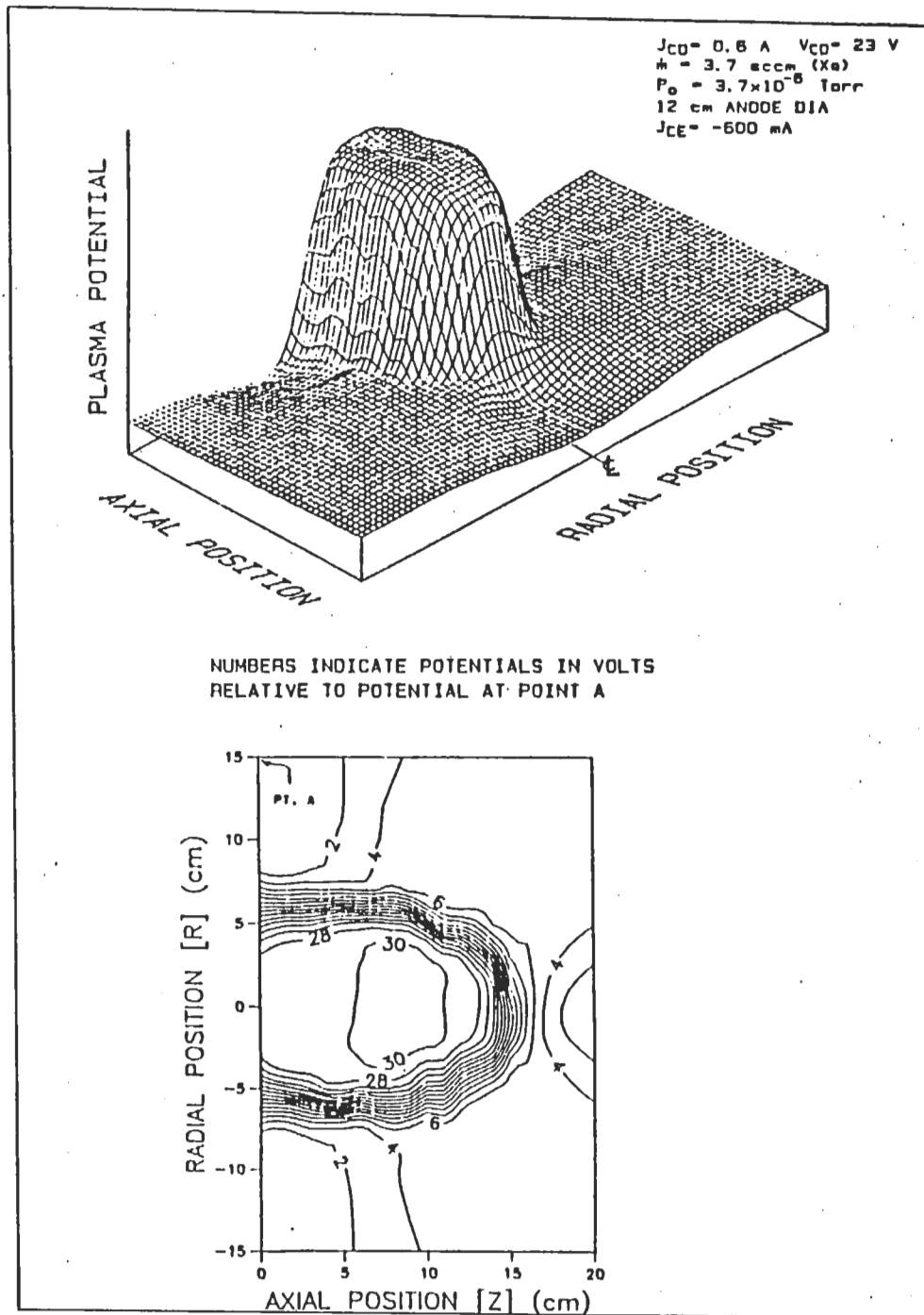


Fig. 3.3 Plasma Potential Contour around Hollow Cathode[Ref. 37]

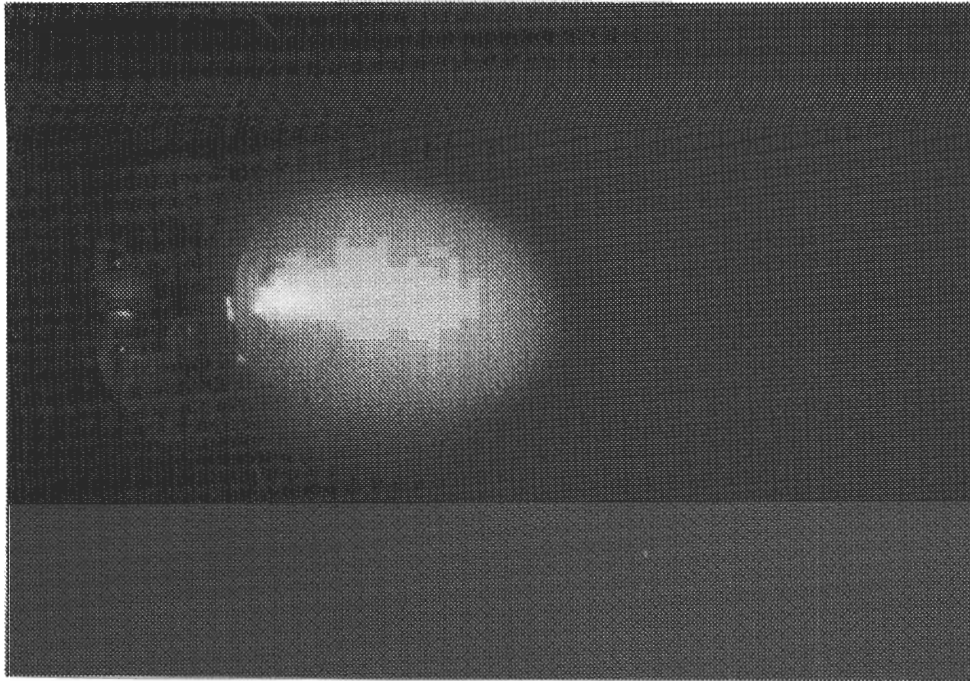


Fig. 3.4 Hollow Cathode Ignited mode Configuration

of relatively high ambient neutral density. Major effects were found due to volume ionization caused by the collected electrons. Recent modifications of the chamber will enable experiments at more reasonable neutral background levels.

Patterson's work focused on high current levels (higher than those studied by Wilbur). Multiampere level (10 A) currents were extracted from the simulated space plasma environment. Figure 3.5 shows the current to the plasma contactor with and without power on for the contactor discharge, at comparable flows and bias voltages. Relatively little difference is found.[Ref. 39]

Figure 3.6 shows the dependence of the collected current on the discharge mode. Substantially higher currents are drawn in ignited mode. Comparison of experiments of the CSU and LeRC facilities indicates the substantial dependence of the results on the chamber size. Figure 3.7 shows the large variation in results for similar operating conditions. Substantially large currents are possible in the LeRC

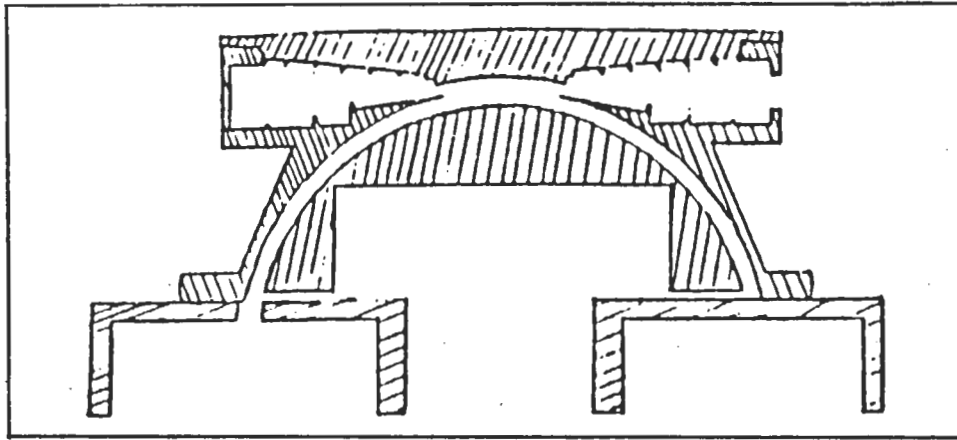


Fig. 4.14 Electrostatic Analyzer

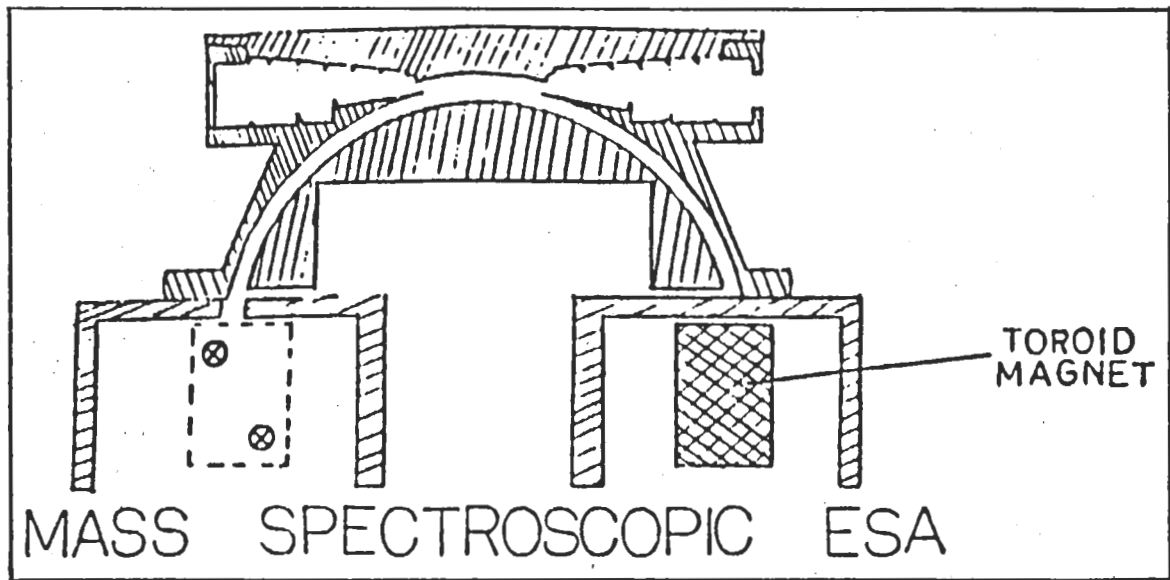


Fig. 4.15 ESA Included Mass Resolution

The unusual capability of resolving extremely heavy ions will allow us to separate locally generated ion distributions from the ambient ions. This is important for making accurate determinations of negative payload potentials, and inferring heating of locally emitted ions, such as  $Xe^+$ . The modification for mass analysis is underway at UAH. Figure 4.16 shows ESA result from ATS-6 ion engine experiment. This is a grey scale presentation of particle data, where the horizontal